2012-10-04

Experimental Analysis and Mechanistic Modeling of Wellbore Strengthening

Mostafavi Toroqi, Seyyed Vahidreza

UNIVERSITY OF CALGARY

Experimental Analysis and Mechanistic Modeling of Wellbore Strengthening

by

Seyyed Vahidreza Mostafavi Toroqi

A THESIS

SUBMITTED TO THE FACULTY OF GRADUATE STUDIES

IN PARTIAL FULFILMENT OF THE REQUIREMENTS FOR THE

DEGREE OF DOCTOR OF PHILOSOPHY

DEPARTMENT OF CHEMICAL AND PETROLEUM ENGINEERING

CALGARY, ALBERTA

SEPTEMBER, 2012

Abstract

Wellbore strengthening refers to the science and technology of increasing the pressure level at which circulation loss to the formation occurs. Although a fairly wide range of technologies have been proposed and tested, the application of engineered drilling fluids has proven to be the most promising approach. Circulation loss, which is one of the most troublesome issues occurring in drilling operations, is experienced at varying levels of severity. It is most expected in highly permeable formations, fractures and caverns. Lost circulation may have several consequences including fluid inflow, wellbore collapse, formation damage, non-productive rig time and environmental contamination. In order to mitigate the risks of circulation loss, a broad range of treatments and preventive methods have been practiced such as application of Lost Circulation Materials (LCM), cement plugs, squeeze gunk, gels and technologies like aerated drilling and stress caging. It has been observed that lost circulation occurs at varying pressure levels dependent on drilling fluid properties. This observation builds the foundation for drilling fluid based wellbore strengthening. Wellbore strengthening has been described previously but a general model to take into account the effects of fluid properties and its constituents does not exist. In addition, the governing mechanisms of this process are not well understood and explained in the literature. In this study a comprehensive literature survey and an extensive experimental analysis was completed to determine the mechanism of and contributing factors to wellbore strengthening. Next, a mechanistic model was developed and verified to predict the formation resistance prior to allowing drilling fluid loss. A field case of wellbore strengthening was also studied where the developed model exhibited a very good agreement. Results from this research are mostly directed towards circulation loss prevention via tensile fractures. However, they might be applicable for pore scale seepage loss through gravels and natural fractures. In the first chapter, an introduction to the circulation loss issue and its consequences is presented. Chapter two is dedicated to a brief review on wellbore stability analysis and a thorough survey on wellbore strengthening. In chapter three, the experimental part of this research is explained and its results are discussed. In chapter four, the experimental results are applied to build a mechanistic model. The model is analyzed and verified using a field case of wellbore strengthening. Conclusions of this research and some recommendation for future studies are presented in Chapter five.

Acknowledgement

I am sincerely thankful to my supervisor, Dr. Geir Hareland, whose encouragement, guidance and full support from the initial to the final level of my PhD. Most importantly, I am deeply grateful for the space he provided me to try new ideas and expand my research area.

I am also grateful to Dr. Bernt S. Aadnoy for his technical support and time during the course of this project. His valuable ideas, extensive knowledge and experience laid the groundwork for this research.

The assistance and technical support of my supervisory and exam committee members, Dr. Maen Husein, Dr. Gordon Moore, Dr. Laurence Lines and Dr. Chris Hawkes is sincerely appreciated.

Kind cooperation of Mr. Ryan Russel from Rheotech Drilling Fluid Services Inc. is acknowledged. The dataset they provided to this research allowed for field verification of the findings.

I am indebted to my colleagues Dr. Mefin Belayneh and Mr. Sivert B Drangeid during the experimental phase of this project in Norway.

I would like to show my gratitude to Talisman Energy, Pason Systems and NSERC for providing the funding and technical support for this research.

Finally, I would like to express my sincere thankfulness to my wife, Tammy for her support, understanding and scientific help during my PhD program.

Dedication

To my life companion, Tahmineh,
my parents and brothers.

Table of Contents

List of Tables

List of Figures

Nomenclature

σ_H	Maximum horizontal stress, MPa
σ_h	Minimum horizontal stress, MPa
σ_V	Vertical stress, MPa
σ_θ	Tangential (hoop) stress, MPa
σ_r	Radial stress, MPa
T_R	Tensile strength of rock, MPa
P_o	Pore pressure, MPa
P_{init}	Fracture initiation pressure, MPa
η	Constant (function of Biot's coefficient and Poisson's ratio)
α	Biot's coefficient
C_o	Compressive strength, MPa
σ_1	Maximum principal stress, MPa
σ_2	Intermediate principal stress, MPa
σ_3	Minimum principal stress, MPa
β	Breakout angle, degree
φ	Angle of internal friction, degree
τ_o	Constant (function of cohesion and angle of internal friction)
m^*	Constant (function of cohesion and angle of internal friction)
σ_{oct}	Octahedral stress, MPa
J_{2D}	Second invariant of the deviatoric effective stress, MPa
c	Cohesion, MPa
Z	Total number of zeros
N	Total number of peaks
P_{P-ave}	Average peak pressure , MPa
P_{max}	Maximum pressure, MPa
N/t	Time averaged number of peaks
Z/t	Time averaged number of zeros
N/Z	Number of peaks per zero

d	Particle size, μm
μ_{app}	Apparent viscosity, cP
PV	Plastic viscosity, cP
YP	Yield point, cP
GS	Gel strength
V_{fil}	Filtration volume, cm^3
MC	Moisture content
d_{max}	Maximum particle diameter, μm
m	Particle size distribution factor
φ_{min}	Minimum porosity
D_v	Constant (function of particle size distribution)
R	Roundness
W_f	Fracture width, μm
D_{P-max}	Maximum particle diameter allowed in the fracture, μm
D^*	Initial width of the particle block, μm
E_P	Elastic modulus of particles, MPa
μ_f	Static friction coefficient of rock
W_{f-max}	Maximum fracture width, μm
W_{f-ave}	Average fracture width, μm
ν_R	Poisson's ratio of rock
E_R	Elastic modulus of rock, MPa
L_f	Fracture length, m
P_f	Fracture net pressure, MPa
H_f	Fracture height, m
W_y	Width of the point at which the plug yields, μm
L_y	Distance of the point at which the plug yields to the fracture mouth, μm
F_N	Normal force, N
σ_N	Normal stress, MPa
A	Cross sectional area, m^2

ε	Strain
f	Friction
F_{Str}	Force required to remove the plug, N
P_{Str}	Plug strength, MPa
A_f	Cross sectional area of fracture planes, m^2
σ_y	Yield stress, MPa
U_r	Modulus of Resilience, MPa
P_{LC}	Lost circulation pressure, MPa
T_{max}	Maximum plug thickness, μm
C_{Cr}	Critical concentration, kg/m^3
ρ_P	Particle density, kg/m^3

CHAPTER ONE: INTRODUCTION

Wellbore strengthening refers to methodologies which aim to increase the resistance of formations to circulation loss during drilling or cementing operations. Lost circulation is known as one of the most prominent drilling problems due to its frequent occurrence and complications. It can also introduce several severe consequences to the drilling operations. Therefore, wellbore strengthening methodologies as preventive approaches towards this issue have attracted attention in the past two decades. Increases in rock strength during drilling operations may be achieved through various technologies described in the past. However, drilling fluid based wellbore strengthening is the most promising approach based on the field and laboratory observations and studies. This approach pursues the engineered design of drilling fluids or specialized pills in order to reach the desired strengthening level. The main focus has been on the properties of the solid contents of the fluids, as they play a key role in the wellbore strengthening process. This methodology is also called particulate-based wellbore strengthening. Despite the vast attention devoted to investigation of the effective parameters in drilling fluid design for rock strengthening purposes, most of the findings are limited to qualitative analyses and explanations and do not provide strong tools for engineering practices. In this chapter, circulation loss, its consequences, severity and zones are discussed in detail. Next, the mitigation approaches and the research methodologies are introduced.

Lost circulation is defined as partial to total loss of drilling fluid or cement slurry to the formation voids[1]. Also known as lost returns, this issue has been known as the most troublesome drilling problem which may initiate as a result of operational shortcomings and natural constraints. In 2003, it was estimated that industry spends almost 800 million dollars per year on circulation loss related issues[2]. Lost circulation may follow other drilling problems and give rise to several other problematic consequences if not prevented or treated promptly during the course of an operation. As shallow hydrocarbon resources deplete, producers need to confront the challenges associated with obtaining hard to reach hydrocarbon reserves. Lost circulation is one of the most prominent, time consuming problems which may be encountered in both conventional and unconventional reservoirs. Therefore studies aiming to mitigate lost circulation

started as early as fifty years ago. Numerous techniques and materials have been tried and recommended with varying degrees of success and efficiency. This issue continues to lengthen the time required to complete drilling operations and introduce inevitable risks. In the next section, circulation loss, its reasons and consequences will be introduced and classified based on previous studies and field experiences.

1.1 Drilling fluid loss

The drilling fluid circulation system is responsible for several essential functions including cuttings removal from the borehole, containment of the pore pressure, mechanical support of the penetrated formations and chemical stabilization of the hole. Excessive accumulation of cuttings in the well leads to several problems such as stuck bit or drill string, differential sticking, high Equivalent Circulating Density (ECD). Loss of mechanical stability in the well increases torque and risk of stuck downhole tools and may even lead to loss of the well. Inflow of pore fluid in the well changes downhole pressure, and if not controlled and stopped can threaten the safety of the rig. Drilling fluid circulation also cools down and lubricates the drill bit, keeps the particles in suspension during the waiting periods, reduces the weight on bit due to buoyancy factor and aids in formation evaluation. Therefore, reduction of the fluid level in the wellbore creates the potential for failing to meet these requirements. From an environmental point of view, loss of oil-based drilling fluid contaminates the porous media and possibly water resources. Formation damage and impaired productivity can occur when circulation loss happens in the pay zone. Therefore, managing to keep the drilling fluid in the borehole is essential to reduce the time and cost of operations and increase the life of the producing well and reservoir. Despite the efforts made by operators and researchers in the past few decades, circulation loss is still known as the number one drilling problem[3].

1.3. Lost circulation severity

Circulation loss may be categorized based on intensity and type of circulation loss zone. Although no generally accepted standard exists to classify the problem in terms of intensity, operators usually use the following terms to describe the severity of the fluid loss.

1.3.1 Seepage loss

Although some studies concluded that seepage loss may happen in any formation[1], seepage loss mostly occurs in porous and permeable formations where a firm low permeability mud cake cannot be formed. Under static conditions, seepage loss rate may vary from in a range of 10 to 20 barrels per hour and under dynamic conditions less than 10% of the fluid may be lost[4]. Some studies have limited seepage loss to less than 10 barrels of fluid loss per hour[5,6,7]. Others have defined the upper limits of 25 barrels per hour and 10 barrels per hour for the seepage loss when drilling with water-based muds and oil-based muds, respectively[8.]

1.3.2. Partial loss

Partial loss of fluids happens in unconsolidated sands and loose gravels as well as zones containing one or more small natural or induced fractures[4]. Some studies concluded that partial losses rarely occur in induced fractures[7]. The loss rate of 20 to 50 barrels per hour in static conditions and 20% to 50% of the drilling fluid in dynamic mode happens during a partial loss of fluids. In another study, ranges of 25 to 100 barrels per hour and 10 to 30 barrels per hour have been presented as the partial loss range for water-based and oil-based muds, respectively[8]. In another classification, all fluid losses in a rate between 10 barrels per hour and 25 barrels per day have been categorized as partial circulation losses[2]. The term “moderate” has also been used to describe partial losses[9].

1.3.3. Severe losses

Severe lost circulations happen in long sections of unconsolidated sands and larger fractures. Fluid is lost in a rate of 50 to 150 barrels per hour and 50% to 100% in static and dynamic conditions, respectively during severe lost circulation. In some studies severe losses have been defined as loss rates of fluid loss higher than 500 barrels per day. Severe losses have also been described as conditions in which more than 30 barrels of oil-based muds or 100 barrels of water-based muds are lost per hour[8] and in another work[2] all circulation losses over 25 barrels per hour have been classified as severe losses. The term "complete loss" has also been used to describe severe circulation losses[7].

1.3.4. Total losses

Total fluid loss happen when no return is observed at the surface. It may happen during drilling through cavernous and vugular formations or while penetrating numerous large fractures. Some studies have defined total losses as conditions under which the level of fluid in the annulus cannot be seen. In some classifications severe and total loss levels are known to be identical.

One may see in the definitions of the fluid loss categories that there is not a general agreement on the definitions. Different operators define these based on intensity and other circumstances. Detecting the level of intensity of fluid loss in combination with the circulation loss zone specifications can assist in developing a treatment plan.

1.4. Lost circulation zones

All kinds of formations and lithologies may be subject to lost returns as this problem has been experienced and reported in various depths and rock types. Although some specific formations are more capable of developing circulation loss environment, a lost circulation zone is defined mostly based on the geometry and shape of the opening. Therefore the zone in this context refers to the path through which the drilling fluid can exit the wellbore rather than geological

description of the formations. Lost circulation zones are introduced in this section and illustrated in Figure 1.

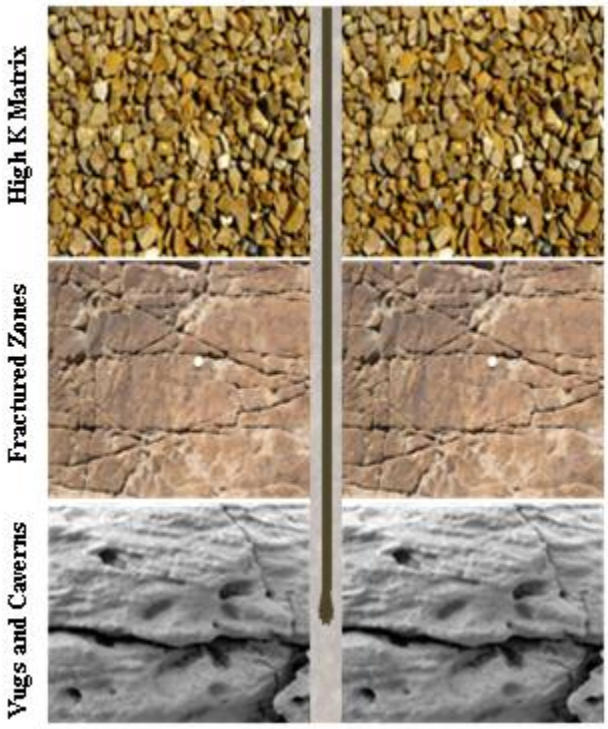

Figure 1: Lost circulation zones

1.4.1. High matrix permeability formations

These zones include porous and permeable formations, unconsolidated sands, loose gravels and micro fractured carbonates[8]. They usually occur at shallow depths and have a permeability of 10 to 100 D (Darcy)[10,8,1] or even more[11]. This type of lost circulation starts with a gradual drop of mud level in pits and may increase if drilling continues with no corrective measures. Since oil and gas permeability values in sands are usually limited to less than 3.5 D, seepage fluid loss is very unlikely to happen for oil and gas fluids unless the loss can be attributed to the case in which the formation fractures.

1.4.2. Natural fractures

Natural fractures and fissures are common in chalk and limestone formations[5]. However, small natural fractures are present in almost all formations[12]. Fluid loss through natural fractures is evidenced by gradual lowering of mud level in mud pits. If the drilling continues and more fractures are exposed, total circulation loss may be experienced[11].

1.4.3. Induced fractures

Induced fractures are usually horizontal at shallow depths and turn vertical if they occur at depths over 2500 ft (~750 m)[10]. In some studies it has been concluded that the induced and natural fractures turn vertical in layers deeper than 4000 ft (~1200 m). Induced fractures may initiate in any formation[7] due to well irregularities, high mud weight, excessive back pressure or choke down, rough handling of drilling tools, or due to a closed hydrostatic system[1]. They are mostly expected in formations with weak planes and low permeability such as shale[1]. Lost circulation through induced fractures is usually sudden and accompanied by total loss of fluid. It is evidenced by experiencing loss at a depth which has been circulation loss free in adjacent wells[11].Induced fractures are very common in high pressure zones because heavy muds are used, however they may be encountered in other pressure zones as well. Unlike naturally occurring fractures, rock strength needs to be overcome to initiate an opening. Wellbore pressure tends to split the rock at enlargements[11]. In this dissertation, circulation loss through induced fractures is investigated and studied in detail. The results, however, may be applicable to other circulation loss zones.

1.4.4. Cavernous and vugular formations

These zones normally occur in limestones[1,10] or dolomites as a result of percolating water which dissolves Calcium leading to quick and total circulation loss. Size of this sort of openings ranges

from fraction of an inch to large tunnels[5]. This type of fluid loss is the most difficult to seal; however, they are not very prevalent[1,11].

1.5. Lost circulation mitigation

Techniques and materials applied to combat circulation loss problems vary based on several factors including circulation loss zone, severity, experiences in adjacent wells, operational constraints and even availability of materials around the drilling location. Although the approaches taken to reduce lost circulation consequences and occurrence have developed over the time, this particular problem continues to increase Non-Productive Time (NPT) of drilling operations and the overall cost as well as bringing up several other hole instability and safety problems. In general, techniques and approaches to mitigate the issue may be categorized as preventive and corrective approaches[1,9], the former being the series of measures and actions to reduce the probability of lost circulation while the latter refers to remedy the loss of fluid after it happens. Avoiding circulation loss requires preparation and an extensive plan which takes into account all influential parameters during the operation. A brief review of the currently acceptable and applied approaches is presented in this section.

1.5.1. Preventive methods

Prevention of circulation loss based on drilling fluid designs which aim to increase the circulation loss gradient, is the topic of this study. It has been observed through different laboratory and field experiments that particles in the drilling fluid may increase the circulation loss gradient beyond the initially estimated values[7,9,11,12,13,14,15,16,17,18,19,20,21,22,23,24,25,26]. Theories such as stress caging have been put forth which claim that an increase of tangential (hoop) stress around the wellbore occurs due to generation of small fractures and filling them with sealant particles. Some other studies have found elasto-plastic behavior of the mud cake as the dominant factor. The idea of designing specific particles and mixing them in the drilling fluid prior to encountering lost circulation problems to reduce the probability of circulation loss was

developed based on the same observations. However, a comprehensive theory to explain the effect of different properties of particles and fluids on the circulation loss gradient has not been developed and verified in previous studies. Another approach to increase the tangential (hoop) stress around the wellbore was proposed based on increasing the temperature of wellbore by using hot fluids. Some authors believe that this method does not have the theoretically predicted effect in the field. Therefore particulate-based methods are the most important preventive approaches towards mitigation of lost circulation. Pre-treatment of drilling fluids with particles was found effective for seepage and partial losses[8]. In general the term "wellbore strengthening" is applied for the approaches which aim to increase the resistance of the well against circulation loss and thus includes all preventive methodologies. Wellbore strengthening will be discussed in more detail in the next chapter.

In some operational reports and studies, lost circulation prevention normally refers to considerations and operational measures and techniques taken in order to reduce the probability of fluid loss. Minimizing hydrostatic pressure to the minimum allowable value, minimize equivalent circulating densities by reducing gel strength of the fluid, yield point and viscosity within safe ranges, controlling surge and swab pressures, avoiding restrictions in the annulus by drilling at a reasonable speed, setting casing to protect the weak upper formations within a transition zone, updating formation pore pressure, and fracture gradient information, underbalanced drilling, casing drilling, application of heated drilling fluids, using expandable casings and liners and having Lost Circulation Materials (LCM) available on the rig site are examples of operational measures for loss circulation prevention[8,10,19].

1.5.2. Corrective methods

Corrective methods are designed based on circulation loss zone, severity and similar experiences in adjacent wells. One of the most widely used techniques applied to remedy circulation loss is the application of Lost Circulation Materials (LCM). LCMs are available in various types, shapes and particle size distributions. They are categorized as granular, fibrous and flake (pellet) particles based on their shapes. Walnut hulls, coconut hulls, peanut hulls, shredder paper, coke,

ground tire rubber, graphite, calcium carbonate, mica, sawdust, cellophane flakes, swellable particulates and polymer gels are the most well-known and widely applied LCMs. As one may observe, some LCMs have been selected based on their redundancy around the drilling location. Typical sizes of LCMs vary between several microns and several thousands of microns. LCM producers usually classify them as coarse, medium and fine particles based on their size. Settable pills are the second type of materials used to solve the issue. They include cements, cross linking polymers (gels) and resin. This sort of pill requires a certain amount of time to penetrate sufficiently into the "thief zones". Once the fluid has penetrated deeply its viscosity increases and the openings becomes sealed off and the fluid flow stops. Settable pills are most likely to be applied when regular LCMs fail to remedy the issue[1]. Deformable Viscous Cohesive (DVC) plugs (soft plugs) are the third type of common corrective materials applied to stop circulation loss. A significant part of previous efforts in the field of lost circulation has been devoted to develop novel corrective materials[15,16,27,28,29,30,31,32,33,34,35].

1.6. Research methodology

As presented in section 1.5, most previous studies have resulted in products to cure circulation loss and practically applicable methodologies to prevent lost circulation are rare. Some researchers and operators have observed, analyzed and described preventive approaches, but a firm verified understanding of particulate-based prevention of circulation loss is still lacking. Therefore, engineering of drilling fluids for this purpose cannot be performed.

One of the main objectives of the current project was to provide a solid understanding of the mechanism of wellbore strengthening and detection of the effective fluid properties that control the success of the strengthening process. Another main purpose of this study was to be able to develop a reliable, verified model for wellbore strengthening to be applied in future engineering practices.

Once a detailed review and evaluation of the previous studies and contributions was completed, an extensive experimental analysis was planned and carried out in the University of Stavanger in Norway, which is one of the leading institutions in the area of wellbore strengthening. All related

facilities of the University of Stavanger including the drilling fluid lab apparatus, particle plugging test apparatus, and core fracturing system were incorporated in this part of the research. In some experiments the available systems were modified to provide the desired information. Details of the experimental results will be presented in Chapter three.

During the second phase of this research, statistical and analytical methods as well as the observed mechanisms during the experiments were applied to develop a mechanistic model for wellbore strengthening. Analysis of the experimental data led to detection of the influential parameters and their magnitude of impact in strengthening the formations. Outcomes of this work were very significant and formed one of the major contributions of this work.

In the next stage of the work, a field trial of wellbore strengthening was analyzed and applied to verify the model. The pursued procedure and approaches were designed based on a detailed review and analysis of previous studies. Results of this work provided a scientifically reliable methodology for wellbore strengthening engineering practices. Stages of this project are illustrated in the chart in Figure 2.

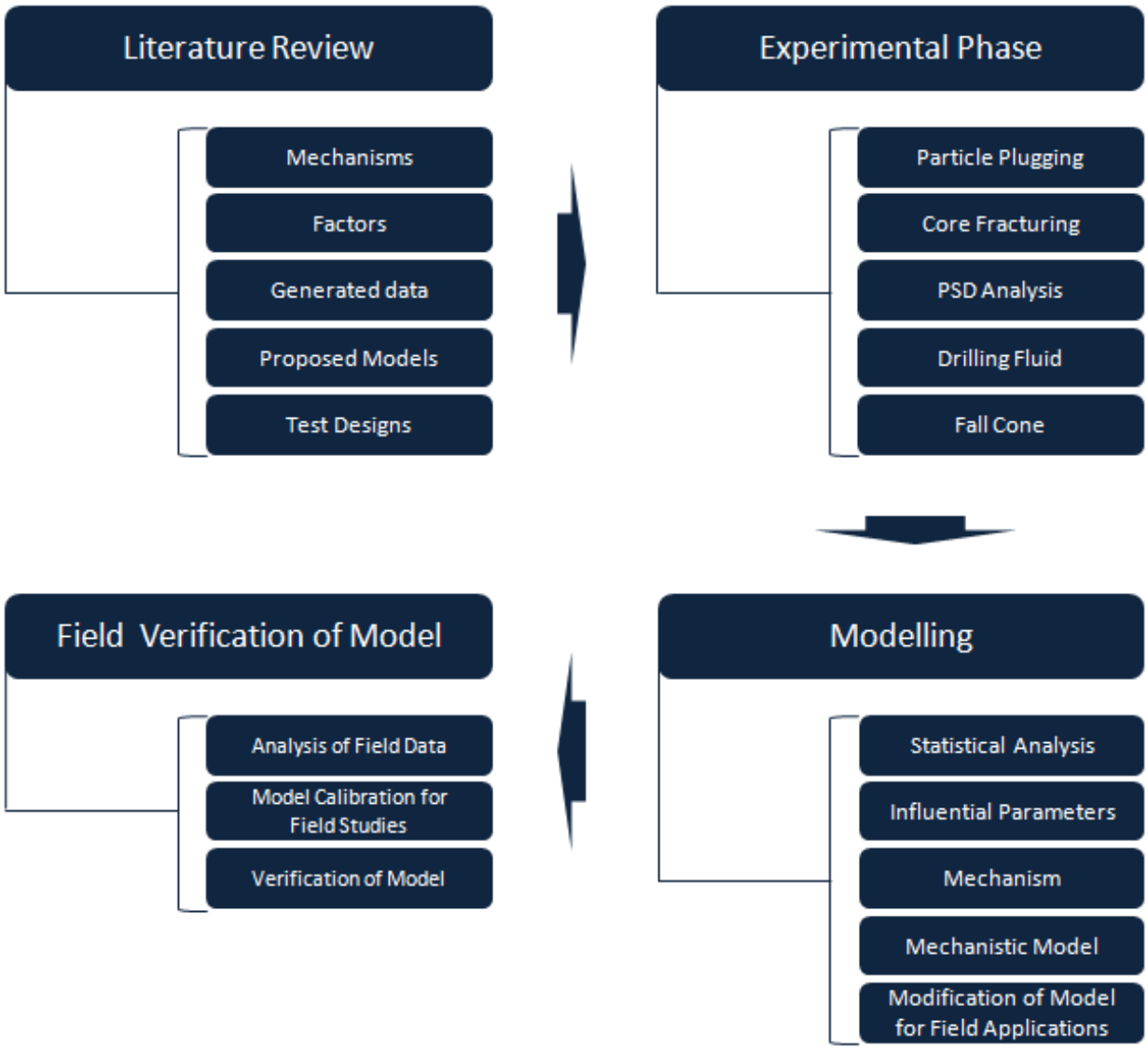

Figure 2: Diagram of the stages of the research

CHAPTER TWO: WELLBORE STRENGTHENING

2.1. Introduction to wellbore stability analysis

Wellbore stability analysis is conducted to obtain knowledge on the stress state around the wellbore in to compare against failure criteria. This knowledge will then be applied for drilling fluid design and well plans. Wellbore stability analysis is strongly attached to wellbore geomechanics and rock physics. Analytical models based on elasticity and plasticity have been developed and applied for stress estimation and failure analysis around the borehole. In addition, application of data analysis, data mining and other statistical tools as well as intelligent estimation of required parameters have attracted attention in recent years.

When the rock body is removed from the well as a result of the penetration of the bit, the stress state around the well is disturbed. Since the drilling process removes the support for the formation around the well and the circulated drilling fluid may provide a lower or higher level of stress, the potential exists for rock failure. Figure 3 shows schematically the stresses around the well.

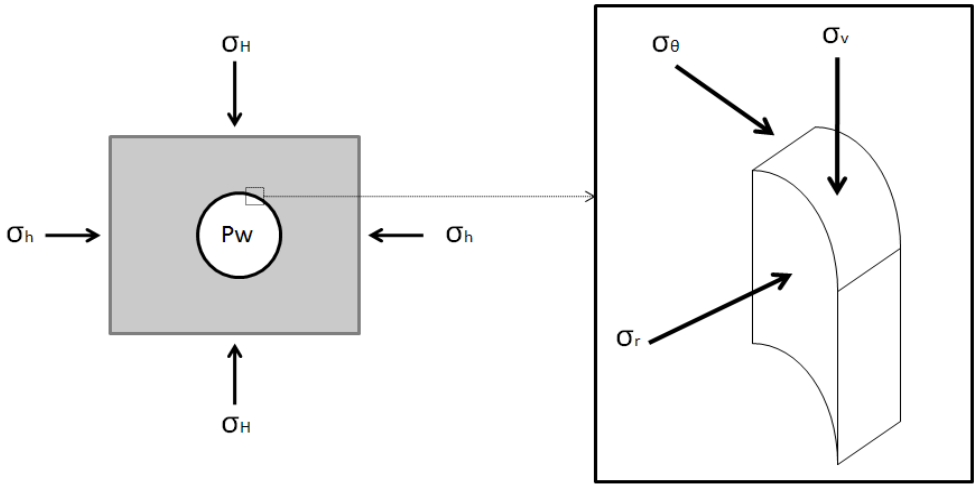

Figure 3: Stress state around the wellbore

As shown, for a vertical well, the stress state around wellbore is usually described in terms of radial, tangential (hoop) and vertical stresses. Wellbore stability analysis usually begins with data

collection. Datasets are collected from logging operations, well tests, offset wells, laboratory experiments of cores, drilling fluid tests, etc. All these sources are associated with some level of uncertainty which needs to be carefully estimated and brought into account before proposing stability plans for the well. In-situ stress state, rock properties, and pore pressure are among the most influential parameters, and several resources should be considered to estimate them as accurately as possible. In some cases, the required parameters and information are not available and thus an assumption within a reasonable range is made. The applied empirical and analytical models and sub-models introduce an extra source of uncertainty to the process.

One of the most important outcomes of a wellbore stability study is the safe range of bottom-hole pressure. As the drilling fluid pressure rises above a certain limit, the extra stress causes the rock to fail in tention. The upper limit for the drilling fluid pressure is considered as the pressure level that causes fracturing and consequently circulation loss. Therefore estimation of the fracturing gradient of the formation is essential to wellbore stability. The lower limit of bottom hole pressure is defined by well collapse or pore pressure in the formation. Pore pressure is the pressure of the fluid in the formation porous media in the vicinity of the well. Low pressure in the well gives rise to high tangential (hoop) stress around the borehole and may cause severe formation collapse. Mohr – Coulomb's criterion is one the most applicable failure criteria utilized for well collapse analysis. Excessive pressure in the wellbore causes a decrease in tangential (hoop) stress. This decrease may turn the tangential (hoop) stress into tension and lead to fracture initiation once the tensile strength is overcome. In most cases, the tensile strength of the rock is assumed to be close to zero since the rock texture is associated with imperfections such as small conductive fissures and fractures. This type of fractures are called tensile fractures and represent one the main causes of partial to total drilling fluid loss once they are sufficiently open. In this work, circulation loss in tensile fractures will be investigated. However, the results may be applicable to lost circulation through natural fractures and highly permeable formations.

The fracturing gradient is dependent on several factors such as rock properties, in-situ stress state and operational practices. In addition, the depletion level of the reservoir and the presence of conductive fractures around the well may affect the fracture gradient significantly. Wang[9] presented a useful collection of the most frequently used equations for fracturing gradient estimation. Figure 4 schematically illustrates the initiation of a tensile fracture in the near wellbore region.

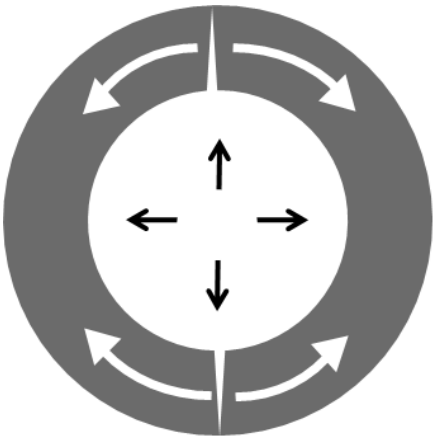

Figure 4: Tensile fracturing in the wellbore

Based on the tensile fracturing criterion, fracture initiates when the following requirement is met.

$$\sigma_\theta = -T_R \qquad \text{Eq. 2-1}$$

where σ_θ is the tangential (hoop) stress around the well and T_R is the rock tensile strength. Based on Kirsch equations, tangential (hoop) stress around the borehole can be estimated using the in-situ stress state. When the wellbore is vertical and perfectly circular without hydraulically conductive fractures and a non-penetrating fluid, the fracturing gradient of the formation may be estimated using equation 2-2.

$$P_{init} = 3\sigma_h - \sigma_H + T_R - P_o \quad \text{Eq. 2-2}$$

where P_{initi} is the fracturing pressure, σ_h is the minimum horizontal stress, σ_H is the maximum horizontal stress and P_o is the pore pressure. When dealing with an isotropic horizontal stress state, the equation may be simplified as below.

$$P_{init} = 2\sigma_h + T_R - P_o \quad \text{Eq. 2-3}$$

When the fluid is fully penetrating, the formation becomes weakened by the fluid penetration. Equation 4 may be applied for such conditions.

$$P_{init} = \frac{3\sigma_h - \sigma_H + T_R - 2\eta P_o}{2(1-\eta)} \quad \text{Eq. 2-4}$$

where η can be estimated using Equation 2-5.

$$\eta = \frac{1-2\nu}{2(1-\nu)} \quad \text{Eq. 2-5}$$

When conductive hydraulic fractures are present, Equation 2-6 estimates the fracture initiation pressure.

$$P_{init} = \frac{3\sigma_h - \sigma_H + T'}{2} \qquad \text{Eq. 2-6}$$

Using Equation 2-6 and assuming an isotropic horizontal stress state and negligible tensile strength the fracture initiation pressure would be simplified to $P_{wf} = \sigma_h$. In some studies where a clear understanding of the well conditions is not available, fracture initiation is assumed to equal the minimum horizontal stress to mitigate the risk of failure.

Equations mentioned in this section are among the most accepted models for fracture gradient estimation. Once the fracture is initiated the fluid does not invade the formation immediately. In general, a higher pressure level is required in the well to push the fluid in the opening and lead to unstable fracture propagation and lost circulation. It has been observed in the past few decades that the pressure level at which the circulation loss initiates, varies with the properties of the drilling fluid. This has often been misinterpreted as an increased fracturing gradient. The maximum pressure that a well can contain before allowing fluid loss to a tensile fracture is called the Wellbore Pressure Containment (WPC) or the circulation loss pressure. This concept will be further investigated in the next section of this chapter.

Wellbore breakouts determine the minimum allowable pressure in the wellbore. In some cases, however, pore pressure is applied as the lower limit. Borehole breakouts are studies using caliper log data and other sources of information. Shear failure is the main mechanism governing the well breakout process. As the shear stress exceeds a certain limit, the rock planes cannot withstand the stress and slide on one another. In terms of modeling, Mohr – Coulomb's criterion is the most widely used criteria for well collapse. It basically states that there exists a linear relation between the shear stress and normal stress at the failure. The slope of this relation is a

function of rock properties. Angle of internal friction and cohesion are the main rock properties which govern the shear failure based on Mohr Coulomb's criterion. The relation between the principal stresses at the failure is expressed by Equation 2-7.

$$\sigma'_1 = C_0 + \sigma'_3 \tan^2\beta \qquad \text{Eq. 2-7}$$

$$\beta = {}^{\pi}/_{4} + {}^{\varphi}/_{2} \qquad \text{Eq. 2-8}$$

Where σ'_1 is the maximum effective principal stress, C_o is the unconfined compressive strength of rock, σ'_3 is the minimum effective principal stress, β is the breakout angle and φ is the angle of internal friction. Figure 5 shows a schematic of a block at the moment of shear failure.

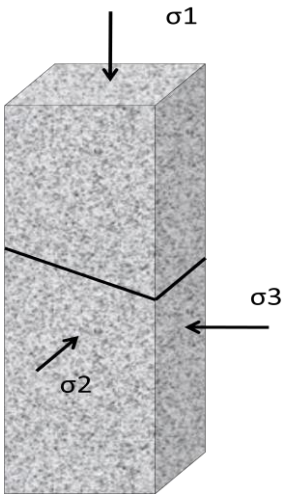

Figure 5: Stress state around a rock block at shear failure

There are several other criteria used to explain the shear failure. Dumans[36] presented a useful set of shear failure criteria that are applied in wellbore stability analyses. One of shortcomings of Mohr – Coulomb's criterion lies within neglecting the intermediate stress. Equation 2-9 presents a generalized version of Mohr-Coulomb's criteria and accounts for all stresses.

$$\sqrt{J_{2D}} = \tau_0 + m^* \sigma_{oct} \qquad \text{Eq. 2-9}$$

where τ_0 and m^* are parameters related to the shear strength of the rock, σ_{oct} is the normal effective octahedral stress which is estimated using Equation 2-10 and J_{2D} is the second invariant of the deviatoric effective stress tensor which is found by Equation 2-11.

$$\sigma_{oct} = \frac{\sigma'_1 + \sigma'_2 + \sigma'_3}{3} \qquad \text{Eq. 2-10}$$

$$J_{2D} = \frac{1}{6}[(\sigma'_1 - \sigma'_2)^2 + (\sigma'_3 - \sigma'_2)^2 + (\sigma'_1 - \sigma'_3)^2] \qquad \text{Eq. 2-11}$$

m^* and τ_0 are estimated as functions of angle of internal friction by Equations 12 and 13.

$$m^* = \frac{6sin\varphi}{\sqrt{3}(3 - sin\varphi)}$$ Eq. 2-12

$$\tau_0 = \left[\frac{2c\ cos\varphi\left(3 - m^*\sqrt{3}\right)}{3\sqrt{3}(1 - sin\varphi)}\right]$$ Eq. 2-13

Shear failure and wellbore breakout analysis can be more complicated in some cases. Specifically when an extended reach well has been planned, operators have to continue drilling with a certain extent of formation collapse. Some studies have referred to the tolerable breakout level in the well as the operational failure as opposed to the rock mechanical failure[37].

2.2. Wellbore strengthening

Fracturing gradient is one of the most critical parameters that govern the stability of the wellbore, circulation loss, drilling rate and therefore plays a key role in well planning. In addition, severe cost and environmental consequences of circulation loss as a result of fracturing highlights the significance of a clear understanding of formation fracturing gradient. The pressure level at which the drilling fluid enters the formation fractures may rise above the fracture gradient. This incremental pressure level shows a strong dependency on drilling fluid properties in addition to the factors which govern the fracturing process[7,9,11,12,13,14,15,16,17,18,19,20,21,22,23,24,25]. These factors include in-situ stress state, pore pressure variations, borehole diameter, mechanical properties of the rock, borehole deviation, intensity and geometry of natural fractures and fissures, formation permeability, formation porosity, wellbore temperature, downhole pressure, injection rate, presence of notches, state of compaction, pore water chemistry, time of exposure, and drilling vibrations.

The process of increasing the Wellbore Pressure Containment (WPC) using engineered drilling fluids is called “wellbore strengthening”. The fact that the maximum allowable pressure in the well can be increased by proper mud design comes with remarkable advantages for the operators. More efficient well control, better hole cleaning, less wellbore breakouts as well as lower overall costs, Non-Productive Time (NPT) and environmental footprint, can all encourage well planners to pursue the application of mud engineering in wellbore strengthening. Although the effect of drilling fluid has been widely appreciated, the exact mechanism of wellbore strengthening is not fully described in the literature. Various explanations provided by drilling operators are mostly qualitative and unverified. Therefore, there exists a great deal of uncertainty about the described mechanisms. In addition, the models and mechanism presented in the literature do not provide a tool for engineering of wellbore strengthening operations.

In the next section, a brief review of the previous studies on wellbores strengthening is presented. Despite the early detection of mud impacts on the circulation loss gradient (Wellbore Pressure Containment), the concept had been barely studied until the last two decades.

2.2.1. Literature review

There exist many studies in the literature which have investigated wellbore strengthening in detail and have shed some light on the mechanics of the phenomenon and the contributing factors. As pointed out previously, when fracture opens up in the formation, drilling fluid particles may be able to bridge the fracture opening and prevent the fluid from flowing into the formation. The upper limit for the Wellbore Pressure Containment (WPC) is defined by the strength of the bridge. Understanding the mechanism of bridge formation and collapse over the fractures and other openings can lay the foundation of modeling of wellbore strengthening. Dominant factors need to be considered in the model to predict their effects on Wellbore Pressure Containment (WPC). In most previous studies, the effects of the size distribution, type and concentration of the particles have been emphasized. Therefore the literature related to each factor and the strengthening mechanism is presented in the following sections.

2.1.1.1. Wellbore strengthening mechanism

DEA-13 was one of the first research projects completed to investigate the mechanism of wellbore strengthening and the influential parameters[13,14]. Fluids with different bases and concentrations of particles were applied in core fracturing tests and fluid loss pressure measurements. Water-based and oil-based drilling fluids were found to initiate fractures at similar pressure levels, however reopening pressure was higher when water-based fluids were used. In addition, they concluded that water-based fluids had a remarkable fracture healing capability which increased the Wellbore Pressure Containment (WPC). This important property was explained by filtration characteristics of water-based fluids which allow deposition of filter cake. They suggested a process called tip screen-out as the governing mechanism of wellbore strengthening. Based on this mechanism, particles form a filter cake inside the fracture so the wellbore pressure is not transferred to the fracture tip and the fracture tip is "screened out". They also recommended the application of sized particles called Loss Prevention Materials (LPM) in drilling fluids to prevent circulation loss. The tip screen out mechanism has been schematically illustrated in Figure 6.

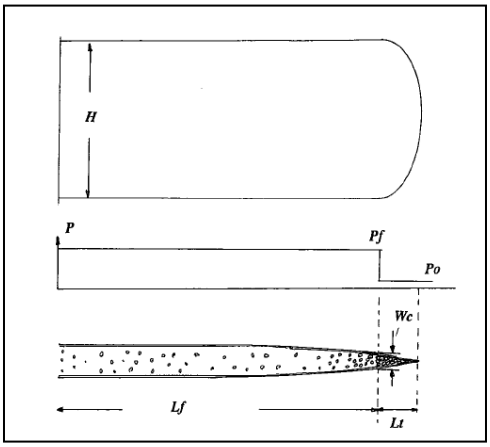

Figure 6: LPM screen-out at fracture tip[14]

Filter cake build-up over the fracture planes may be the case when dealing with widely open natural fractures. In the case of tensile ruptures, the small width of the fractures at the moment of initiation does not allow large particles to pass through. This might be one of the main shortcomings of this description of the strengthening mechanism for tensile fractures. Another phenomenon which was explained in DEA-13 was the occurrence of saw tooth peak shapes in pressure trend during fracture propagation using water-based muds. They believed that water-based fluids screen out the fracture tip after each step of fracture propagation and heal the fracture to some extent. Therefore a higher pressure level is necessary in the fracture to continue to propagate. They stated that low permeability formations exhibit more unstable fracture propagation since lower filter cake deposition occurs. Some other studies related internal filter cake to increased rock strength[38]. Another major study dedicated to wellbore strengthening was a university – industry collaborative research project known as GPRI 2000[18]. This study was mainly focusing on estimation of fracture reopening pressure. Reopening pressure is directly related to the impaired conductivity of the fractures. They concluded that plugging governs the wellbore strengthening process for the most part and Wellbore Pressure Containment (WPC) does not necessarily depend on the filtration process. A split sample used in GPRI 2000 is shown in Figure 7. Goud and Joseph[21] also believed that plugging the fractures occurs by large particles.

Figure 7: A split core sample during GPRI 2000 tests[9]

A series of field and laboratory experiments and observations led to description of another mechanism for wellbore strengthening called stress caging. Stress caging describes the strengthening mechanism based on the assumption that fractures initiate at pre-determined pressure levels. Then, particles in the fluids prop the fractures and thus increase the tangential (hoop) stress around the boreholes based on the increased tangential (hoop) strain, leading to higher fracture gradients around the wellbore. The mechanism has been schematically shown in Figure 8. In some studies the wellbore strengthening term is applied exclusively to refer to the stress caging theory. In this research, we use this term in a generalized manner describing all methodologies which lead to increased Wellbore Pressure Containment (WPC).

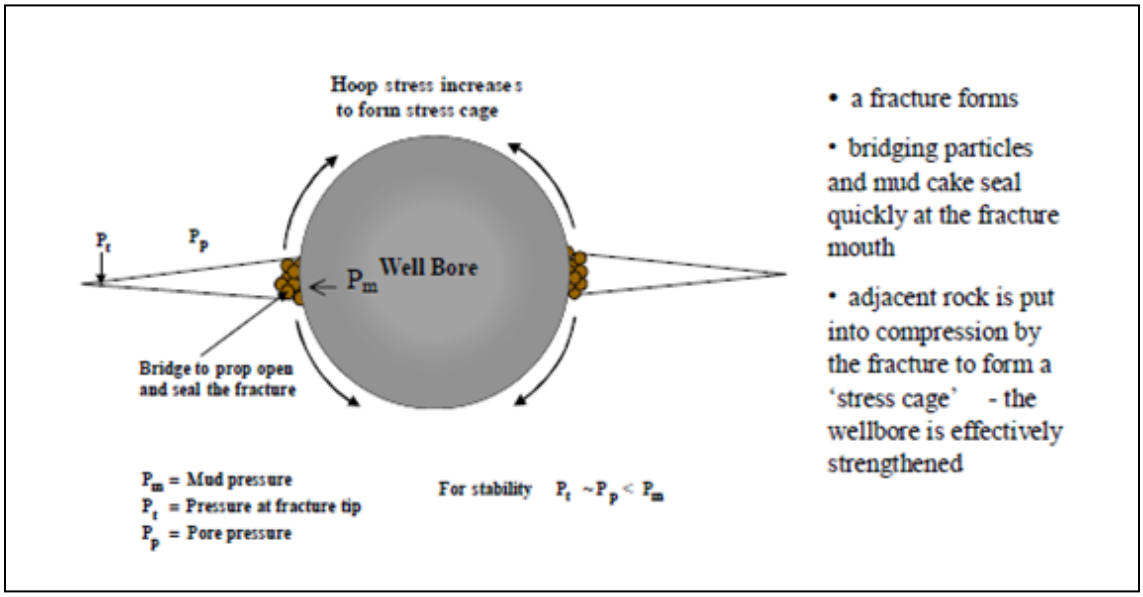

Figure 8: Stress cage concept to enhance wellbore strength[24]

This theory has been widely studied in the past decade[9,12,19,23,24,39,40,41,42,43,44,45,46,47,48,49]. However, there are some skeptics about the mechanical foundations of the phenomenon. Some also believe that the stress caging mechanism is not dominant in the case of unconsolidated sand formations[20].

The University of Stavanger started investigating the drilling fluid based wellbore strengthening in the last decade by conducting numerous core fracturing tests[50,51,52]. Based on their test results and interpretation, they concluded that as the fracture initiates a quick filtration occurs over the rupture and the particles form a bridge over the opening. They suggested that the bridge failure followed a Mohr – Coulomb failure criterion and thus varied with the compressive strength and angle of internal friction of the particles. They developed an elasto-plastic model based on elastic and plastic deformation of the filter cake over the fracture. The mechanism they described is illustrated in Figure 9. This study was amongst the few which correlated the wellbore strengthening capabilities of the drilling fluids to the mechanical properties of the suspended solids.

Event	Fig.	Main Controlling Parameters
Filter-cake formation	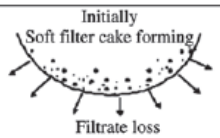	Filtrate loss
Fracture initiation	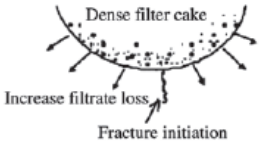	Filtrate loss, stress
Fracture growth	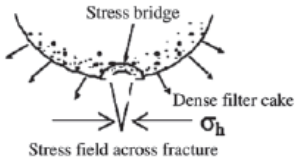	Bridge stress, rock stress
Further fracture growth	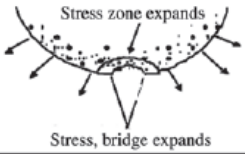	Bridge/rock stress, particle strength
Filter-cake collapse	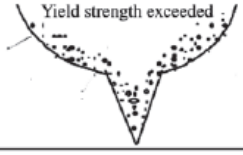	Particle strength

Figure 9: Qualitative description of fracturing process[50]

Messenger[1] explained a plugging sealing mechanism for fractures up to ¼ inch wide. He concluded that fractures were plugged and then sealed over the plugging particles and failure of the bridge would occur if the plug breaks through or gets "scraped off" the fracture mouth. White[17] stated that the sealing mechanism in high matrix permeability fluid losses was different to that of circulation losses through fractures. Howard[11] believed that sealing occurred at the entrance of the openings. Nayberg[7] concluded that forming the seal inside the formation is more desirable since it does not break down by pipe movement or erode off. Based on the review of the literature, internal filter cake seems to be seen as the cause of strengthening in most cases.

2.1.1.2. Particle type

In most previous studies, the particle type has been concluded to be the most significant factor in wellbore strengthening. There are several particles which have been widely investigated and applied such as Calcium Carbonate and Resilient Graphite. However, there are only a few researches in which the influential particle properties have been detected and introduced. The optimum particle is expected to seal large openings with small amounts of filtrate[17], so that the fracture pressure remains below the fracture propagation pressure. Resilient Graphite was found in the experimental and field tests to be the most effective drilling fluid additive due to its compressive strength and resiliency in increasing fracture reopening pressure and stress caging while $CaCO_3$ particles have not exhibited a good sealing performance despite their wide applications[18,21,22,24]. A mixture of graphite and $CaCO_3$ showed acceptable efficiency in fracture reopening tests as well as the field[18,21,22,23]. Goud and Joseph[21] showed that resilience of graphite particles is five times larger than that of $CaCO_3$. Based on their theory, plugging particles may slip out of the fracture as a result of fracture width reduction as pumps are shut down and the fracture pressure declines; therefore more resilient particles are capable of deforming and keeping the fracture sealed. Using the Mohr – Coulomb failure criterion and elasto – plastic model, Aadnoy *et al.*[50,51,52] found the compressive strength and internal friction angle of the particles to be effective. They were one of the pioneers in correlating the particle properties of additives to the wellbore strengthening capability of the drilling fluid. They suggested that Mohs scale of hardness as presented in Table 1 may be applied for evaluation of strengthening capabilities of materials as they are mixed in the fluid. Catalin *et al.*[15] stated that high compressive strength may be detrimental to the sealing efficiency because it does not allow the

particles to reach the fracture tip. Instead, they highlighted the positive effect of shear strength of the plug.

Table 1: Mohs scale of hardness for some materials[25]

Scale	Mineral	Test
1	Talc	Softest
2	Gypsum	
2.5		Fingernail
3	Calcite	Copper coin
4	Flourite	
5	Apatite	
5.5-6		Knife blade
6	Orthoclase	
6.5-7		Steel file
7	Quartz	
8	Topaz	
9	Corundum	
10	Diamond	Hardest

2.1.1.3. Particle size distribution and shape

The importance of wide particle size distributions has been emphasized in almost all published studies in the area of wellbore strengthening, but an optimum particle size distribution has been rarely defined for Lost Circulation Materials (LCM)[7]. Catalin *et al.*[15], Aston *et al.*[24] and Whitfill[23] stated that 90% of particles must be smaller than the opening size to enter the fracture and seal it off. In order to handle the uncertainty in fracture geometry estimation it was recommended to tune the particle size distribution to have a D_{50} equal to the fracture opening[19,23.] They found the ideal packing theory to be useful to determine the particle size distribution of the added Lost Circulation Materials (LCM). They also emphasized the importance of having large particles in the mixture as well as very fine ones. The significance of properly sized particles in the fluid is illustrated in Figures 10 and 11. In another work, granular particles with angular shapes in the range of 150 µm to 4.75 mm were mentioned to be effective in sealing fractures.

The maximum size of particles to be mixed in the fluid is strongly dependent on the fracture size. Fractures up to the size of ¼ inch and openings of up to 1 inch large in gravels may be sealed off by Lost Circulation Materials (LCM)[1,17]. The maximum size of the fracture to be sealed depends on the maximum particle size and concentration while the impact of maximum particle size is dominant. Some studies stated that when the opening is more than three times larger than the size of the largest particle in the fluid, sealing is unlikely to happen[17] and the upper limit for the particle size is the pumping capacity. Particles close to the fracture size are necessary in the LCM mixture to plug the fracture[1] and blends of coarse and fine materials were found to reach improved results[17]. Three main shape categories of particles were defined: granules, flakes and fibers. Some studies recommended fibers when dealing with high matrix permeability to tie the granules and flakes to the formation but their effectiveness in fractures seems to be limited to fractures smaller than 0.125 inch[17]. In GPRI 2000, fibers were concluded to be effective in the field but not in the laboratory. They showed more efficiency when added in small amounts[18]. Efficiency of fibers was found to be mostly a function of size rather than type[7]. Mixtures of granules, flakes and fibers were stated to be more efficient than each of them alone[1,17]. In some experimental studies, granules were found to be the most effective particles[11]. It was concluded by Nayberg[7] that granules may sometimes lead to channeling due to low concentration. White[17] stated that granules and flaky particles do not mix well unless fibers are present in the mixture.

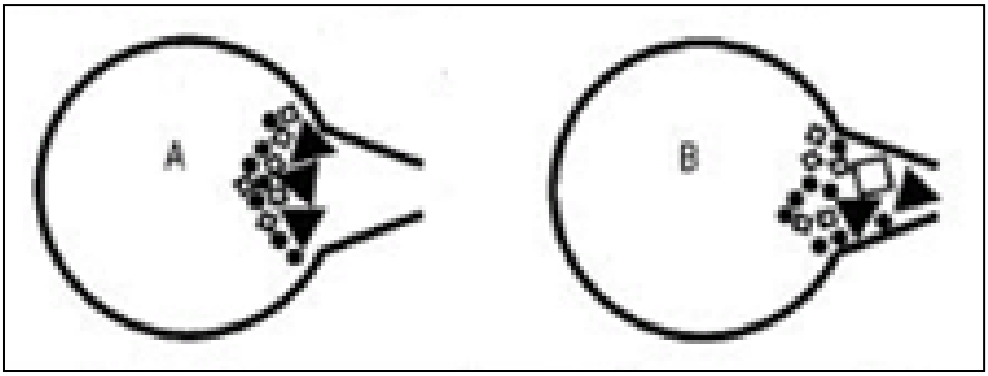

Figure 10: A: Results using very large LCMs - builds on the wellbore and erodes away; B: proper bridging[21]

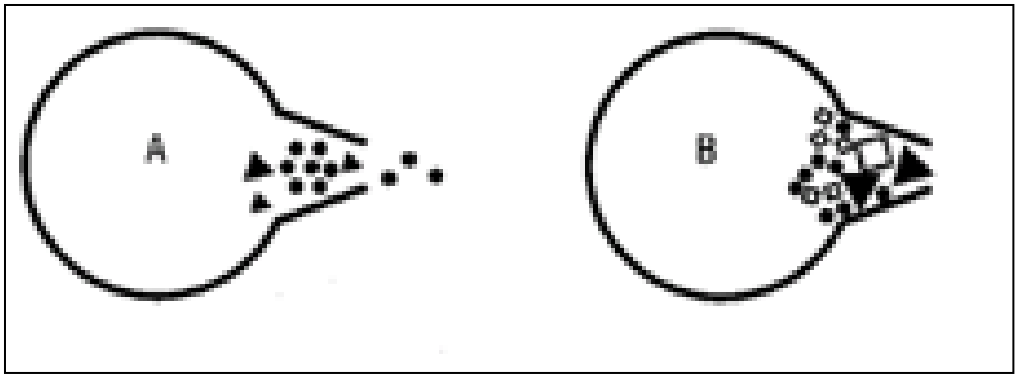

Figure 11: A: Results using very fine LCMs - goes through opening and does not form a bridge; B: proper bridging[21]

CHAPTER THREE: EXPERIMENTAL ANALYSIS OF WELLBORE STRENGTHENING

3.1. Introduction

In this chapter, procedures and results of the experimental part of this research are presented and discussed. This phase was completed in the drilling fluid and wellbore strengthening laboratories of the University of Stavanger in Norway. The main objective of this part of the research was to obtain a solid understanding of the governing strengthening mechanism and detecting the influential parameters. One of the main shortcomings of the previous researches in this area lies within the unclear strengthening mechanisms. Besides, the effective parameters were described qualitatively and did not provide strong tools for engineers to design their practices. The generated data in this stage of the research fed the modeling process leading to a reliable strengthening model which is one the most significant outcomes of this study. The experimental plan was pursued in two main parts: particle plugging and core fracturing tests, which are explained in the following sections in more detail.

3.2. Particle plugging system

Particle plugging testing systems have been applied widely in the drilling fluid industry. The apparatus consists of a steel cylinder of known diameter and height which is connected to atmospheric pressure from the bottom through an opening of known width. In most particle plugging systems of this type the opening size may be altered. The cell is filled with the drilling fluid and water is pumped from the top to force the drilling fluid to flow through the opening at the bottom of the vessel. The pressure inside the vessel is recorded by the water pump. Figure 12 shows the schematic of the experimental setup. As the fluid flows through the fracture, particles form a sealing barrier and prevent the loss of more fluid. Once the pressure in the vessel elevates sufficiently, the barrier collapses and the fluid flow continues. The sequence of forming and breaking the barrier continues until all the drilling fluid exits the vessel. The fracture sizes at the bottom of the vessel may be varied and manipulated with respect to particle size distribution and

the average particle size in the fluid to evaluate the strengthening capability of a certain drilling fluid. This experimental setup was fabricated and applied at the University of Stavanger and was believed to simulate the fractures in horizontal wellbores[53]. However, due to the lack of dynamicity in the fluid during the experiments and simplified geometry of the fracture, the particle plugging tests does not allow for an accurate simulation of the well conditions. The main objective of using this setup in this work was to closely investigate the strengthening mechanism. The system functions in a simple manner and allows multiple tests and changes. Each test takes around thirty minutes and generates a significant amount of data. The system in general consists of three main parts: pump, vessel and fracture openings which are described in the following sections.

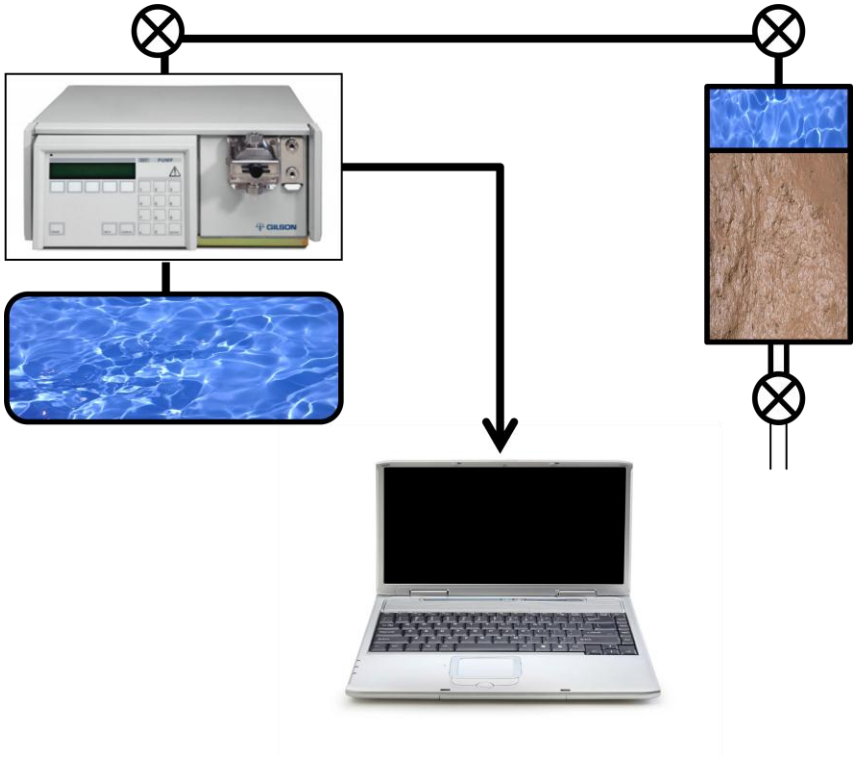

Figure 12: Schematic illustration of the particle plugging test setup

3.2.1. Pump

The pump used was a Gilson pump of the type 307 HPLC. It was possible to change the injection rate within the range of 0.05 ml/min (8.33×10^{-10} m^3/s) to 10 ml/min (1.6×10^{-7} m^3/s). However the injection rate was kept constant at 4 ml/min (6.7×10^{-8} m^3/s) in all tests. The pump was capable of functioning up to 600 bar (60 MPa).

3.2.2. Vessel

The vessel was a steel hollow cylinder used as the mud container. It was connected to the pump from the top and to the atmospheric pressure through the fractures and a valve from the bottom. It was possible to disassemble to vessel and all joints were sealed completely after assembling to avoid leakage. The outer diameter of the vessel was 64 mm, the inner diameter was 35 mm and it was 150 mm long.

3.2.3. Fractures

The fractures consisted of two steel half cylinders which formed an opening of a known size when connected. Figure 13 shows the picture of one of the fractures. It is possible to fabricate fractures of desired size or shape. Therefore an extensive experimental plan was designed and implemented using the particle plugging system.

3.2.4. Test procedure

Each experiment starts with preparation of the drilling fluid. Then the desired fracture is selected and the system is assembled. The bottom valve is closed and the vessel is filled with the drilling fluid. Then the lid is put in place and the water injection initiates. When water starts overflowing, the top valve is closed and the bottom valve is opened. From this point water is injected in a pre-determined rate. The pump pressure is recorded in a known frequency and the experiment

completes when all the drilling fluid passes through the fracture or the pump pressure reaches its maximum allowable level. In our tests, we used 3.5×10^{-4} m^3 of drilling fluid and each test took almost 30 minutes. The data recording frequency was 0.17 Hz (once per six seconds).

Figure 13: Fabricated steel fractures[53]

3.3. Core fracturing system

University of Stavanger owns a well-equipped core fracturing facility. A core fracturing experiment basically includes the circulation of a drilling fluid in a hollow concrete core followed by isolation of the hole and injection of more drilling fluid until the fracture initiates and propagates. The experiment is very similar to the normal hollow cylinder tests with the added feature of circulation. It is also similar to the well-known leak off tests performed in the field to estimate the fracture gradient and minimum horizontal stress. Circulation of the fluid allows for deposition of the filter cake prior to initiation of the fracture. The core fracturing setup is shown in Figure 14.

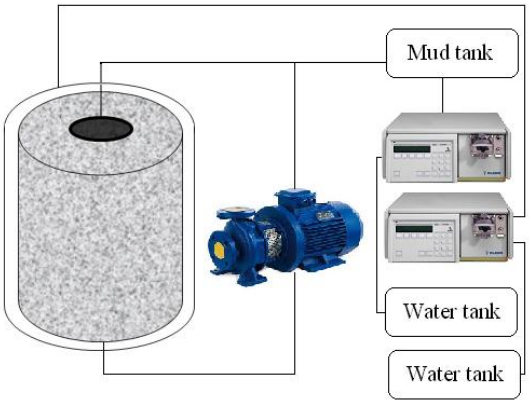

Figure 14: Schematic illustration of core fracturing system

3.3.1. Description of cores

The concrete cores used in the core fracturing system were produced in the material laboratory at the University of Stavanger for use in previous studies[53]. They tested several different ingredients and compositions. The final composition of the concrete core specimen is presented in Table 2. Physical and mechanical properties of the core specimens were estimated by Drangeid[53] as presented in Table 3. The applied cores were 20 cm long and 10 cm wide. The well in the center was circular with a diameter of 1 cm.

Table 2: Composition of the core specimen

Ingredient	**Mass**
Durasplit 0-2 mm (stone)	25.000 kg
Norcem industry cement	5.800 kg
Water	3.425 kg
HP-SF dispersing agent	0.115 kg

Table 3: Mechanical properties of the cores[53]

Property	Value
Tensile strength	84.1 bar (8.41 MPa)
Compressive strength	364.3 bar (36.43 MPa)
Permeability	20 μD
Porosity	22%
Density of dry specimen	2116 kg/m^3
Density of water saturated specimen	2299 kg/m^3

3.3.1. Test procedure

Before starting the experiment, the core needs to be placed in the steel jacket which provides the confining pressure. The jacket's diameter is almost 11 cm and the space between the jacket's wall and the core is filled with water. The pump pressure is recorded as the jacket is filled and is fixed at 4.5 MPa. An axial load is also exerted on the core to represent the overburden pressure. The system is then manually filled with the drilling fluid and a centrifugal pump is used to circulate the mud in the well. The circulation continues for eight minutes to build up a filter cake. The well is then isolated and more drilling fluid is injected while the pressure is being recorded and plotted. There are several parameters that can be studied in the core fracturing tests such as fluid properties, flow rate, well geometry and confining pressure. In this work only the fluid properties were the only topic of interest. Belayneh[53] studied the wellbore geometry using the same facility.

3.4. Experimental phase I

The experimental phase started with a series of preliminary tests using the particle plugging and the fracture reopening systems. Objectives, fluid design, and results of these series of tests are discussed in this section.

3.4.1. Objectives

Experimental phase I was planned and implemented to achieve the necessary training to operate the experimental systems, obtain sufficient information for fluid design for the main series of experiments, shed some light on the mechanism and initiate the modeling process. These objectives are briefly explained below.

a) *Lab training*: One of the main objectives of this part was to learn the operational procedures for the lab facilities and investigate possible modifications. Each system had its own limitations and constraints which needed to be considered prior to planning for the main series of experiments. The available spare parts for each system were also revisited and the necessary components were provided to avoid any time-consuming breakdown of the system during the experimental period. For instance, steel fractures of the particle plugging system were measured to mitigate uncertainties about the fracture opening size and some new slots were fabricated to enhance the generality of the results.
b) *Fluid design*: The drilling fluid which is applied in the particles plugging apparatus needs to be viscous enough to keep the particles in suspension as no circulation occurs during the experiment. Therefore an optimum procedure for preparation of the base mud was found during the first experimental stage. The core fracturing system, on the other hand, is capable of circulating the fluids which are less viscous than a certain limit. Therefore, thinners were essential in designing the fluids for the fracturing tests.
c) *Investigation of mechanism*: Analyzing the data generated during the preliminary tests, a few mechanisms were proposed to be further studied during the experimental phase. This data analysis clarified the plug forming principles and assisted in planning for the main series of tests. Possible governing mechanisms and influential parameters were selected, based on which the main experiments were designed.
d) *Initiation of modeling*: The modeling process was started based on statistical analyses and learning gained studying the physics of the process.

3.4.2. Particle plugging experiments in phase I

These series of particle plugging experiments were designed and implemented using a mixture of three types of LCMs. Barite was also present in the mixture and contributed to the plugging and sealing process. Each test was performed three times and the results were averaged to increase the confidence level of the outcomes. Descriptions of the drilling fluid and particles as well as the results of these series of tests are presented in this section.

3.4.2.1. Drilling fluid

The designed drilling fluid for the particle plugging tests contained water barite, Bentonite, and three types of LCMs. The applied LCMs included Mica flakes, Resilient Graphite and Solu-Flake. These particles are widely used in the industry to control fluid loss. Properties of the Resilient Graphite and Solu-Flake are presented in Table 4. Resilient Graphite has shown promising outcomes in the past as mentioned before. Calcium Carbonate forms more than 97% of Solu-Flake and the rest is Silica, crystalline and Quartz[54]. The base mud needed to contain sufficient Bentonite to provide keep the LCM in suspension. Various Bentonite contents were tried to test the settlement of particles. The final composition of the base mud is presented in Table 5.

Table 4: Properties of Resilient Graphite and Solu-Flake[54]

Particle	Resilient Graphite	Solu-Flake
Appearance	Powder	Fiber
Color	Grey	White
Physical state	Solid	Solid
pH	6.5 – 10.5 in 10% aqueous solutions	8.4 – 10.2 in 5% aqueous solutions
Melting point	> 5000 °F (>2760 °C)	Not available
Specific gravity	2.25	2.7
Decomposition temperature	> 482 °F (250 °C)	Not available
Bulk density	> 450 kg/m^3	Not available

Table 5: Drilling fluid formulation applied for the preliminary tests

Component	Mass	Density	Volume
Water	4000 gr	1 gr/m^3	4000 ml (4×10^{-3} m^3)
Bentonite	260 gr	2.6 gr/m^3	100 ml (1×10^{-4} m^3)
Mica	4.22 gr	1.602 gr/m^3	2.63 ml (2.63×10^{-6} m^3)
Resilient Graphite	9.04 gr	2.25 gr/m^3	4.02 ml (4.02×10^{-6} m^3)
Solu-Flake	4 gr	2.7 gr/m^3	1.48 ml (1.48×10^{-6} m^3)
Barite	4.06 gr	4.2 gr/m^3	0.97 ml (9.7×10^{-7} m^3)

3.4.2.2. Particle size distribution

For the preliminary tests, all particles were smaller than 1 mm in a smooth size distribution. The particle size distribution is presented in Figure 15. Barite and LCMs were used as the bridging particles.

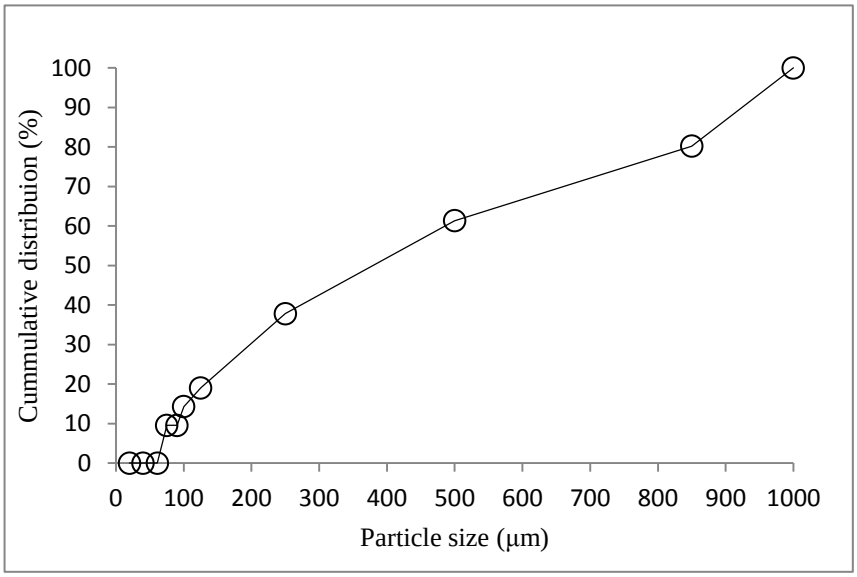

Figure 15: Particle size distribution of the bridging particles in the preliminary particle plugging tests (phase I)

3.4.2.3. Results and discussion

Particle plugging tests using the drilling fluid described above were completed using 10 sizes of slots. The slots were fabricated and measured prior to the experiments. The plugs formed through the slots smaller than 200 μm were resistant up to the maximum pump pressure, 60 MPa and therefore, it was not possible to record the maximum bridge resistance. In addition, no sealing barrier was formed in any of the tests when using the 1 mm slot. Therefore the analysis was performed based on the data set collected during the experiments using slots in the range of 300 μm to 900 μm.

Pressure records of the particle plugging tests using 400 μm, 500 μm, 600 μm, 700 μm 800 μm and 900 μm are illustrated in Figures 16-21. When water is injected in the cell fluid tends to flow out through the fracture. The particles accumulate and manage to seal the opening. This leads to an increase in the pump pressure as a result of a constant injection of water in the cell. When the pump pressure overcomes the resistance of the plug, the fluid breaks down the plug and exits the cell through the fracture. This flow results in the decrease of the pressure in the cell until another plug builds up at the opening.

Observation of the pressure recordings during the particle plugging tests indicates the higher capability of the drilling fluid to seal the smaller openings. As the opening size grows, zero values of pressure become more frequent and the pressure level decreases. Although these observations are helpful in the analysis it is difficult to go beyond the qualitative assessment of the fluid using the pressure recording plots.

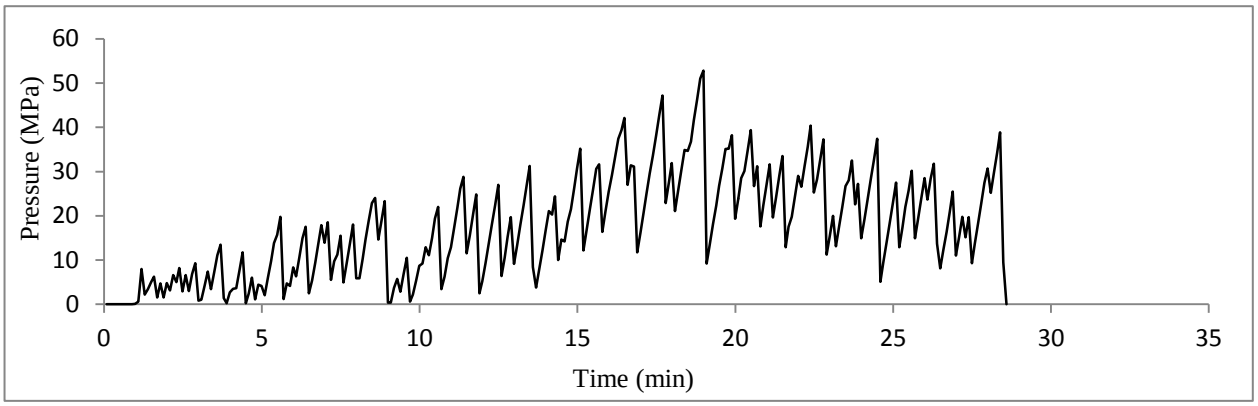

Figure 16: Pressure recording during particle plugging test using the 400 μm wide slot

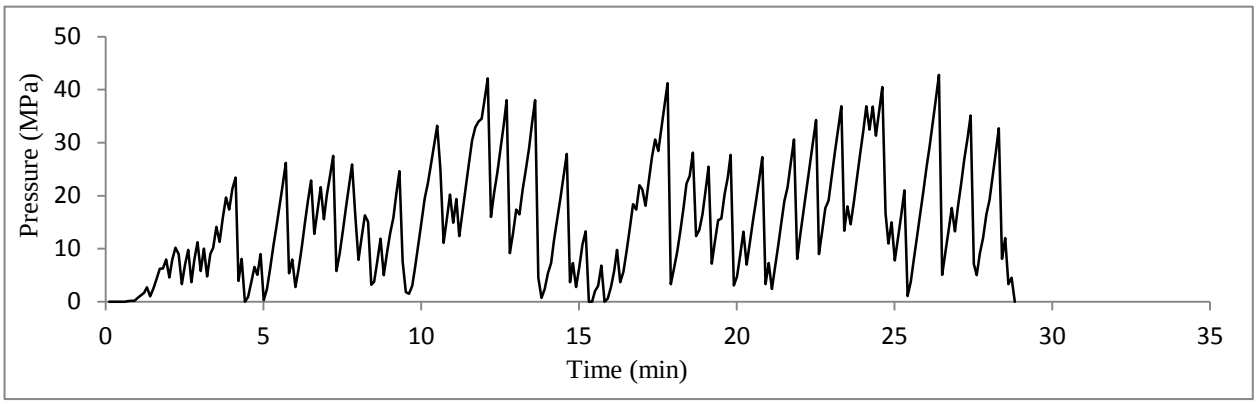

Figure 17: Pressure recording during particle plugging test using the 500 μm wide slot

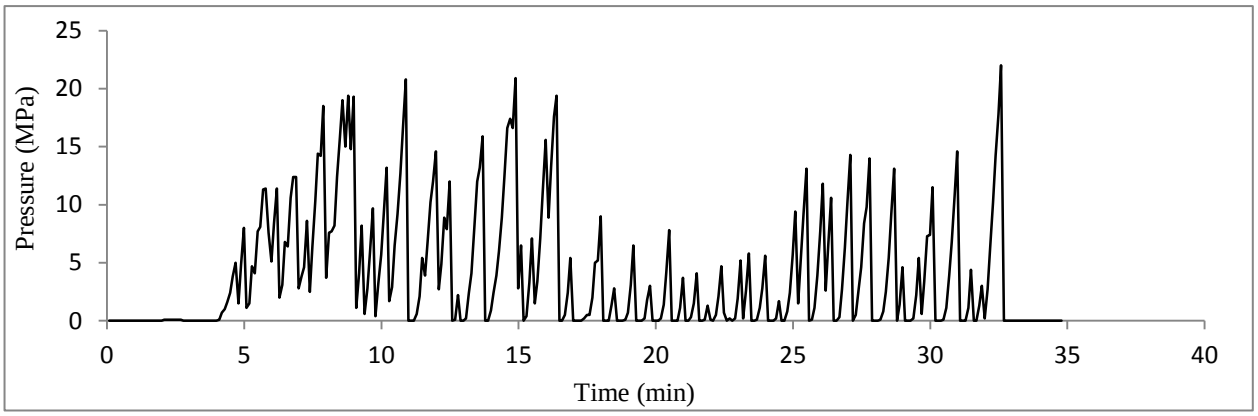

Figure 18: Pressure recording during particle plugging test using the 600 μm wide slot

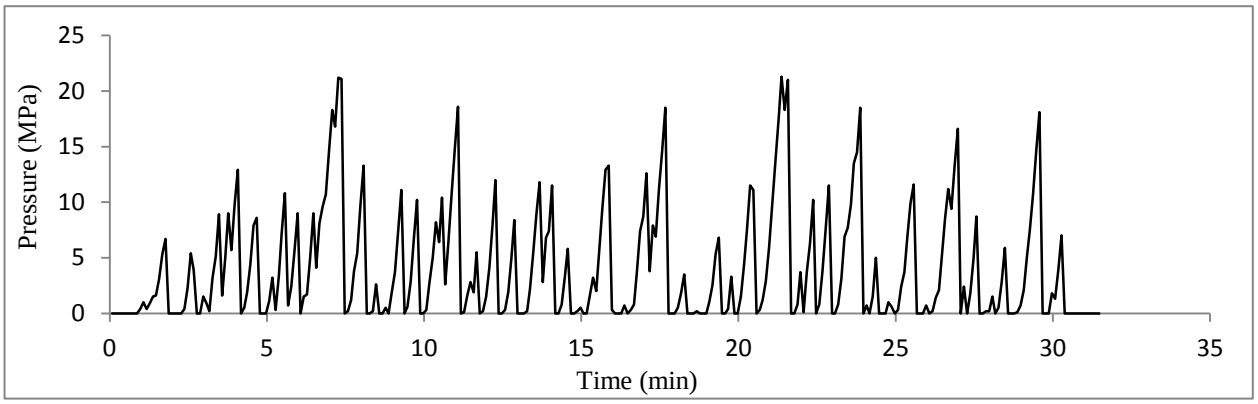

Figure 19: Pressure recording during particle plugging test using the 700 μm wide slot

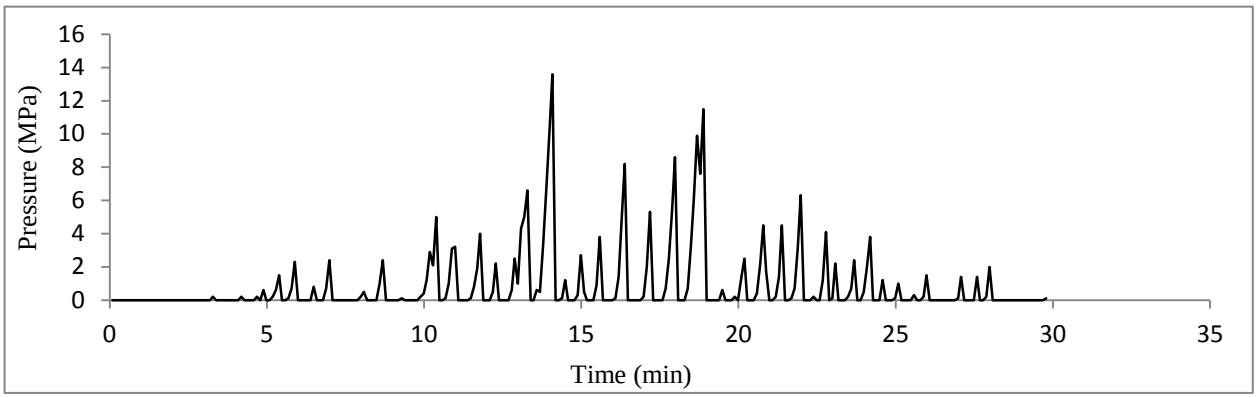

Figure 20: Pressure recording during particle plugging test using the 800 μm wide slot

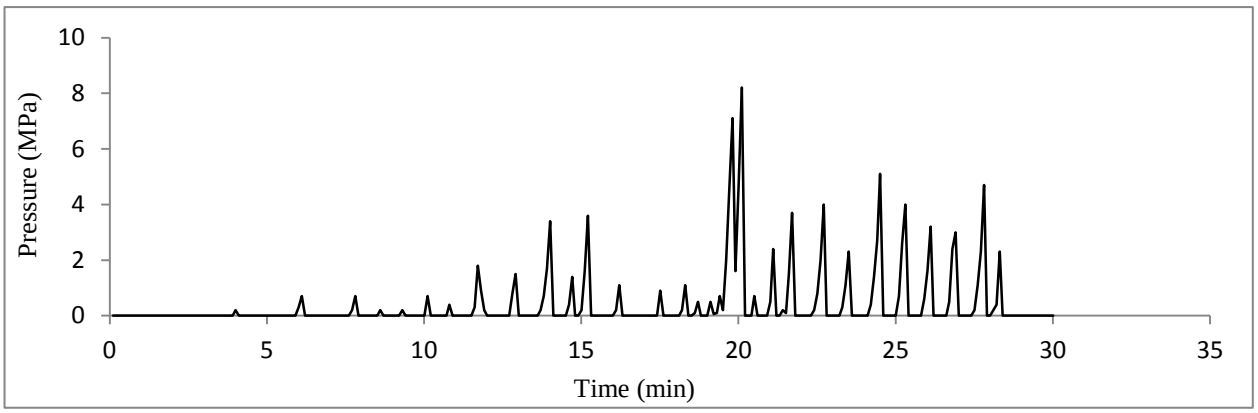

Figure 21: Pressure recording during particle plugging test using the 900 μm wide slot

Particle plugging tests have been applied in the industry to evaluate the capability of the particles to plug the fractures and inter-granular spaces for a very long time. This system of evaluation of LCMs has been used to see if the particles are strong enough to minimize the filtration to openings in the formations such as natural and induced fractures or highly permeable formations. Traditionally, application of this system has been mostly limited to industrial applications for designing lost circulation pills. In most of these experiments the amount of filtration has been the parameter of interest. In some cases, certain requirements were determined initially to evaluate the particles in a certain concentration and particle size distribution, such as the time required to form the bridge or a certain level of pressure that a plug should withstand before allowing fluid invasion through the slot. Although the traditional analysis methodology provides some insight about the strength of the sealing and capabilities of the fluid, insufficient data analysis has led to poor correlation between the lab results and the field tests. This is partly due to the qualitative essence of particle plugging data analysis. In the present work, the datasets provided by industrial and academic studies were closely reviewed to inspect and enhance the data analysis techniques. A new data analysis methodology was devised for particle plugging tests leading to more detailed investigation of the data and extracting richer knowledge on performance of the fluid. Eight new parameters were defined to evaluate the sealing potential of drilling fluids. These parameters provide quantitative information on the performance of particles in terms of particle plugging and resistance and are introduced in the following.

Total number of peaks (N): Each peak in the pressure plot shows the failure of a bridge formed during the test. Therefore the total number of the peaks represents the ability of the fluid to form a plug, regardless of its strength. Figure 22, shows the pressure recording during one of the preliminary tests using a 400 μm wide slot. The peak pressures have been shown in dots.

Average peak pressure ($P_{P\text{-}ave}$): The average peak pressure is the average strength of the plugs formed by the fluid. This parameter is one of the most important parameters obtained during the analysis of particle plugging test results. In our system it was possible to measure the pressure up to 60 MPa. This parameter was further applied in modeling of the process. The modeling part of this research will be discussed later. This value indicates the pressure differential through the opening.

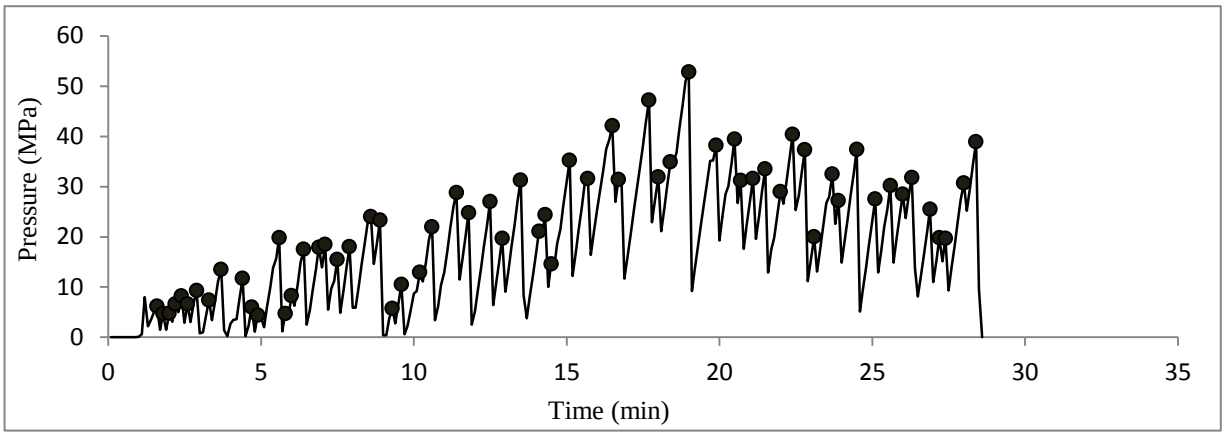

Figure 22: Peak pressure values in the pressure recording during the particle plugging test using a 400 μm wide slot

Total number of zeros (Z): Total number of zero values recorded during the test indicates the amount of filtration since the fluid is allowed to pass freely through the slot when the pump pressure is zero. Figure 23 illustrates the zero values in hollow dots. In this case filtration has occurred only at the beginning of the test.

Maximum pressure (P_{max}): The maximum pressure experienced during the course of an experiment is usually influenced by the distribution of the particles and degree of uniformity of the fluid. Therefore the results are usually scattered to some extent.

Number of peaks per minute (N/t): Time - averaged number of peaks can be used to compare results of the experiments of different time length.

Number of Zeros per minute (Z/t): Time – averaged number of zeros represents the average filtration per minute during a test and may be used for comparison of filtration between two tests of different time length.

Number of peaks per zeros (N/Z): As will be discussed later in the modeling section, this parameter provides valuable information regarding the strengthening capabilities of the fluid. It describes the inverse average amount of filtration occurring to form a plug.

Average pressure (P_{ave}): The average pressure in the cell may also be used for comparison of strengthening capabilities of fluids.

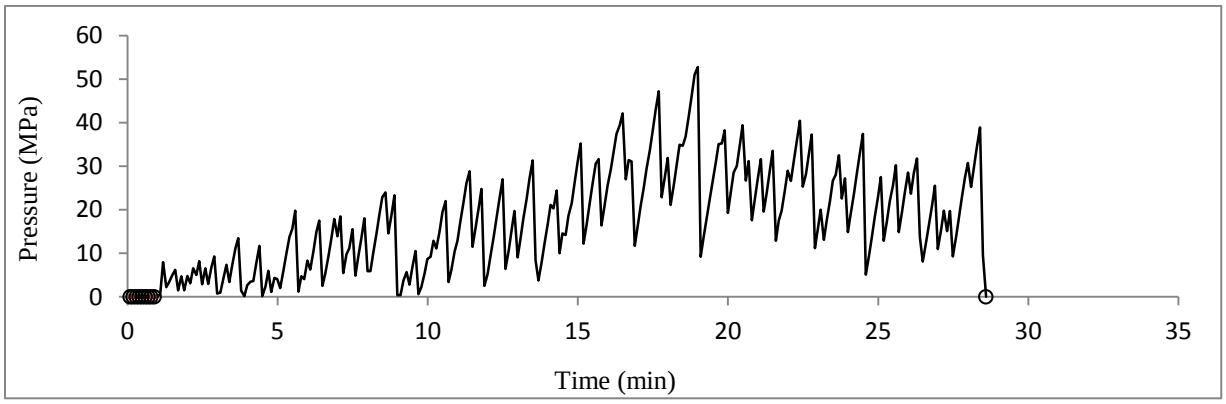

Figure 23: Zero pressure values in the pressure recording during the particle plugging test using a 400 μm wide slot

Based on the parameters described above, results of the preliminary tests are plotted in Figures 24 -31. Close analysis of the plots reveals valuable information about the sealing mechanism. Since the particle type, size distribution and concentration has been kept constant in these series of tests, the only variable against which the parameters are studied is the opening size. As the opening size grows, a smooth drop in the number of peaks is observed. The number of peaks describes the ability of the fluid in building a plug over the fracture, regardless of its strength. As the fracture becomes wider, more particles flow in the opening and the probability of forming a sufficiently resistant plug decreases. The average peak pressure is the most important parameter which provides information on the average strength of the sealing barrier formed by the particles and exhibits a steep drop as the fracture opening increases. The total number of zeros represents the cumulative filtrate volume since the zero pump pressure occurs when the fluid flows through the opening. This value rises for the most part for larger fractures as they allow more fluid flow. The maximum pressure decreases as the fracture size grows. The time average of zero values and peaks also increase and decrease respectively, versus the opening size, as expected. As the

fractures become wider, the average peak per zero decreases, indicating higher amount of filtrate required to build a plug.

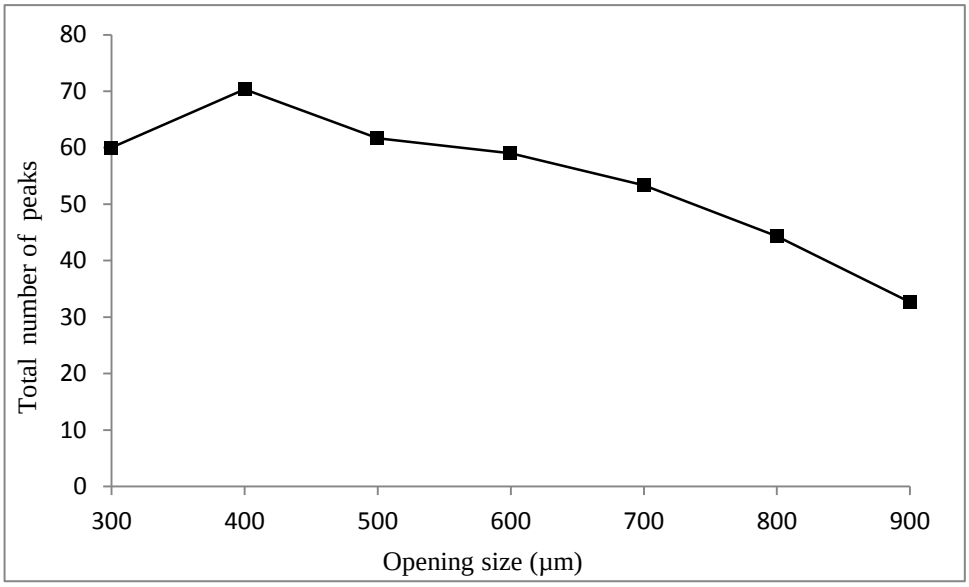

Figure 24: Total number of peaks during the preliminary tests versus the opening size

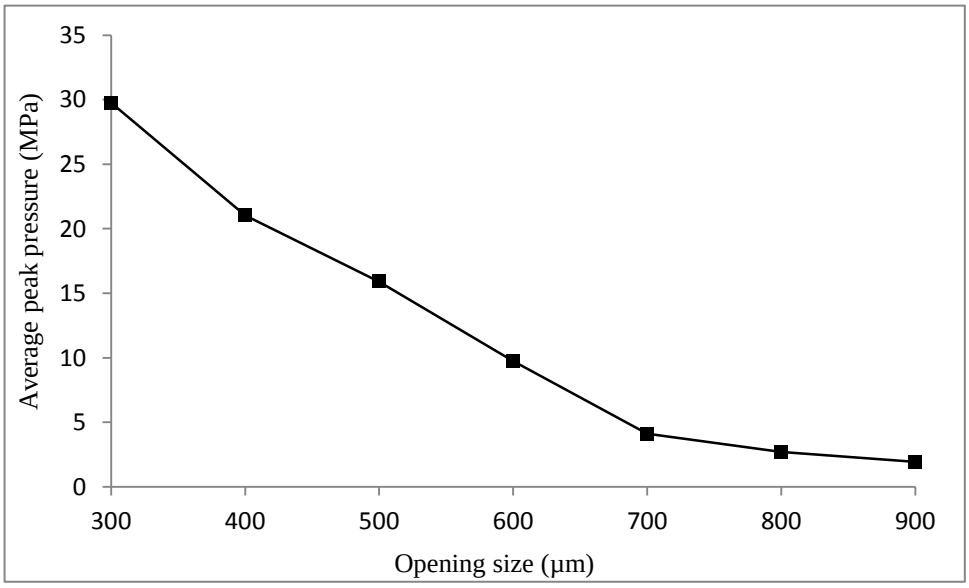

Figure 25: Average peak pressure during the preliminary tests versus the opening size

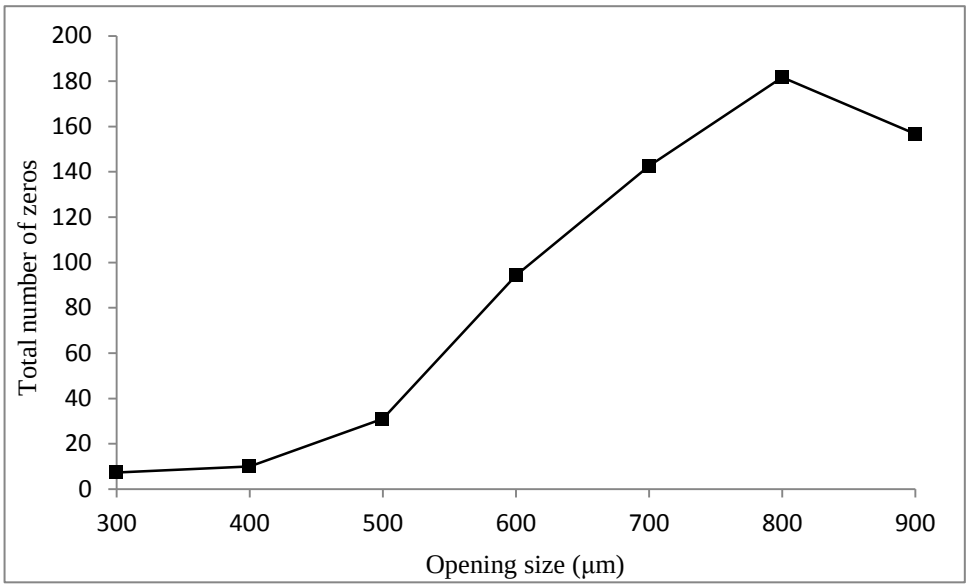

Figure 26: Total number of zeros during the preliminary tests versus the opening size

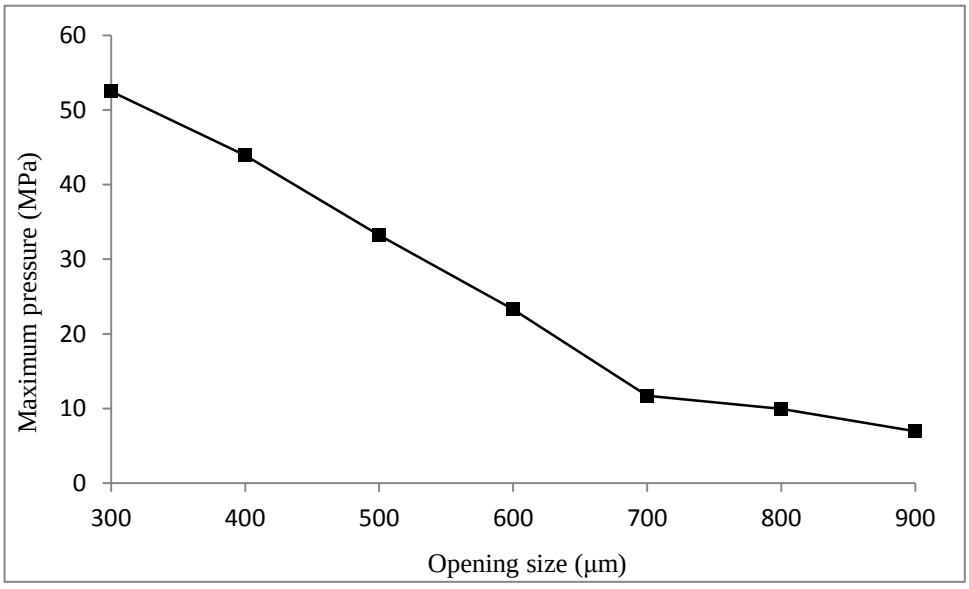

Figure 27: Maximum pressure during the preliminary tests versus the opening size

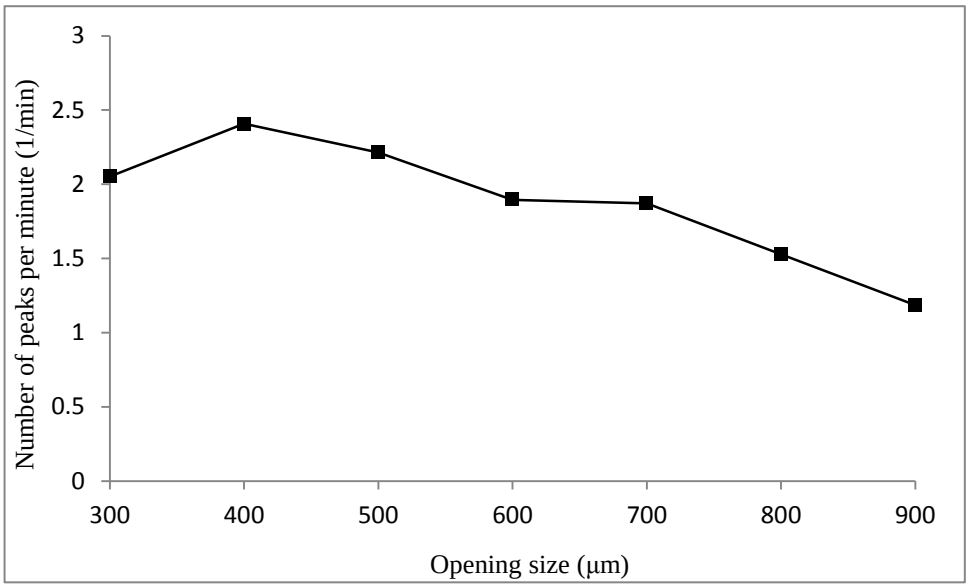

Figure 28: Number of peaks per minute during the preliminary tests versus the opening size

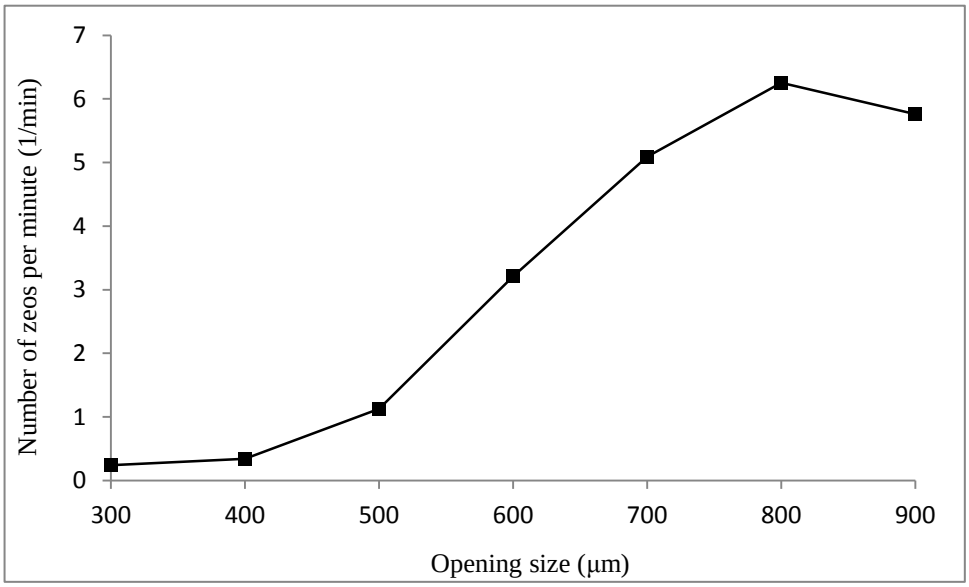

Figure 29: Number of zeros per minute during the preliminary tests versus the opening size

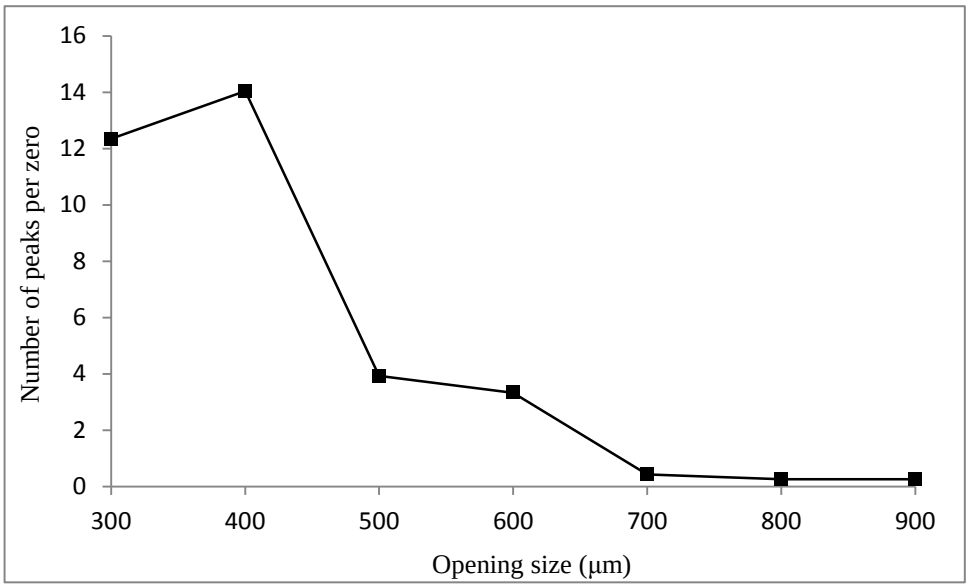

Figure 30: Number of peaks per zero during the preliminary tests versus the opening size

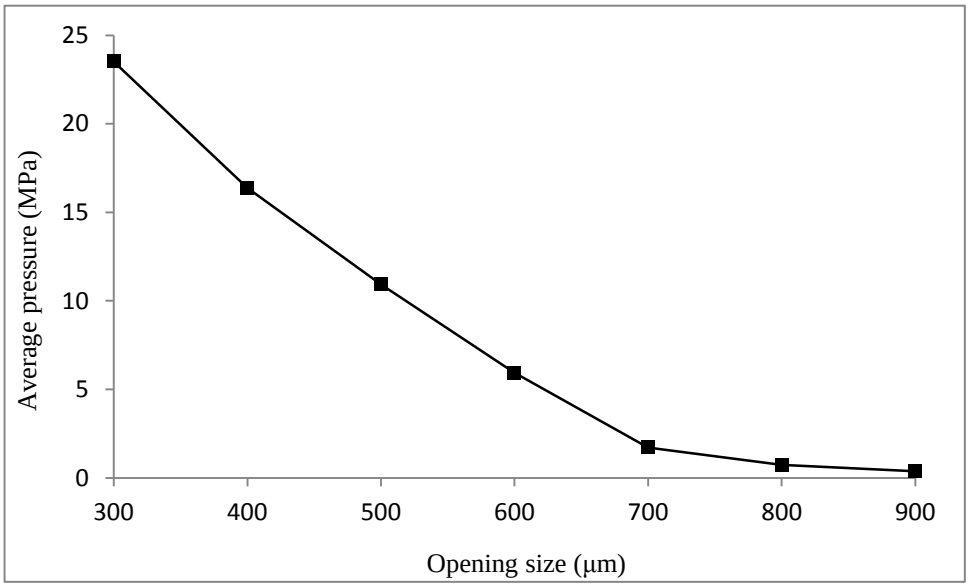

Figure 31: Average pressure during the preliminary tests versus the opening size

3.4.3. Core fracture reopening experiments in phase I

In these series of tests, several drilling fluids using the available LCMs were prepared in a constant concentration and particle size distribution to study the effect of particle type in the

fracture reopening pressure. The fracture reopening tests were performed using concrete cores that were previously fractured and tested. The cores were first washed and saturated with water. Particle size distribution and concentration of the particles were kept constant for all tests of these series.

3.4.3.1. Drilling fluid

Composition of the applied drilling fluid is presented in Table 6. As mentioned before, this composition was kept constant during the whole series of reopening tests and the results were analyzed versus the LCM type only. The total solid content of the fluid was 13% by mass. The size distribution of the particles was the same for all LCMs in the whole series of experiments and is presented in Table 7.

Table 6: Composition of the drilling fluid used in the fracture reopening tests

Component	**Mass**
Water	803.7 gr
Bentonite	32.1 gr
Low viscosity CMC	16.1 gr
Lignite	16.1 gr
Barite	84 gr
LCM	48 gr

The LCM mixture that was used for the fracture reopening tests included the Resilient Graphite, Solu-Flake, Mica and Calcium Carbonate. Barite was also present in all the fluids and contributed to the sealing process. Properties of the Resilient Graphite and Solu-Flake are presented in Table 5. The Mica particles are groups of sheet silicate (phyllosilicate) minerals which include several closely related materials. Calcium Carbonate or limestone is one of the most applied Lost Circulation Materials (LCM) that has a wide application in the drilling industry for circulation loss purposes. In these series of tests, these particles were either tried alone or in dual combinations

Table 7: Particle size distribution of the LCM applied in the fracture reopening tests

Parameter	Value
Maximum particle size (µm)	850
D_{90} (µm)	590
D_{10} (µm)	25
Barite	84
m	0.4
Median	60
Inner spread	165
Outer spread	352
Inner skewness	15.5
Outer skewness	2.91
Kurtosis	0.53

3.4.3.2. Results and discussion

Results of the fracture reopening tests are presented in Figures 32 - 43. The only parameter that can be attained from a fracture reopening or a core fracturing test is the pressure level at which the fluid starts to invade the fracture. This pressure level varies for different drilling fluids. In Figure 44 the maximum pressure values experienced using all samples have been plotted. The Resilient Graphite exhibited the best performance in the tests. This is in agreement with previous findings in the area of wellbores strengthening[18]. In some tests, an abrupt failure of the plug was observed while in other cases only a smooth drop was seen. Mica particles also managed to form a resistant plug. However the Mica containing fluid invaded the fracture at a much lower pressure compared to the Resilient Graphite containing fluid. Fracture reopening pressure values also revealed the poor performance of limestone (Calcium Carbonate), in granular and fiber (Solu-flake) form. Although some previous researchers have found Calcium Carbonate particles to be effective in mixture with Resilient Graphite, their presence was found detrimental to the strengthening process in these series of tests. Description of abbreviations used in Figure 44 may be found in Table 8.

Table 8: Description of the abbreviations used in Figure 44

Drilling fluid sample	Abbreviation
Base mud	BM
Barite	B
Mica	M
Solu-Flake	SF
Resilient Graphite	LC
Calcium Carbonate	CC
Fiber	F

Rheology parameters of the applied fluid samples were also measured to seek possible correlation between the sealing capability of a drilling fluid and its rheological properties. The rheological measures of the fluid samples are presented in Table 9. In this table, P_{max} is the maximum recorded pressure, μ_{app}, is the apparent viscosity, PV is the plastic viscosity, YP is the yield point, GS is the 10 second gel strength, V_{fil} is the filtration volume and MC is the moisture content of the filter cake. The correlation coefficients between the maximum recorded pressure values and different rheology measures of the fluids are plotted in Figure 45. Values of the correlation coefficients indicate a poor correlation and thus it was concluded that rheology measurements may not solely lead to a reliable estimate of sealing properties of a fluid.

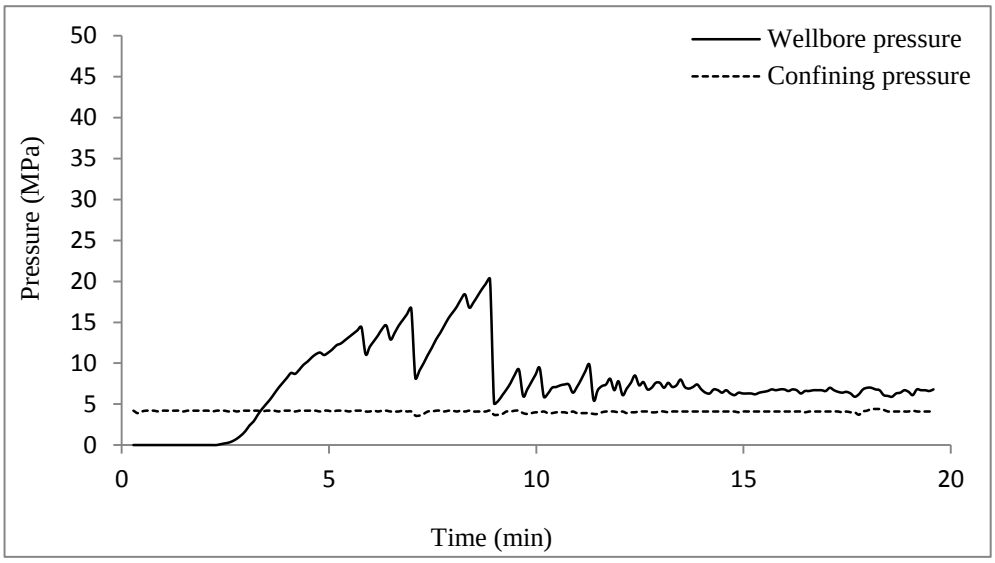

Figure 32: Wellbore and confining pressure profiles during the fracture reopening test using the base mud

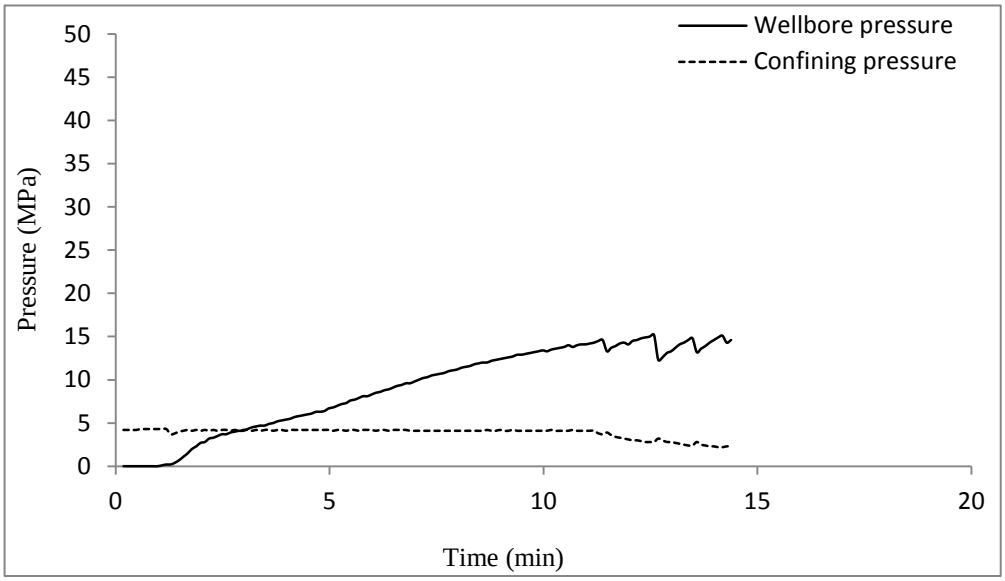

Figure 33: Wellbore and confining pressure profiles during the fracture reopening test using the base mud and barite

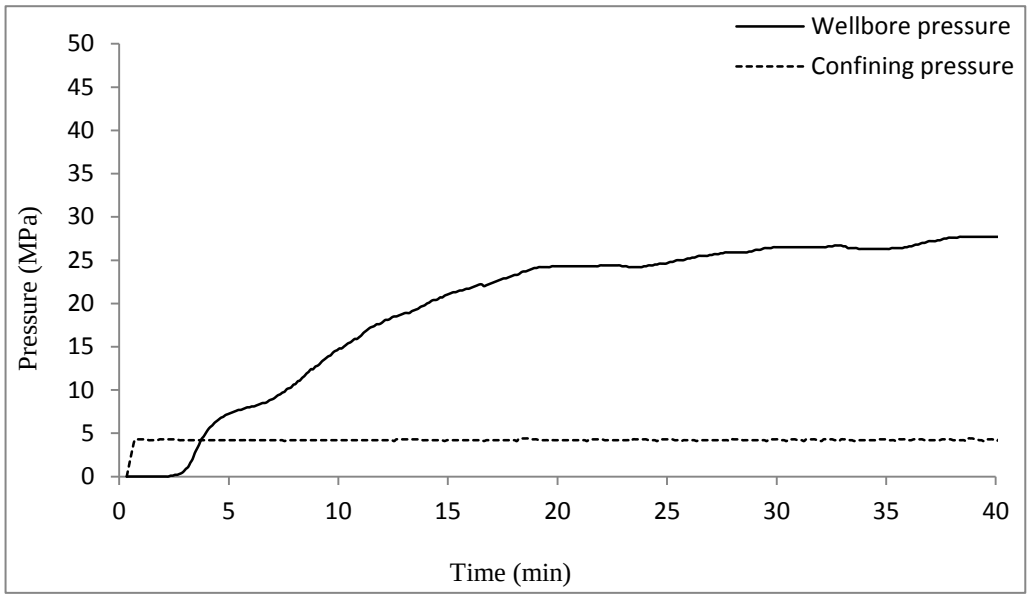

Figure 34: Wellbore and confining pressure profiles during the fracture reopening test using the base mud + Barite + Mica

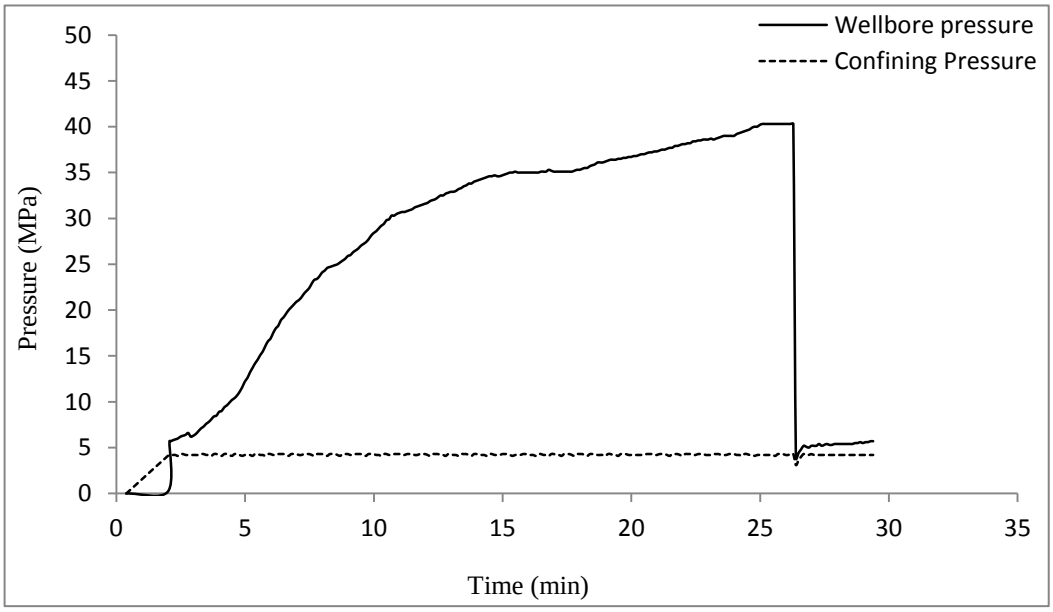

Figure 35: Wellbore and confining pressure profiles during the fracture reopening test using the base mud + Barite + Resilient Graphite

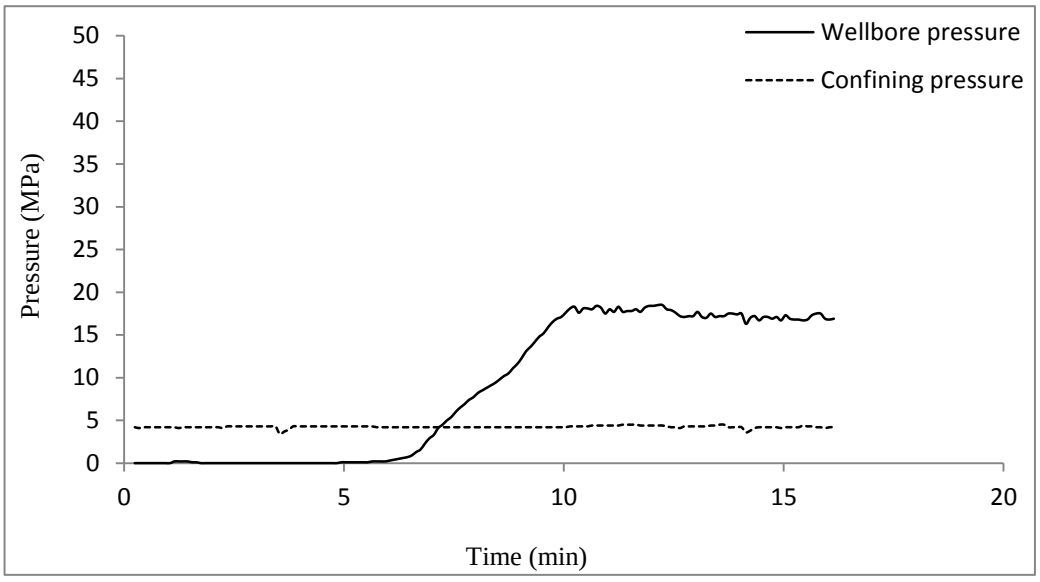

Figure 36: Wellbore and confining pressure profiles during the fracture reopening test using the base mud + Barite + Solu-Flake

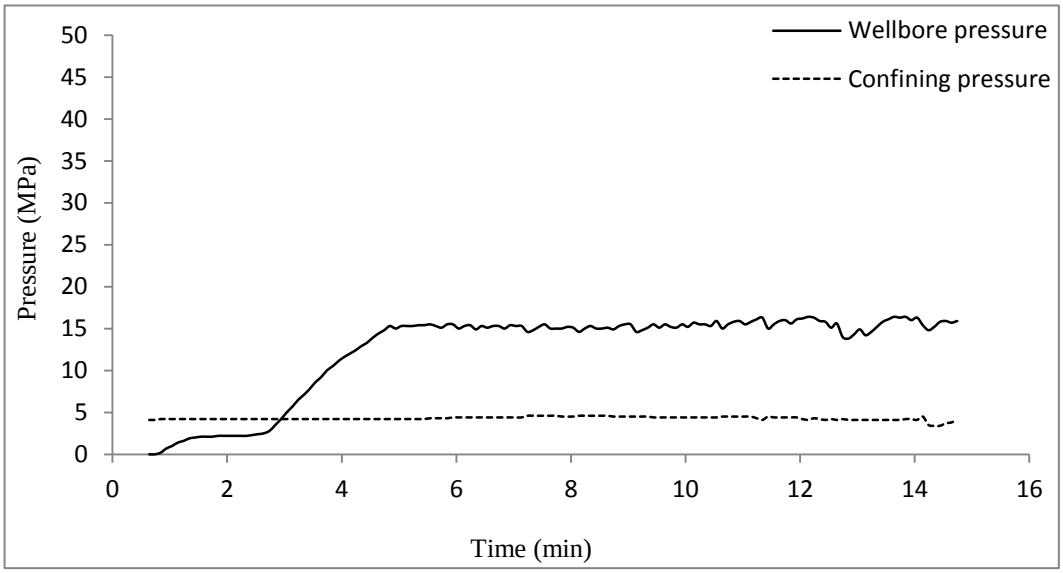

Figure 37: Wellbore and confining pressure profiles during the fracture reopening test using the base mud + Barite + Mica + Solu-Flake

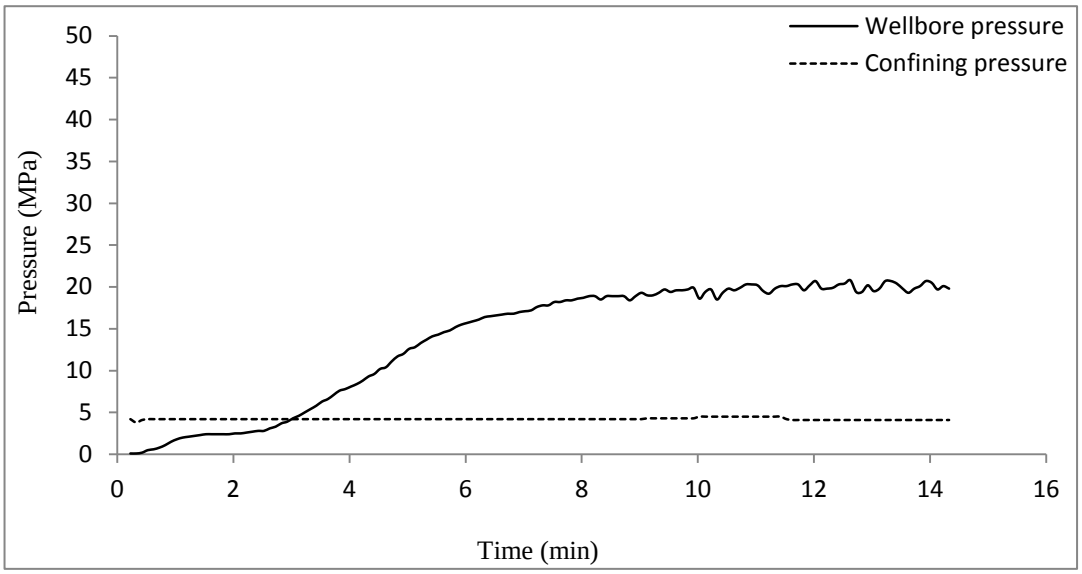

Figure 38: Wellbore and confining pressure profiles during the fracture reopening test using the base mud + Barite + Resilient Graphite + Mica

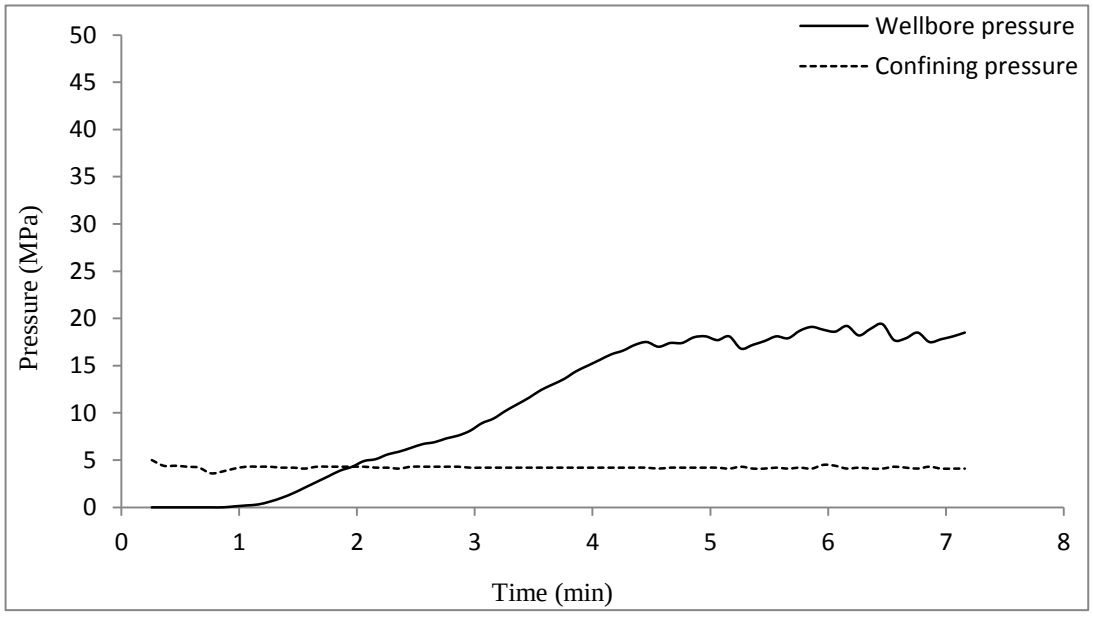

Figure 39: Wellbore and confining pressure profiles during the fracture reopening test using the base mud + Barite + Resilient Graphite + Solu-Flake

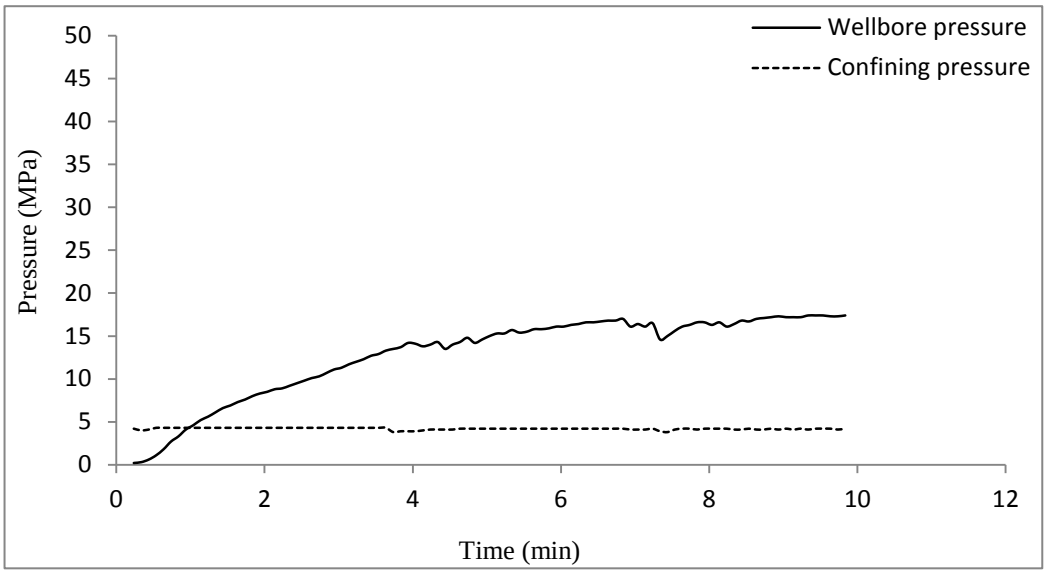

Figure 40: Wellbore and confining pressure profiles during the fracture reopening test using the base mud + Barite + Calcium Carbonate

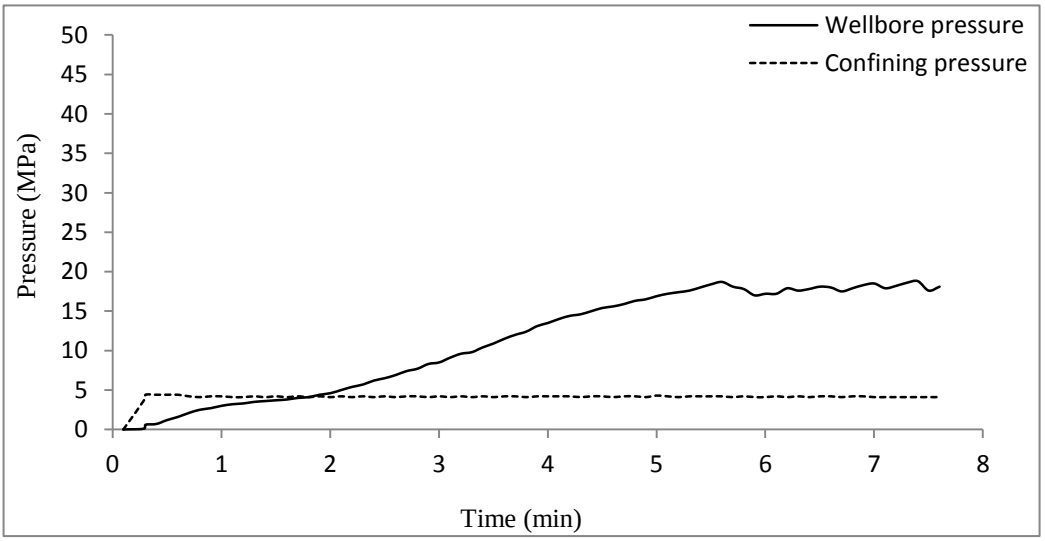

Figure 41: Wellbore and confining pressure profiles during the fracture reopening test using the base mud + Barite + Calcium Carbonate + Mica

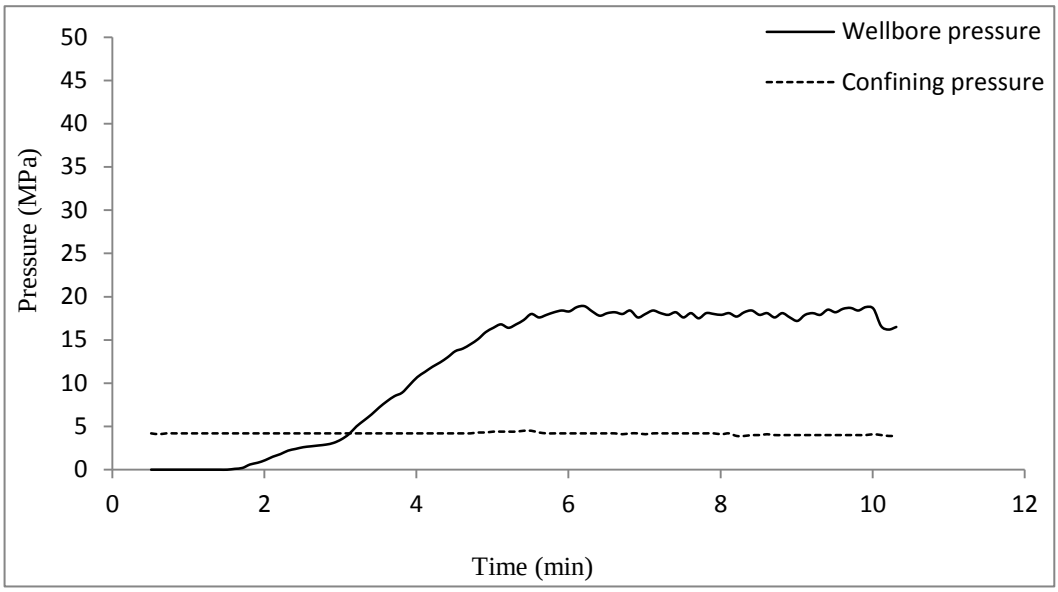

Figure 42: Wellbore and confining pressure profiles during the fracture reopening test using the base mud + Barite + Calcium Carbonate + Solu-Flake

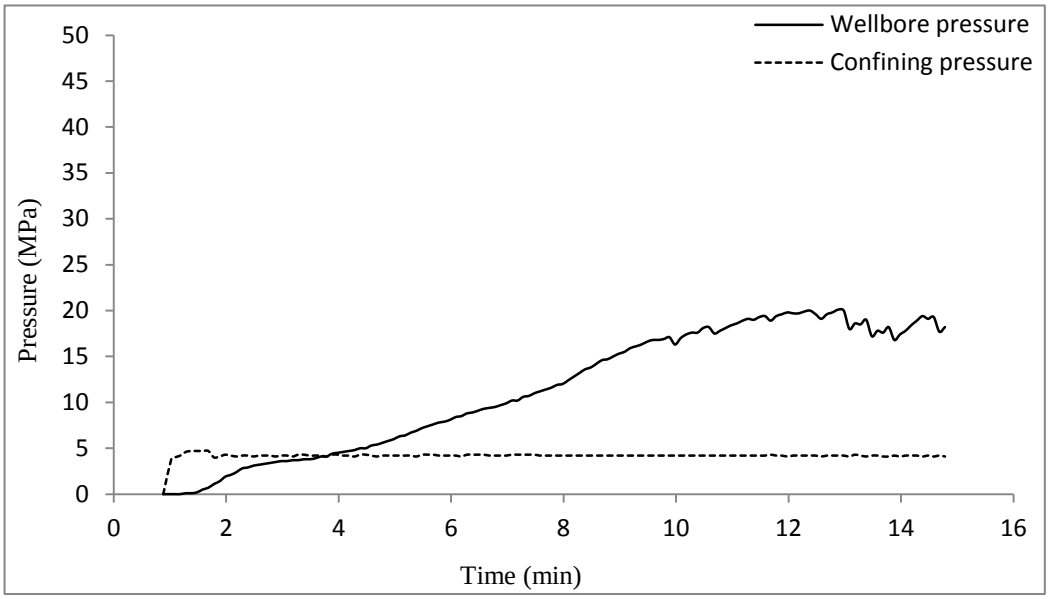

Figure 43: Wellbore and confining pressure profiles during the fracture reopening test using the base mud + Barite + Calcium Carbonate + Resilient Graphite

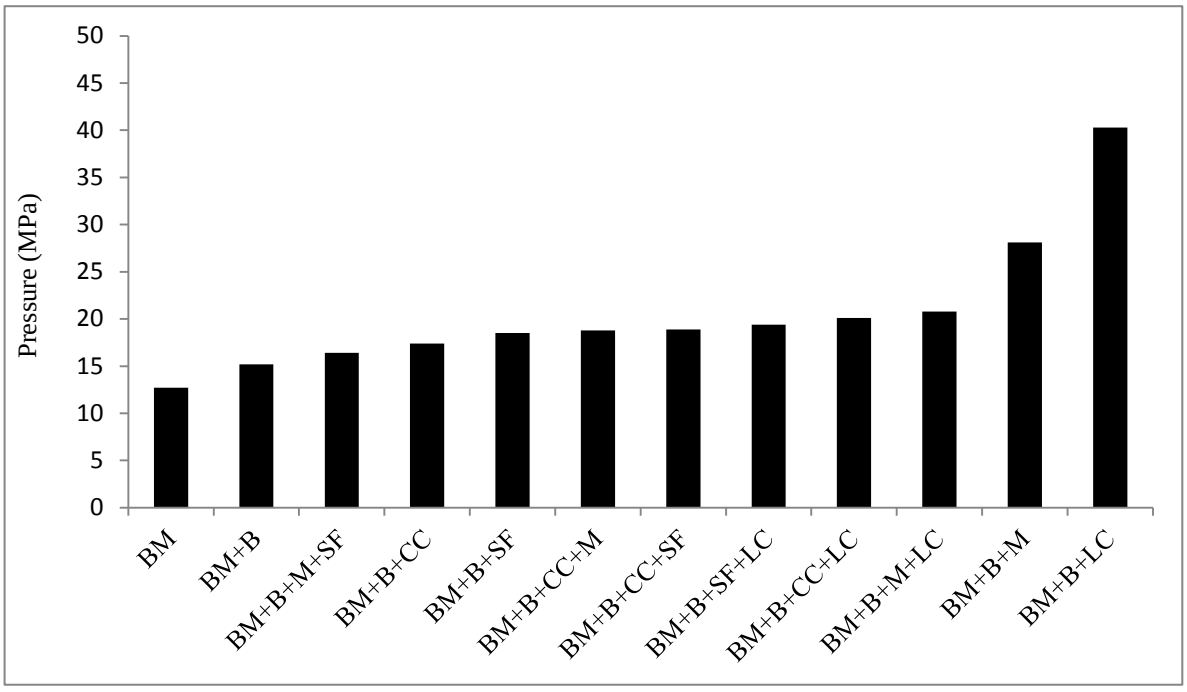

Figure 44: The maximum reopening pressure values obtained by using different drilling fluids

Table 9: Rheological properties of the drilling fluids applied in the fracture reopening tests

Drilling Fluid	**P_{max} (MPa)**	**μ_{app} (cP)**	**PV (cP)**	**YP (cP)**	**GS (cP)**	**$V_{fil.}$ (cm^3)**	**MC**
BM	12.7	59	37	22	3	1.8	0.89
BM + B	15.2	45.5	35.5	20	3	1.45	0.74
BM + B + M + SF	16.4	50	36	14	3	1.25	0.74
BM + B + CC	17.4	58	36	22	4	1.3	0.70
BM + B + SF	18.5	60.5	34	22	4	1.1	0.74
BM + B + CC + M	18.8	55	36	19	4	-	0.72
BM + B + CC + SF	18.9	54	33	21	4	1	0.72
BM + B + SF + LC	19.4	57	36	21	5	1.8	0.72
BM + B + CC + LC	20.1	58	34	24	4	1.2	0.71
BM + B + M + LC	20.8	54	32	22	5	-	0.71
BM + B + M	28.1	39	33	12	2	1.15	0.74
BM + B + LC	40.3	55	37	18	4	1.4	0.74

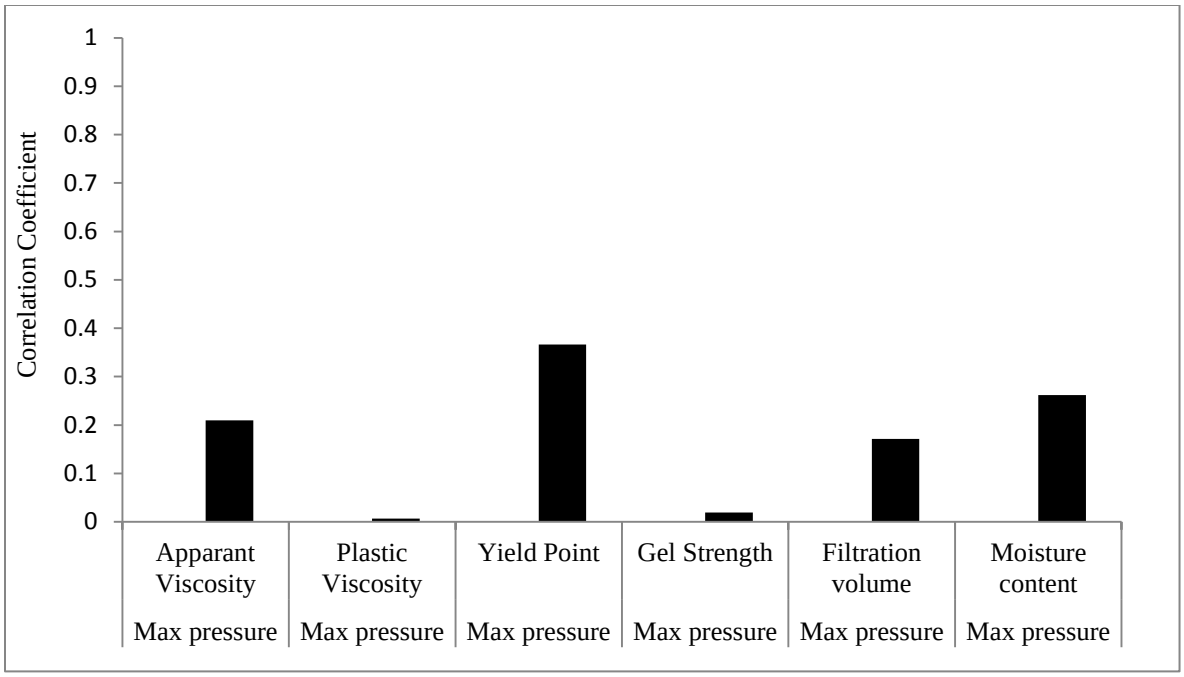

Figure 45: Correlation coefficients between the rheological parameters and the reopening pressure values

3.5. Experimental phase II

Based on the analysis of the results of the first series of tests, an extensive experimental plan was prepared to detect and analyze the contributing parameters in the strengthening process and to study the strengthening mechanism itself. Particle plugging tests were planned and implemented followed by the modeling process. In this section, the studied parameters as well as the tests results and analyses are presented and discussed. Particle plugging equipment was used for the most part in this phase and the core fracturing system was only used to confirm the extracted conclusions.

3.5.1. Objectives

The experimental phase II was planned and performed to build a reliable foundation based on which the mechanistic modeling could be initiated. One of the main objectives was to assess the

parameters which were found to be influential in the experimental phase I. Based on the observations and analysis during the experimental phase I, particle size, friction coefficient of the fracture planes, particle type, concentration of the fluid and the opening size were selected to be further studied as the major influential factors using the particle plugging tests. These parameters are introduced in this section. Our experimental and analytical approach is also explained

3.5.1.1. Particle size distribution

Particle size distribution has been widely identified in the literature as one of the most effective parameters in wellbore strengthening. However, an applicable quantified description of this factor is scarce. In order to numerically describe the particle size distribution, a long list of parameters have been used by researchers in various areas of engineering including soil mechanics, rock mechanics, bioengineering, nano-technology etc. In the present work, a very practical parameter was applied which had been previously used in the sand pack technology to estimate the minimum porosity[55]. Using this parameter, the size distribution of particles may be described using equation 3-1.

$$f = 100\left(\frac{d}{d_{max}}\right)^{m} \qquad \text{Eq. 3-1}$$

where f is the percentage of the particle size d in the mixture, d_{max} is the size of the largest particle and m is the particle size distribution parameter. In this dissertation, m is referred to the particle size distribution parameter as the m factor. The m factor, can define the shape of the particle size distribution for a given maximum size. Peronius and Sweeting[55] proposed this parameter based on research to seek a correlation between the m factor and the porosity of a sand pack and proposed Equation 3-2 for this purpose.

$$\varphi_{min} = 0.106 + 0.079D_v + 1.367{D_v}^3 + 0376(1-R)^3 \quad \text{Eq. 3-2}$$

where φ_{min} is the minimum porosity of the sand pack, D_v is a parameter estimated by Equation 3-3 based on the m factor, and R is the roundness of particles.

$$D_v = \begin{cases} 1 - 2^{-2(0.5-m)} & m \leq 0.5 \\ 1 - 2^{-(m-0.5)/m} & m > 0.5 \end{cases} \quad \text{Eq. 3-3}$$

Roundness of particles can be estimated using various methodologies, some of which include complex mathematical algorithms. In some cases, sedimentologists use diagrams to roughly estimate the roundness of soil particles. Roundness changes between zero and one for completely angular and completely circular particles, respectively. Peronius and Sweeting[55] found that the minimum porosity in a sand pack is obtained when m=0.5.

The m factor can take any positive value. Lower values of m correspond to a higher amount of smaller particles with respect to larger particles within the size range determined by d_{max} while larger m values indicate a more significant portion of larger particles. Figures 46 and 47 show the particle size distribution of a mixture with the maximum particle size of 1 mm with two different values of m. In the present research two values of m were used, m=0.5 and m=0.2, for fluid preparations and the results were compared to evaluate the importance of particle size distribution. In addition, several experiments were performed to evaluate the importance of all sizes of particles. In each test a certain range of particle size was eliminated and the results were compared to the tests with drilling fluids that contained the full range of particle size.

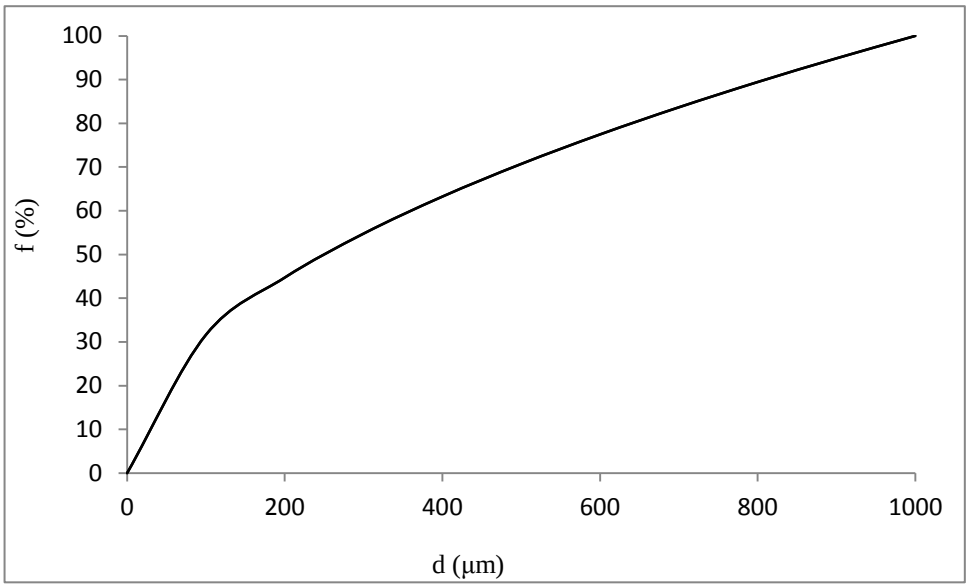

Figure 46: Particle size distribution of a mixture with the maximum particle size of 1 mm and m = 0.5

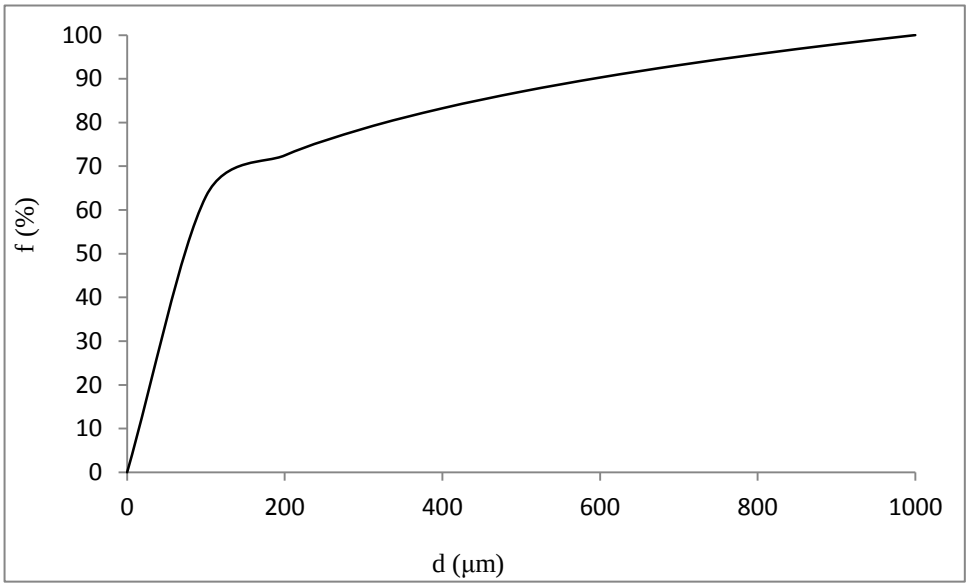

Figure 47: Particle size distribution of a mixture with the maximum particle size of 1 mm and m=0.2

3.5.1.2. Particle type

The selection of particles for lost circulation and strengthening purposes depends on several factors including high strengthening performance, low formation damage, easy removal during the completion and production stages, cost and availability near the well location. In the present research, Resilient Graphite, Mica, Fiber and Solu-Flake were selected for the particle plugging tests. The selected particles were in granular, flake and fiber shapes. The mentioned LCMs were either mixed in the fluid alone or in combination with other LCMs to study the interactive effects between two or three different types of materials.

3.5.1.3. Friction coefficient

The friction coefficient of the fracture plane was selected for experimental analysis since the observation of abrupt failure of the bridges in experimental phase I highlighted the possibility of a significant plugging process as the governing mechanism of strengthening as suggested in most previous studies. Based on this theory, higher friction between the plug and the fracture planes can lead to a more resistant plug. In order to study this hypothesis in more detail, two types of fracture planes were used, as shown in Figure 48. In order to make higher friction coefficient on the fracture planes, small wrinkles were made artificially on the fracture planes. The size of the wrinkles were negligible compared to the fracture opening and thus did not impact the opening size significantly. The exact value of the friction coefficient was unknown; however it was obvious that the wrinkled fracture planes were capable of providing a much higher friction.

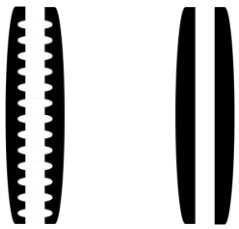

Figure 48: Schematic illustration of artificial simulation of high friction coefficient using wrinkled fracture planes

3.5.1.4. Solids Concentration

Literature suggests that increased solids concentration of the fluid boosts the strengthening process and promotes the chance of fracture initiation or opening. In some cases, a critical concentration has been found above which no significant improvement was observed in the previous studies. Some results even indicated a drop in the strengthening capability of the fluid as the concentration reached a certain point. In this research three concentrations of 16.85 lb/bbl (48.11 kg/m^3), 8.49 lb/bbl (24.25 kg/m^3) and 33.16 lb/bbl (94.70 kg/m^3) were selected to investigate the effect of higher concentration of solids on wellbore strengthening.

3.5.2. Experimental plan

The experimental plan for the particle plugging system of this phase is shown in Table 10. Note that each test was repeated at least three times to increase the reliability of the results. The tests were divided into four sections to evaluate the impacts separately.

The effect of particle type was studied separately in the first part of this phase. Resilient Graphite, Solu-Flake, Fiber and Mica were selected and tested. In some experiments, particles were mixed together in the fluid to study the possible interactions between the particles.

In the second part, in order to investigate the significance of particle size distribution, two fluid samples were prepared with the constant concentration of 16.85 lb/bbl (48.11 kg/m^3). One of the samples contained Mica while the other one contained Resilient Graphite as the Lost Circulation Material (LCM). For all tests of this section, fracture planes with normal surfaces were applied. The m factor was changed from 0.5 to 0.2 to study the importance of the particle size distribution. In addition, the importance of smoothness of particle size distribution was investigated using a series of experiments with fluid samples with certain ranges of particle size eliminated. Elimination of a certain size ranges allows for investigation of the necessity of having all ranges of particle size in the fluid for wellbore strengthening enhancement.

The third section of the particle plugging tests was dedicated to investigation of effect of friction of the fracture surface on the strengthening of the wellbore. Therefore, the opening size, the concentration and the particle size distribution parameter of the fluids were kept constant and equal to 500 μm, 16.85 lb/bbl (48.11 kg/m^3) and 0.5, respectively. The fluids contained either Mica or Resilient Graphite as the Lost Circulation Material (LCM).

The fourth part of the particle plugging experiments was designed to study the effect of the fluid concentration. Several drilling fluids containing different types of LCMs were used for this part. The m factor was kept constant and equal to 0.5 and a 500 μm wide fracture was used. The concentration of the fluids was changed from 16.85 lb/bbl (48.11 kg/m^3), 8.49 lb/bbl (24.25 kg/m^3) and 33.16 lb/bbl (94.70 kg/m^3).

In the final part of the tests, particle type was studied with respect to changing fracture opening size. Each particle was tested using a 300 μm, a 500 μm and a 700 μm wide fracture. For these experiments, normal fracture planes and fluid samples with the constant concentration of 16.85 lb/bbl (48.11 kg/m^3) and m factor of 0.5 were used.

Table 10: Description of the sections of the particle plugging tests in the experimental phase II

Section	**Studied parameter**	**Constant parameters**
Section I	Particle type	Particle size distribution, concentration, friction and opening size
Section II	Particle size distribution	Particle type, concentration, opening size and friction
Section III	Friction	Particle type, concentration, opening size and particle size distribution
Section VI	Concentration	Particle type, opening size, particle size distribution and friction
Section IV	Opening size	Particle type, concentration, particle size distribution and fraction

3.5.3. Results and discussion

Results of the experimental phase II laid the groundwork for the modeling process in the present research. The experiments were designed to evaluate the effects of the above described parameters. The results are presented in the following four sections to discuss the effects of each factor separately.

3.5.3.1. Effect of particle type

The eight parameters defined to investigate the results of the particle plugging tests are utilized to evaluate the performance of LCMs. In order to compare the effects of different types, all tests of this section were performed using a 500 μm side fracture. All fluids had the concentration of 16.85 lb/bbl (48.11 kg/m^3) and the m factor was kept equal to 0.5. The fracture planes were also normal. Mixtures of particles were done in equal portions.

Total number of peaks (N) and number of peaks per minute (N/t)

Figures 49 and 50 reveal that application of Resilient Graphite in the fluid increases the number of peaks. In addition, Solu-Flake had the lowest ability to build bridges over the openings.

An analysis of Figures 49 and 50 also shows that the application of fiber in the drilling fluid with Resilient Graphite leads to acceptable results in terms of N and N/t, even though the amount of Resilient Graphite has been reduced by half when mixed with fiber. It may be desirable due to cost reduction since Resilient Graphite is relatively costly. On the other hand, fibers have been reported to have a remarkable impact on the rheology. Solu-Flake, on the other hand, decreased the performance of Resilient Graphite and Mica as added in mixtures.

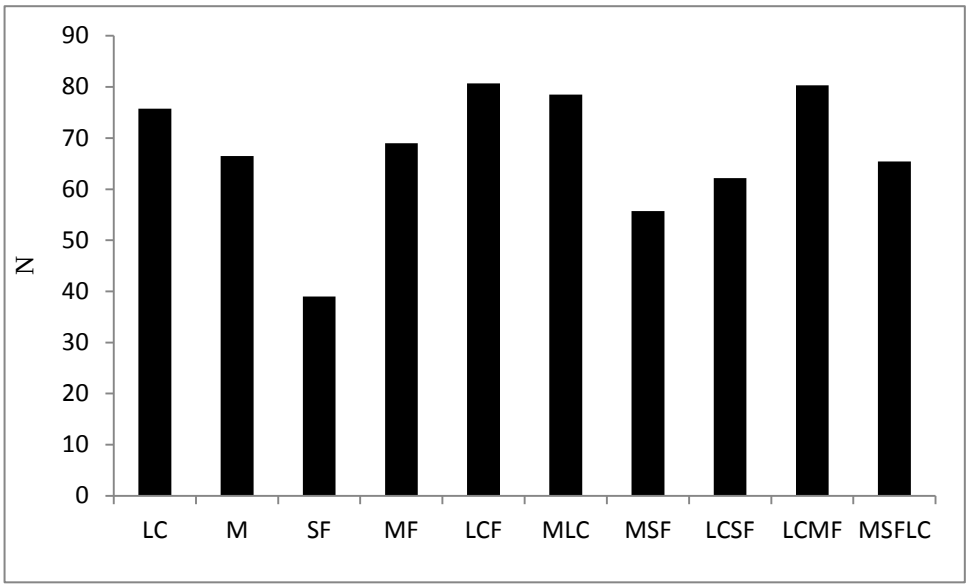

Figure 49: Total number of peaks using fluids containing different particles

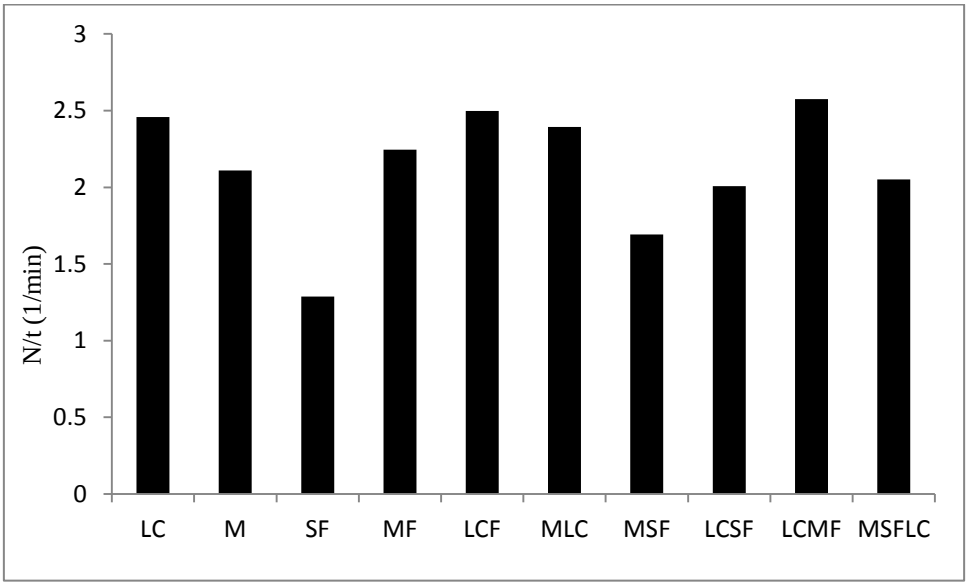

Figure 50: Number of peaks per minute using fluids containing different particles

The pressure recordings of the tests using a Resilient Graphite containing fluid and a Solu-Flake containing fluid are illustrated in Figures 51 and 52. It is clearly seen that the Resilient Graphite particles are capable of forming more bridges.

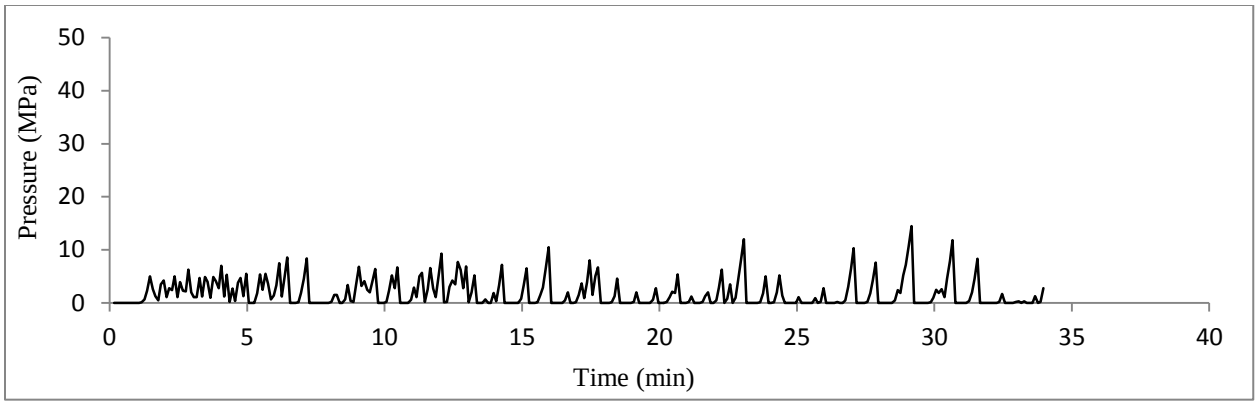

Figure 51: Pressure recording during particle plugging tests using a Resilient Graphite containing fluid

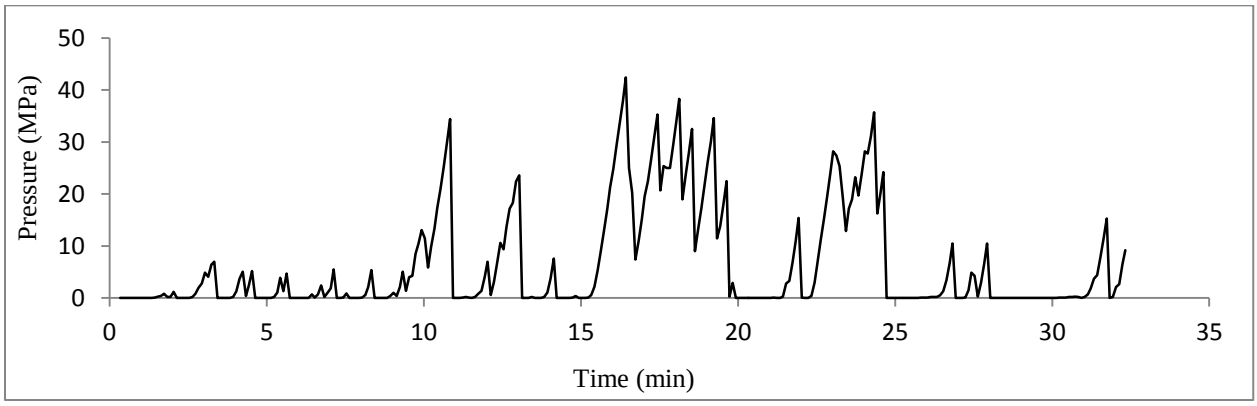

Figure 52: Pressure recording during particle plugging tests using a Solu-Flake containing fluid

Average peak pressure ($P_{P\text{-}ave}$)

Figure 53 illustrates the average peak pressure for the tested fluids. Average peak pressure, is the most important parameter recorded during the particle plugging tests which provides information on the strengthening capability of the fluid. Surprisingly, the Resilient Graphite bridges show lower failure resistance compared to Solu-Flake. Fiber does not significantly affect the average peak pressure either. Solu-Flake, which was shown to build fewer bridges compared to other particles, forms bridges of the highest resistance. It also increases the resistance of the bridges as added in mixtures. A glance at Figures 51 and 53 shows that although the Resilient Graphite

particles form more bridges, the resistance of each bridge is significantly less than the bridges that Solu-Flake particles build.

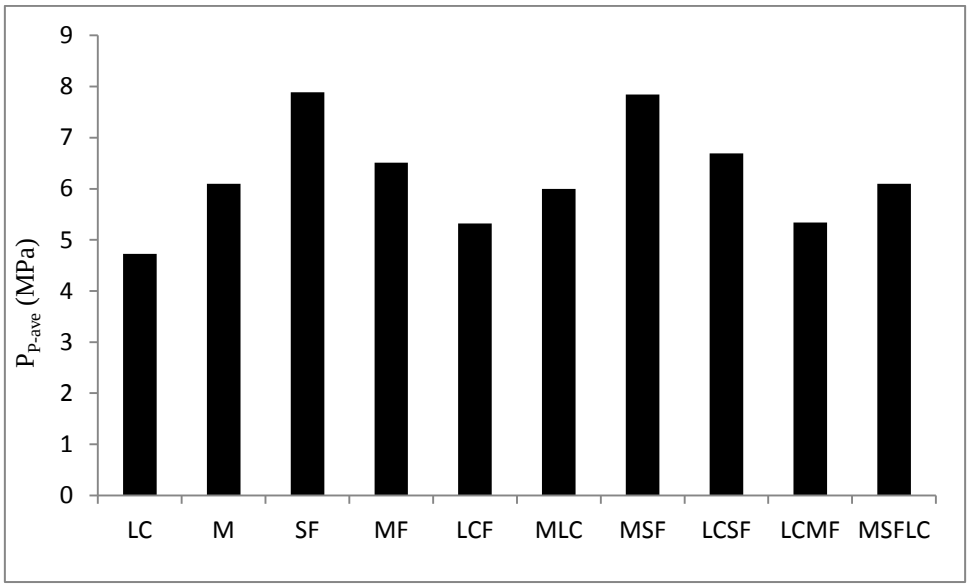

Figure 53: Comparison of the average peak pressure values for different fluids during particle plugging tests

Total number of zeros (Z) and number of zeros per minute (Z/t)

Total number of zeros is a very good indication of the amount of filtration. Less filtration volume leads to better strengthening and lower risk of fracture growth and circulation loss. Figures 54 and 55 show the total number of zeros for particle plugging tests using different LCMs. Resilient Graphite is very efficient in terms of reducing the filtrate loss. This was expected since this particle manages to build bridges as soon as one is broken down and thus does not allow for significant filtration. Solu-Flake allows for the largest amount of filtration compared to other particles. Fiber does not change of the filtration volume when added to the fluid.

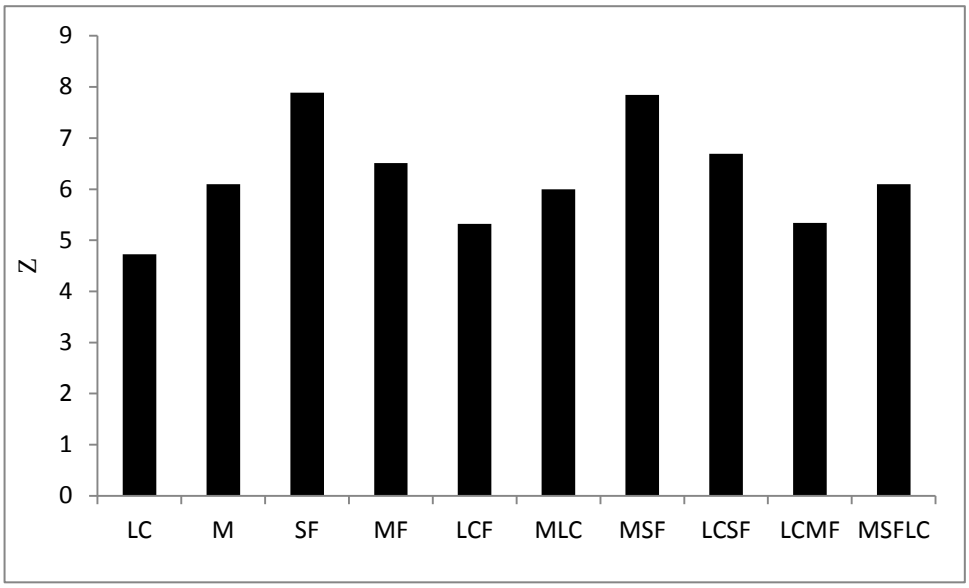

Figure 54: Comparison of the total number of zeros for different fluids during particle plugging tests

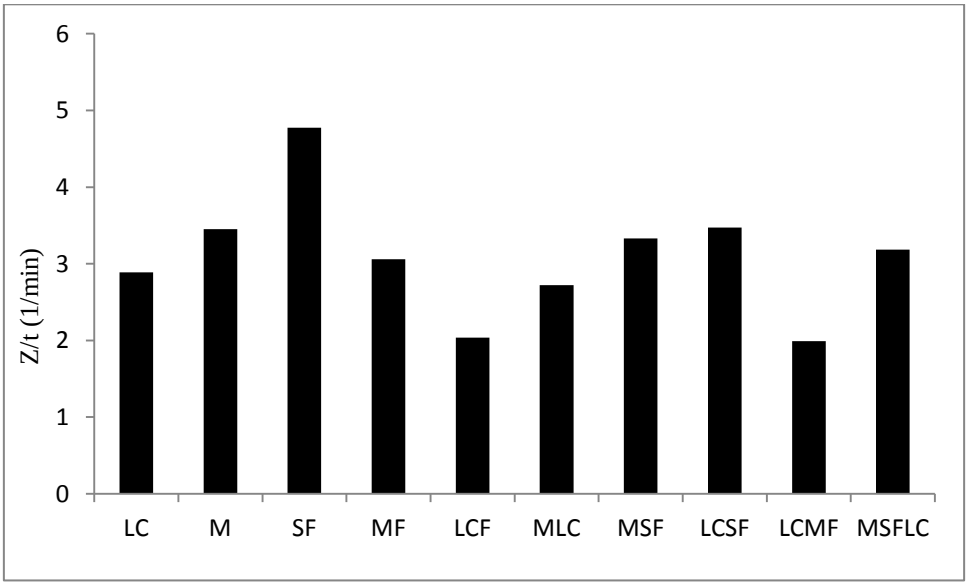

Figure 55: Comparison of the time averaged number of zeros for different fluids during particle plugging tests

Maximum pressure (P_{max})

Maximum pressure values recorded in the particle plugging experiments are a strong function of the uniformity of the particle distribution in the fluid. Figure 56 shows that the Solu-Flake containing mixtures were able to build the strongest bridges.

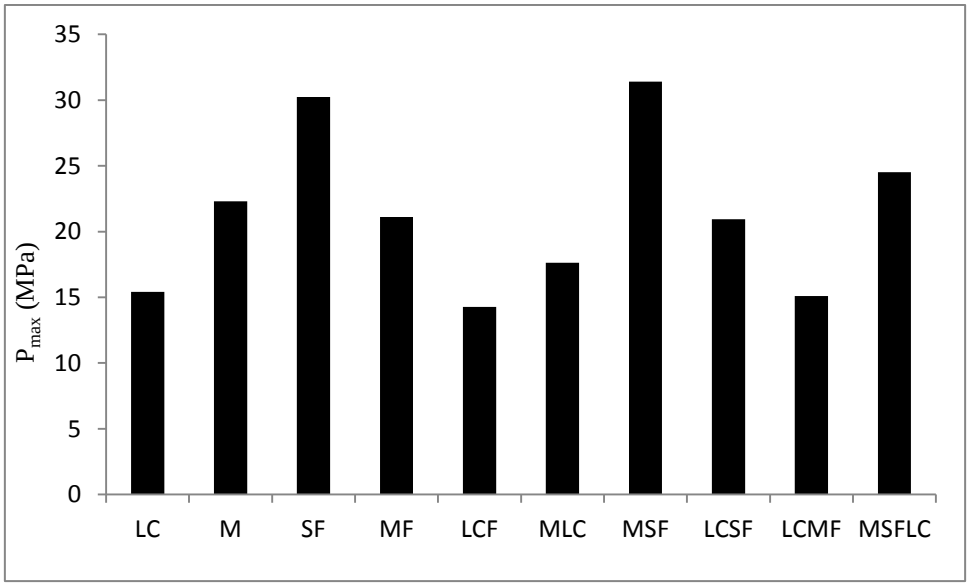

Figure 56: Comparison of the maximum pressure values for different fluids during particle plugging tests

Number of peaks per zeros (N/Z)

The number of peaks per zeros shows the number of bridges built for a certain amount of filtration. Its reciprocal, indicates the amount of filtration required to build one bridge over the fracture. As Figure 57 indicates, when Resilient Graphite is present in the mixture, this parameter grows. In this case fiber has also shown a good performance in increasing the number of formed bridges. Solu-Flake shows poor results and was found detrimental to mixtures in terms of this number of peaks per zeros.

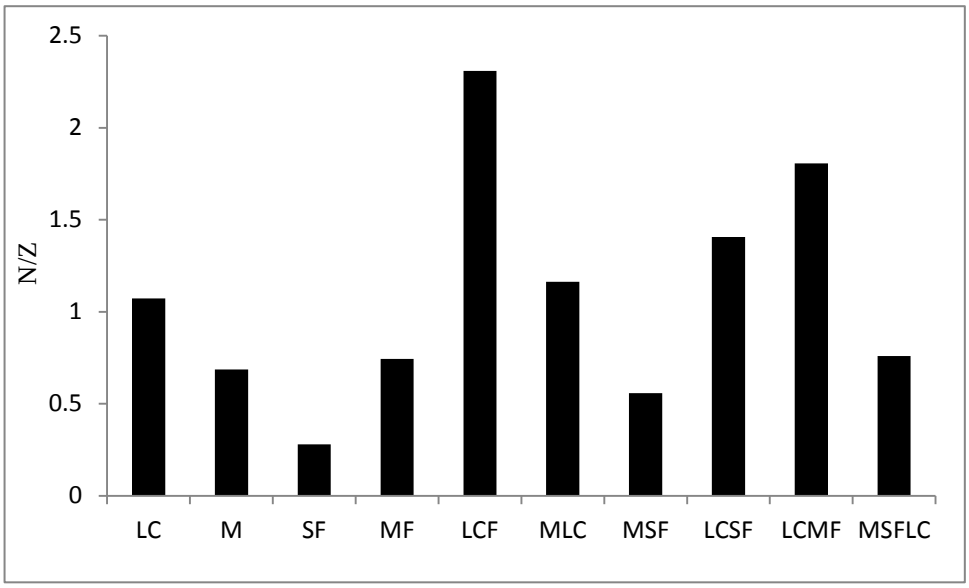

Figure 57: Comparison of the maximum pressure values for different fluids during particle plugging tests

Average pressure (P_{ave})

The average pressure in the cell is illustrated in Figure 58. This parameter does not provide reliable information on the wellbore strengthening capabilities of the drilling fluids. Solu-Flake containing samples show high values of average pressure while Resilient Graphite exhibits a poor performance in increasing the average pressure values in the cell.

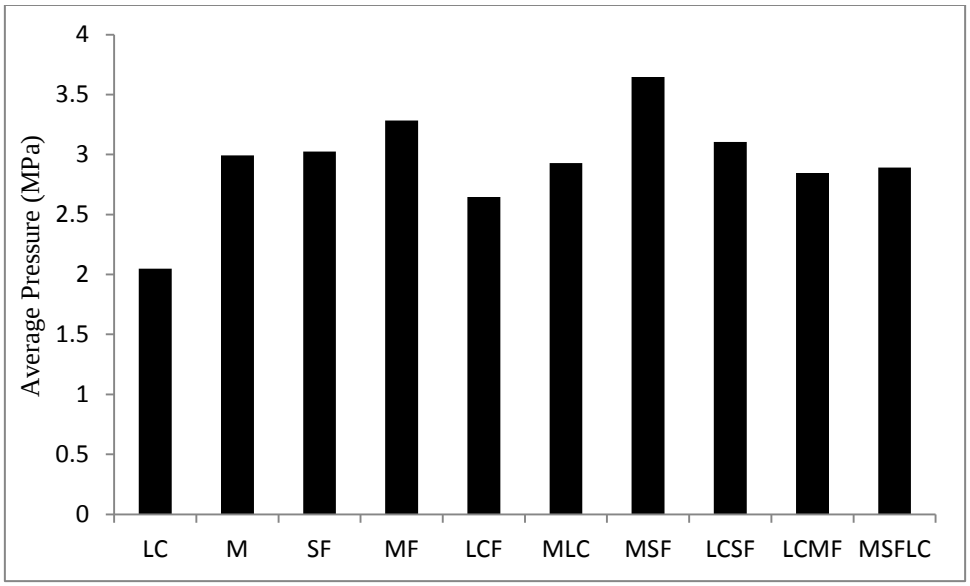

Figure 58: Comparison of the average pressure values for different fluids during particle plugging tests

Summary of particle type effect

One of the main findings based on the results of this section is the fact that the efficiency of a particle in wellbore strengthening may not be easily deduced from its shape. In the completed series of experiments to investigate the importance of the particle type, the fiber showed a totally different performance compared to the Solu-Flake, which is fiber-shaped as well. Resilient Graphite was unable to build strong bridges. This might partly root from its slippery nature which makes it difficult to form sufficient shear strength within the plug. Resilient Graphite exhibited a high capability in building immediate bridges though. The low number of zeros and high number of bridges demonstrably prove that this particle is capable of forming a new bridge as soon as the old one fails. As previously mentioned in this dissertation, qualitative descriptions regarding the application of particles are found in the literature frequently. In this research one of the main objectives is to describe the wellbore strengthening capability of particles in terms of their mechanical properties. Once the rest of predetermined parameters are studied, this objective will be pursued.

3.5.3.2. Effect of particle size

Our approach towards the investigation of effect of particle size distribution was discussed before. In addition to the size distribution, the necessity for the presence of all sizes of particles was also evaluated. Therefore, the results are presented in two sections.

3.5.3.2.1. Effect of particle size distribution

Two m values of 0.5 and 0.2 were selected for the particle size distribution parameter and the results were compared. The lower m factor indicates the presence of higher amounts of smaller particles. The particle size distributions are shown in Figure 59. Two fluid samples were prepared, one of which contained Resilient Graphite as the LCM while the other one contained Mica as the LCM. Results are shown in Figures 60 - 65. It was concluded that the fluids which contained larger particles were capable of building more bridges and allowed for less filtration. Both of these characteristics led to improved strengthening. In addition, all pressure parameters ($P_{P\text{-}ave}$, P_{max} and P_{ave}) are enhanced in the fluids with the m factor of 0.5. The number of peaks per zero (N/Z), which describes the number of bridges formed per unit of filtration, was also much higher for the fluids that contained larger particles.

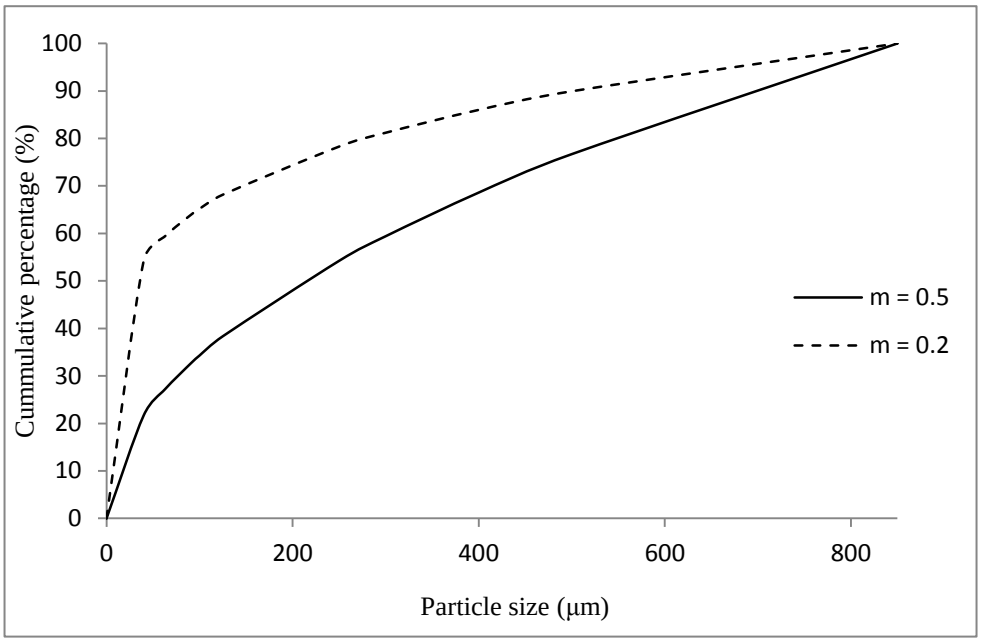

Figure 59: Illustration of particle size distribution for m=0.5 and m=0.2

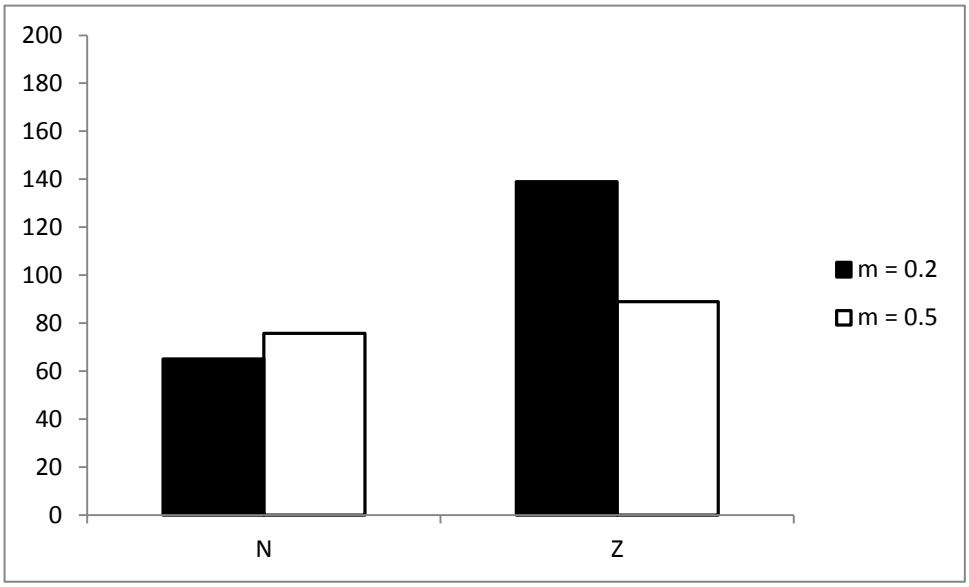

Figure 60: Effect of m factor on total number of peaks and total number of zeros during particle plugging tests using a Mica containing fluid

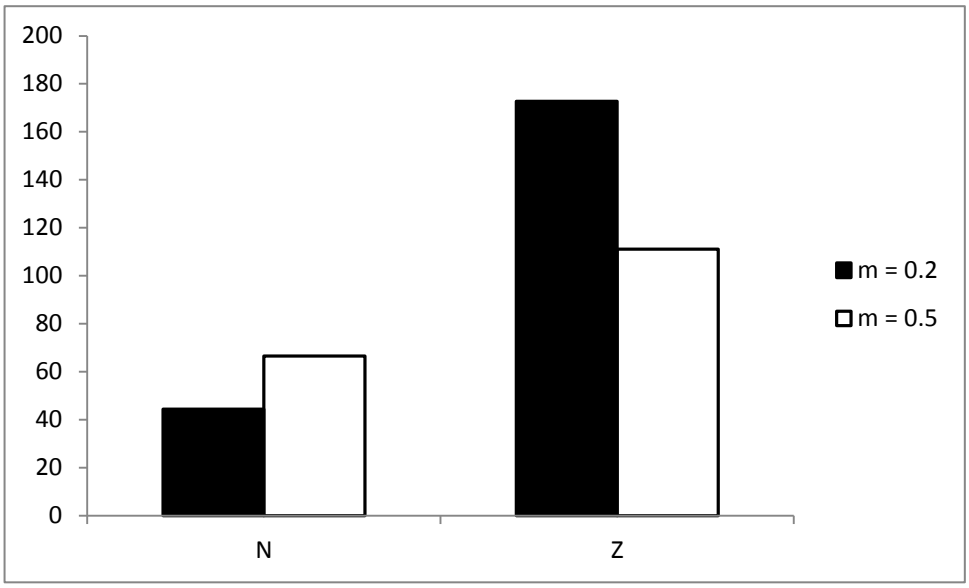

Figure 61: Effect of m factor on total number of peaks and total number of zeros during particle plugging tests using a Resilient Graphite containing fluid

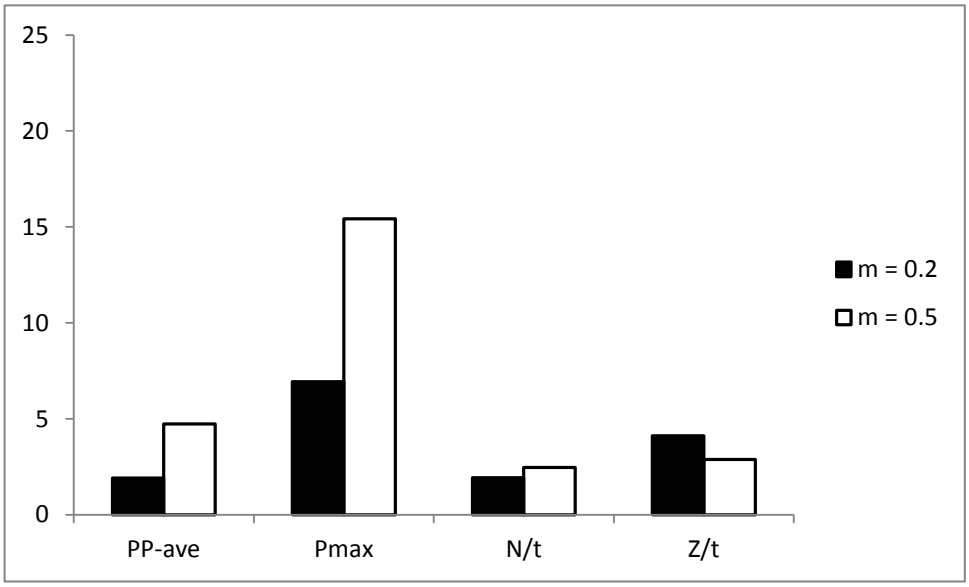

Figure 62: Effect of m factor on average peak pressure (MPa), maximum pressure (MPa), time averaged number of peaks (1/min) and time averaged number of zeros (1/min) during particle plugging tests using a Mica containing fluid

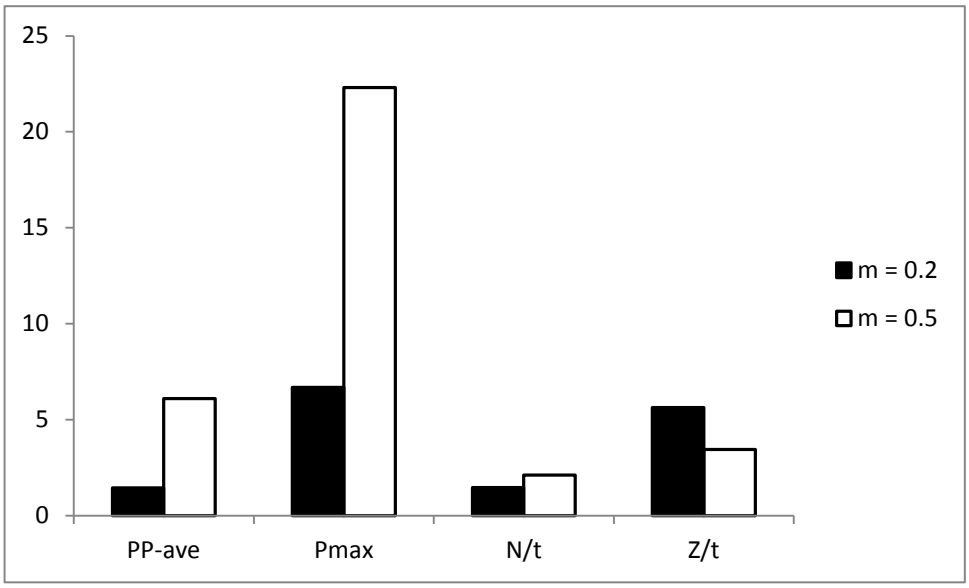

Figure 63: Effect of m factor on average peak pressure (MPa), maximum pressure (MPa), time averaged number of peaks (1/min) and time averaged number of zeros (1/min) during particle plugging tests using a Resilient Graphite containing fluid

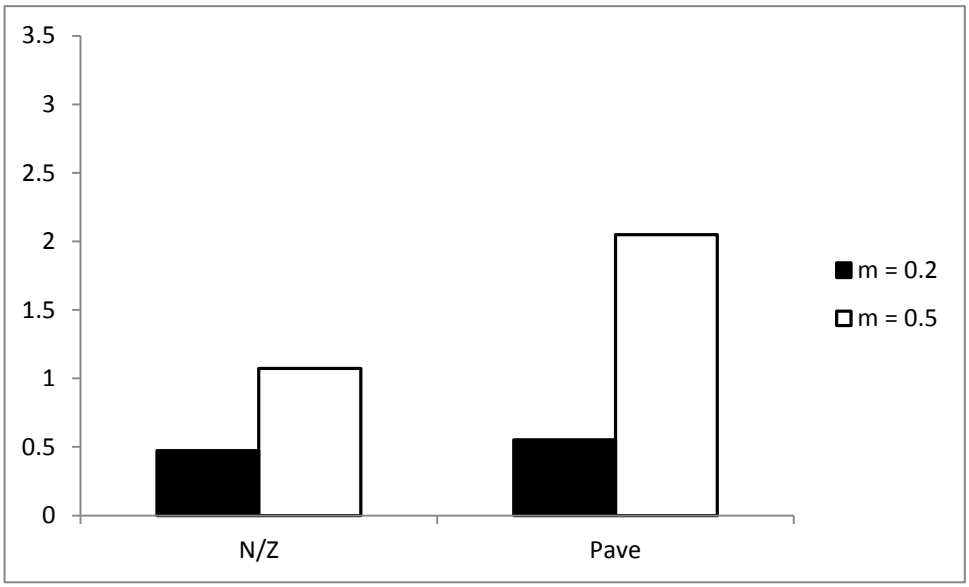

Figure 64: Effect of m factor on number of peaks per zero and average pressure (MPa) in the cell during particle plugging tests using a Mica containing fluid

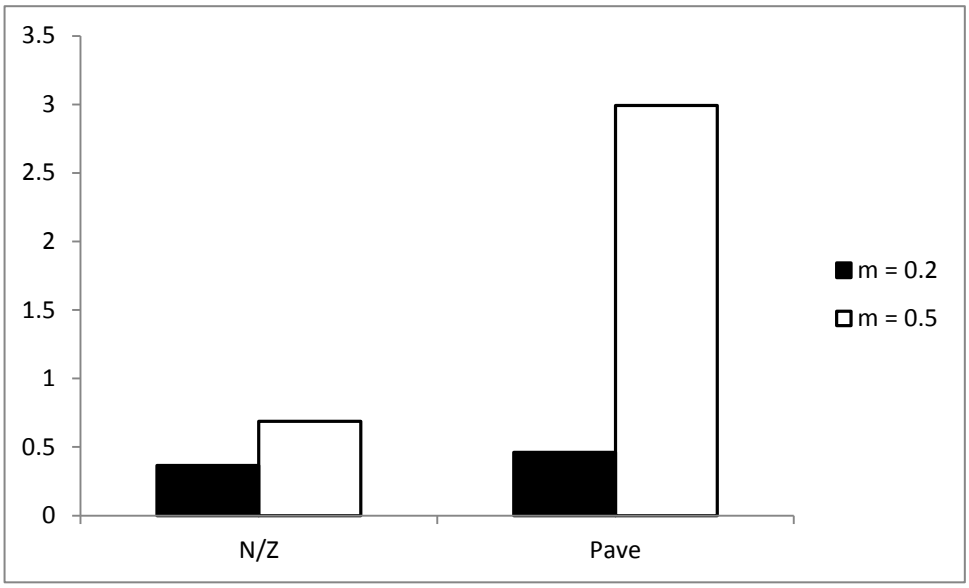

Figure 65: Effect of m factor on number of peaks per zero and average pressure (MPa) in the cell during particle plugging tests using a Resilient Graphite containing fluid

Results of this section are very important in the modeling of the process. The significance of larger particles in the strengthening process shows the importance of the plugging mechanism. Larger particles enter the opening and plug the fracture mouth. Smaller particles can then fill the gaps between larger particles and form a low porosity and low permeability bridge. In order to assess the significance of the presence of all particle sizes, another series of experiments was performed using fluids in which certain part of the particles of a predetermined size were absent. The results were then compared to the fluids containing the full range of sizes and the results are presented in the next section.

3.5.3.2.2. Effect of particle size range

As mentioned above, certain size ranges were eliminated from the LCM mixtures to assess the significance of the presence of all sizes. All particle plugging tests of this section were carried

out using a 300 μm opening. Results were then compared to the fluids containing the same particles in the full size range. In the first series of experiments, a fluid containing Resilient Graphite was prepared using particles in the size range of 500 μm to 850 μm. Basically the large portion of the particles were kept in the fluid while all particles smaller than 500 μm were eliminated from the particle size profile. Results are illustrated in Figures 66 and 67.

Results vividly indicate the importance of particle smaller than 500 μm when the fracture opening is 300 μm. There is almost no resistance in the bridges compared to the regular fluid which contains the whole range of particle sizes. These tests were repeated using Mica as the LCM and the results are presented in Figures 68 and 69.

In another series of tests, particles larger than 400 μm were removed from a Mica containing fluid. Results are presented in Figures 70 and 71. The opening size applied in this series of tests was 300 μm. Results indicate that the presence of large particles is very essential to forming a resistant bridge. All parameters exhibit the poor performance of fluids with no large particles.

In order to investigate whether the particles around the size of the opening would suffice for building a resistant bridge, a mica containing fluid was prepared using particles in the range of 300 μm to 400 μm and tested using a 300 μm fracture. Results of particle plugging tests using this fluid are presented in Figures 72 and 73. Similar to the previous experiments, the narrow size range is detrimental to the strengthening capabilities of the fluid.

In the final series of tests in this section, a narrow range of particles smaller than the opening size was selected using a Resilient Graphite containing fluid and tested using a 300 μm wide fracture. Again, the results emphasize the importance of having a wide range of particles. In this case, no bridge was formed. This conclusion also confirms the detected plugging mechanism of the formation of a bridge over the opening. Since particles smaller than the opening size are unable to form a bridge at this concentration, plugging of particles larger than the fracture size is concluded to be the key to success of a strengthening process. Results of these experiments have been compared to those of the normal fluid containing all sizes of LCM in Figures 74 and 75.

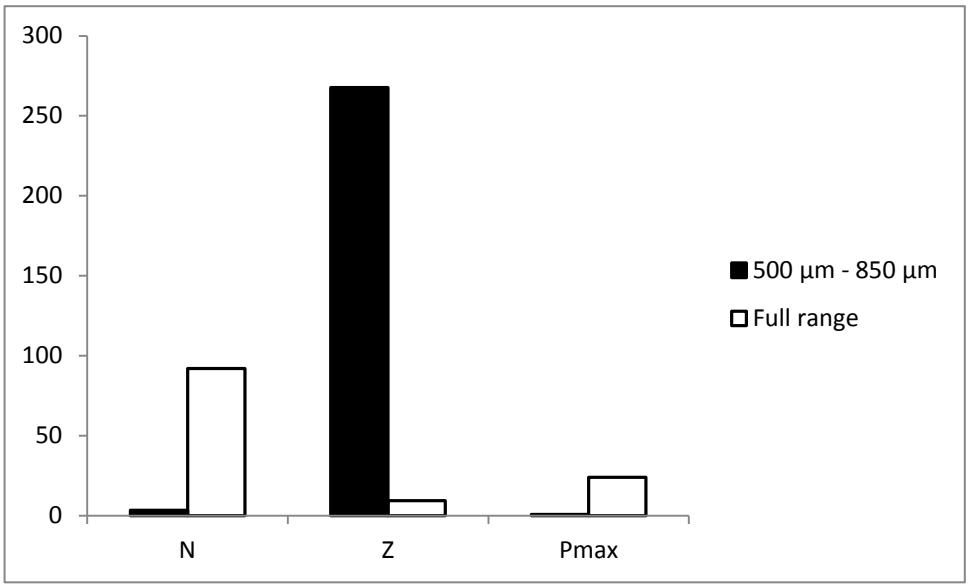

Figure 66: Effect of elimination of the particles smaller than 500 µm on the total number of peaks, total number of zeros and the maximum pressure (MPa) experienced during particle plugging tests using a Resilient Graphite containing fluid

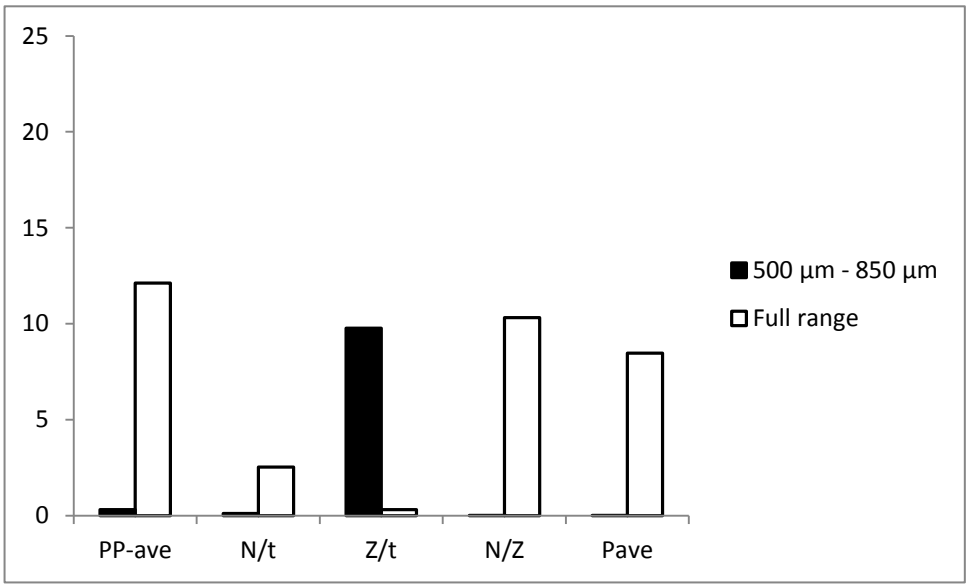

Figure 67: Effect of elimination of the particles smaller than 500 µm on the average peak pressure (MPa), time averaged number of peaks (1/min), time averaged number of zeros (1/min), number of peaks per zero and the average pressure (MPa) experienced in the cell during particle plugging tests using a Resilient Graphite containing fluid

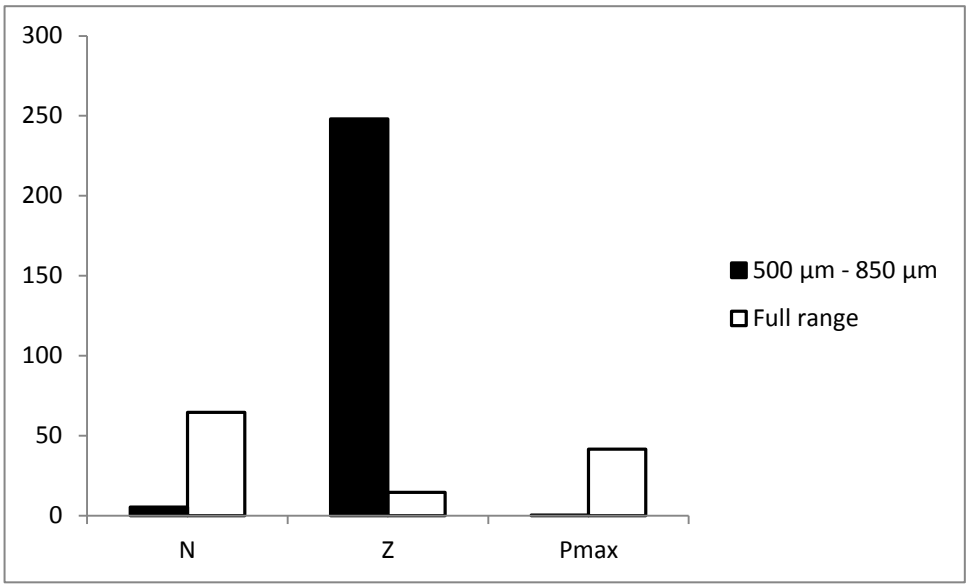

Figure 68: Effect of elimination of the particles smaller than 500 µm on the total number of peaks, total number of zeros and the maximum pressure (MPa) experienced during particle plugging tests using a Mica containing fluid

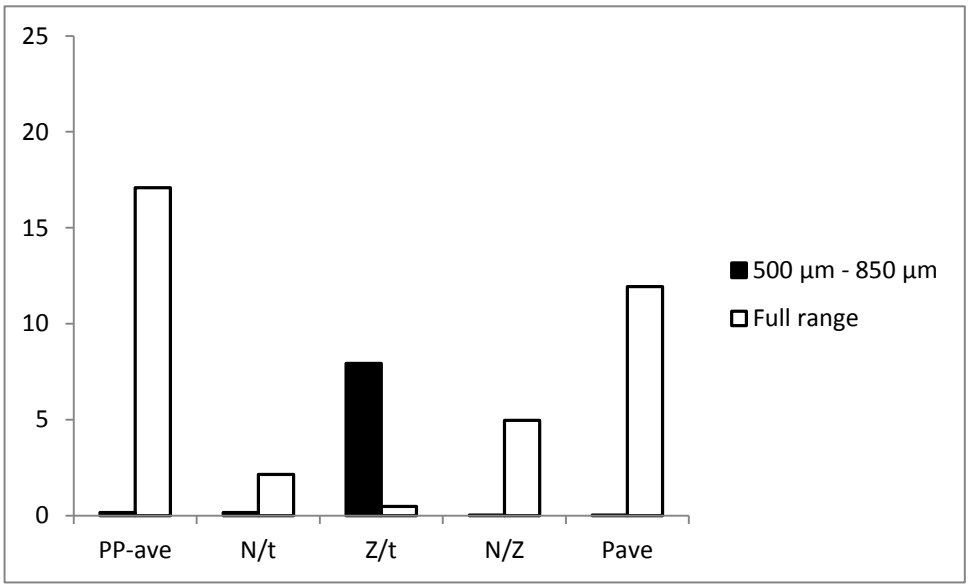

Figure 69: Effect of elimination of the particles smaller than 500 µm on the average peak pressure (MPa), time averaged number of peaks (1/min), time averaged number of zeros (1/min), number of peaks per zero and the average pressure (MPa) experienced in the cell during particle plugging tests using a Mica containing fluid

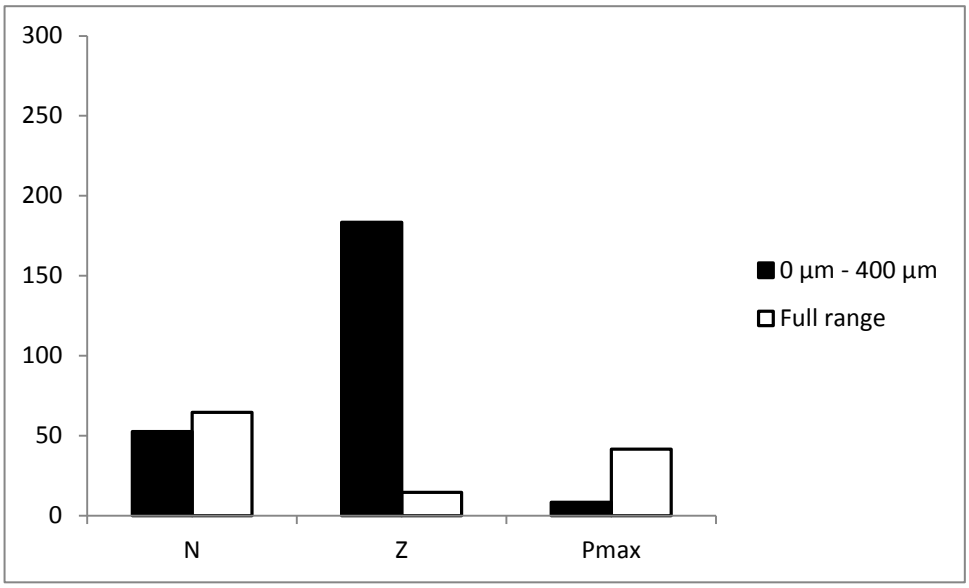

Figure 70: Effect of elimination of the particles larger than 400 µm on the total number of peaks, total number of zeros and the maximum pressure (MPa) experienced during particle plugging tests using a Mica containing fluid

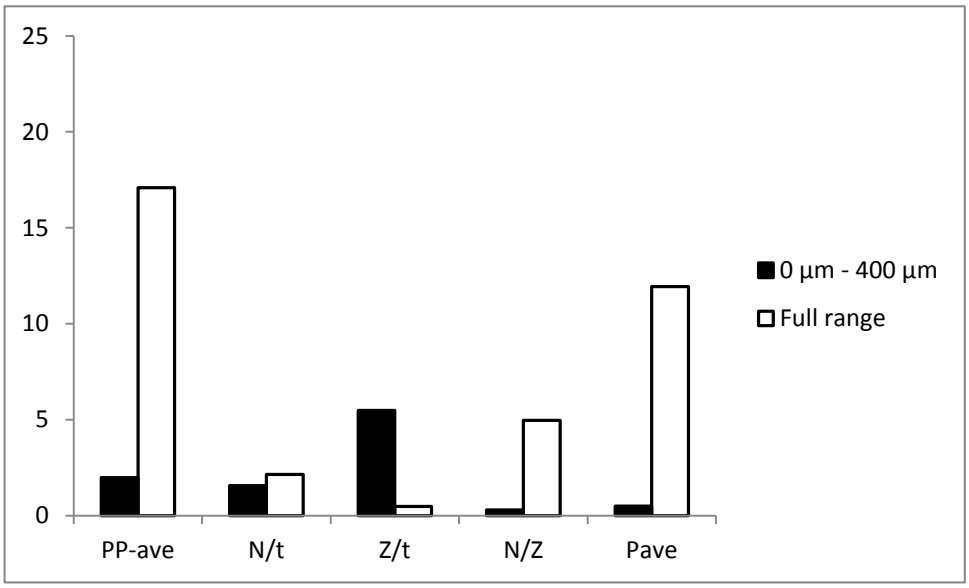

Figure 71: Effect of elimination of the particles larger than 400 µm on the average peak pressure (MPa), time averaged number of peaks (1/min), time averaged number of zeros (1/min), number of peaks per zero and the average pressure (MPa) experienced in the cell during particle plugging tests using a Mica containing fluid

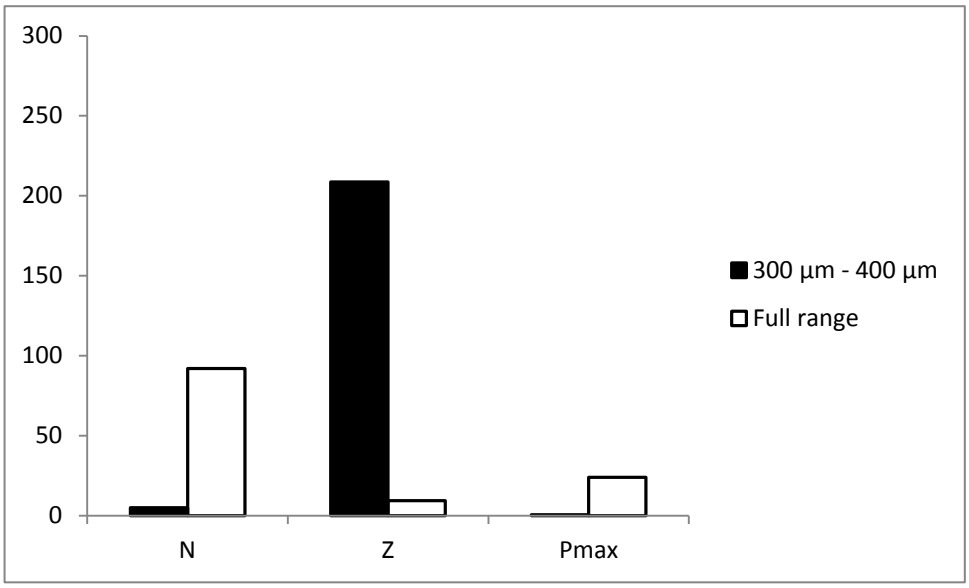

Figure 72: Effect of elimination of the particles larger than 400 µm and smaller than 300 µm on the total number of peaks, total number of zeros and the maximum pressure (MPa) experienced during particle plugging tests using a Resilient Graphite containing fluid

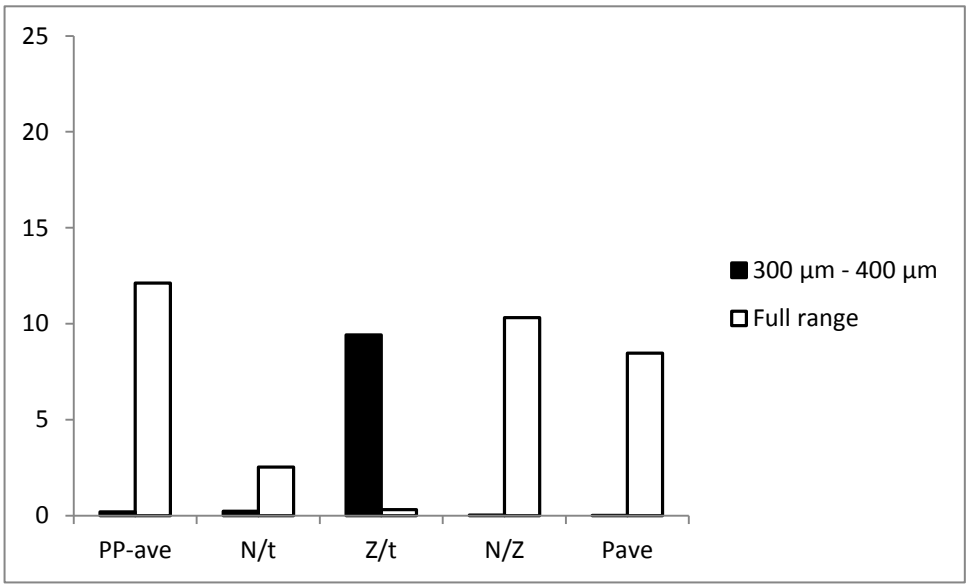

Figure 73: Effect of elimination of the particles larger than 400 µm and smaller than 300 µm on the average peak pressure (MPa), time averaged number of peaks (1/min), time averaged number of zeros (1/min), number of peaks per zero and the average pressure (MPa) experienced in the cell during particle plugging tests using a Resilient Graphite containing fluid

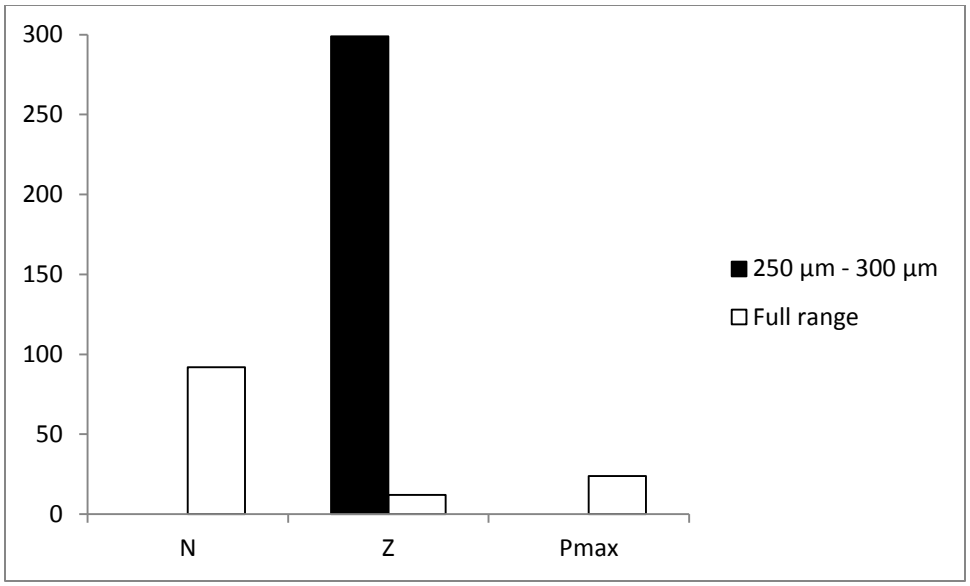

Figure 74: Effect of elimination of the particles larger than 300 µm and smaller than 250 µm on the total number of peaks, total number of zeros and the maximum pressure (MPa) experienced during particle plugging tests using a Resilient Graphite containing fluid

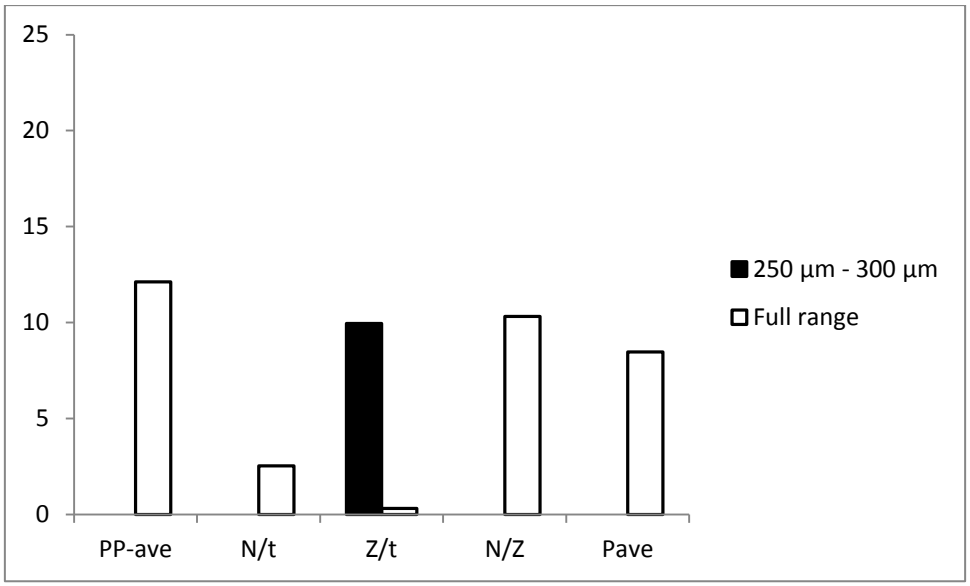

Figure 75: Effect of elimination of the particles larger than 300 µm and smaller than 250 µm on the average peak pressure (MPa), time averaged number of peaks (1/min), time averaged number of zeros (1/min), number of peaks per zero and the average pressure (MPa) experienced in the cell during particle plugging tests using a Resilient Graphite containing fluid

In order to further investigate the importance of each portion of the size range the same values have been plotted in Figures 76 - 91 in order to compare the relative efficiency of each portion in the strengthening process. Figures 76 - 83 illustrate the comparison of the parameters for Resilient Graphite containing fluids and Figures 84 - 91 show the same comparison for Mica containing fluids. Results have been categorized based on the type of the LCM to eliminate the factor of particle type in the analysis.

Comparison of the strengthening capabilities of fluids with eliminated particle size ranges results in a fundamental understanding of the strengthening mechanism. In addition to the fact that the fluid with the full size range of particles gives the best results, it was realized that particles that are smaller than a certain size above the fracture opening size are most essential for forming a resistant plug. This is because they get the chance to enter the fracture and form a plug at the fracture mouth while the particles that are much larger than the fracture, can just form an external sealing over the opening as shown in Figure 93. In static tests such as the particle plugging tests external sealing leads to higher strength of the bridge. However, the conditions might be different in real cases, where the vibration of the drill pipe and the fluid velocity can erode off the external sealing or limit its growth. This is the main reason the fluids which contain LCMs in the size range of 500 μm to 850 μm could form fairly resistant bridges as shown in the figures. However, they are able to form fewer bridges than fluids which particles in the size range of 300 μm to 400 μm.

In Figure 92, the findings of the latter series of experiments of this section are summarized. There is a critical particle size above which the particles cannot enter the opening and thus do not contribute to the plugging mechanism ($D_{P\text{-}max}$). This critical size is usually slightly higher than the fracture width (W_f). As previously explained, particles which are significantly larger than the opening size, form an external seal over the opening in static tests. However in dynamic tests, this external seal may not be as efficient. Figure 93 schematically shows how particles isolate the fractures from the cell pressure in a particle plugging test.

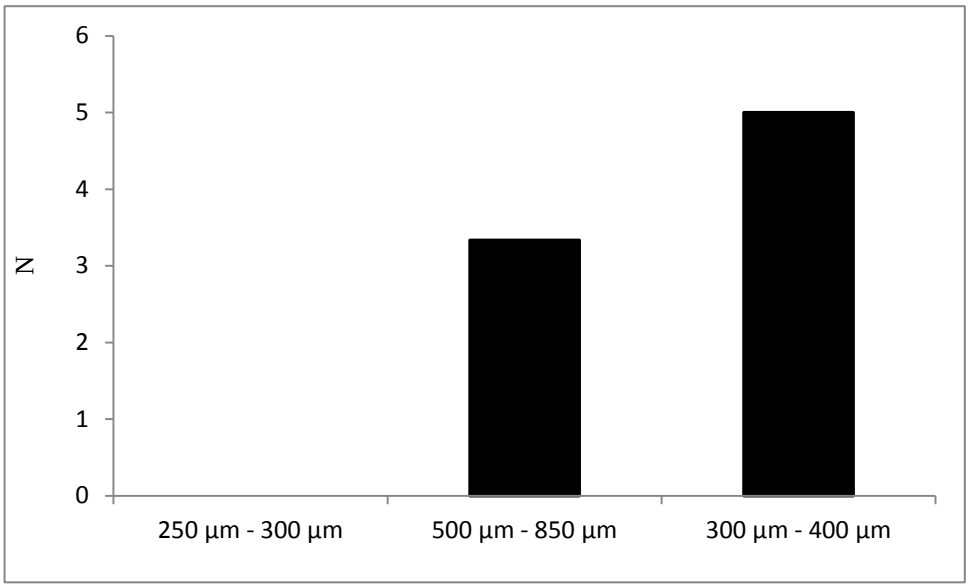

Figure 76: Total number of peaks for Resilient Graphite containing fluids with various particle size ranges

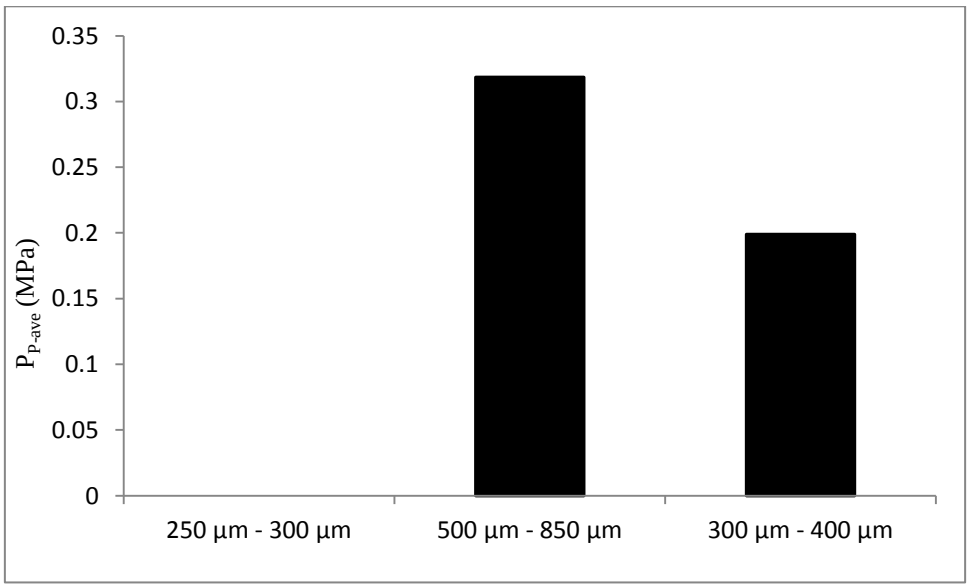

Figure 77: Average peak pressure for Resilient Graphite containing fluids with various particle size ranges

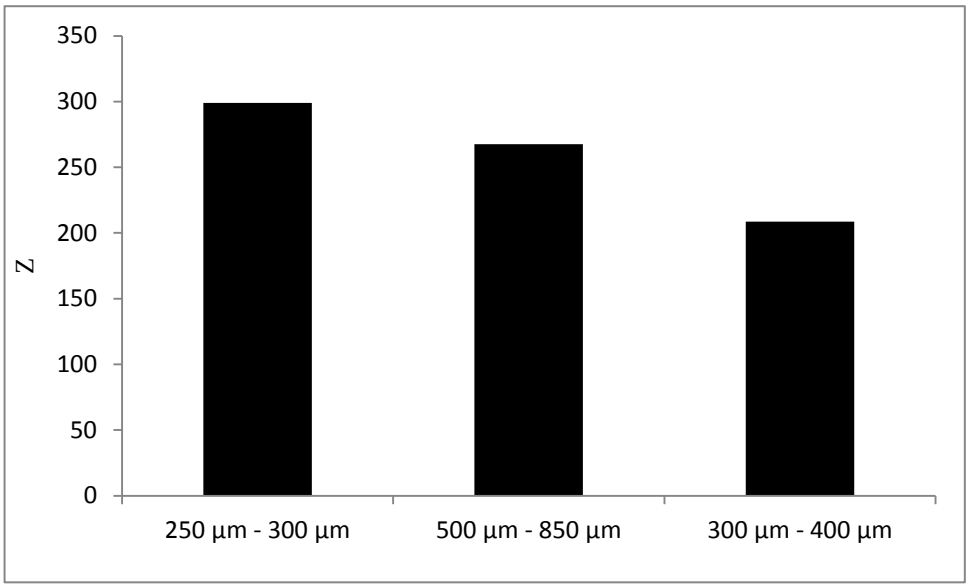

Figure 78: Total number of zeros for Resilient Graphite containing fluids with various particle size ranges

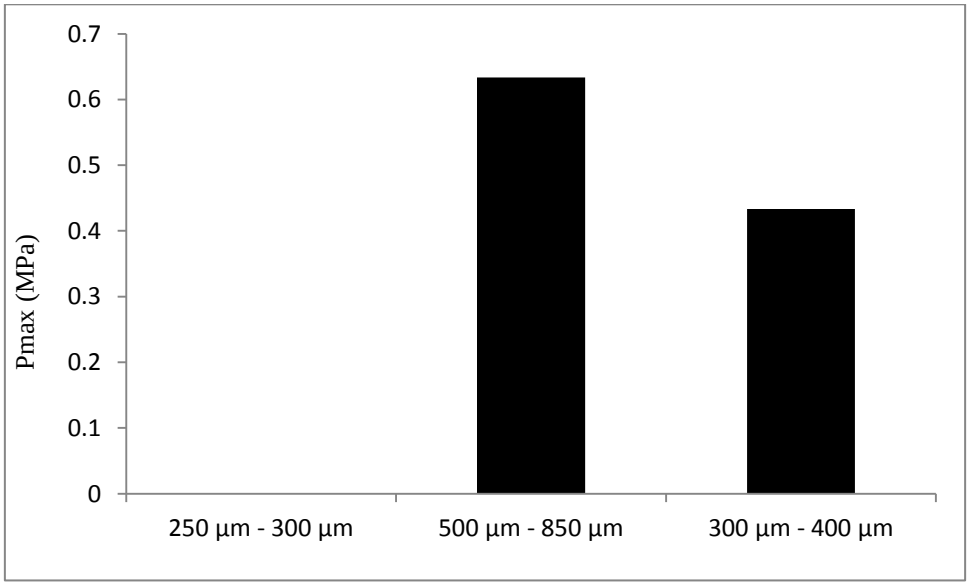

Figure 79: Maximum pressure values for Resilient Graphite containing fluids with various particle size ranges

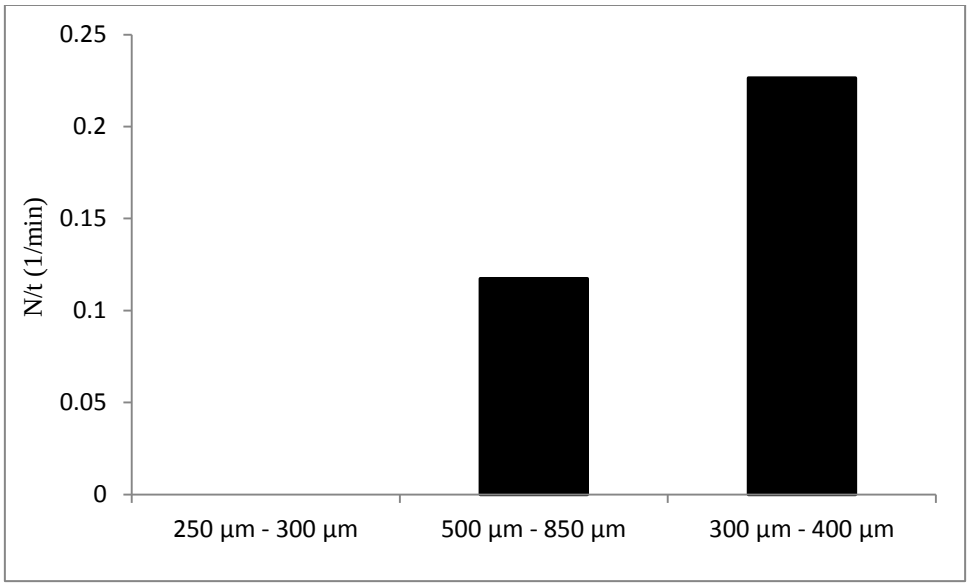

Figure 80: Time averaged number of peaks for Resilient Graphite containing fluids with various particle size ranges

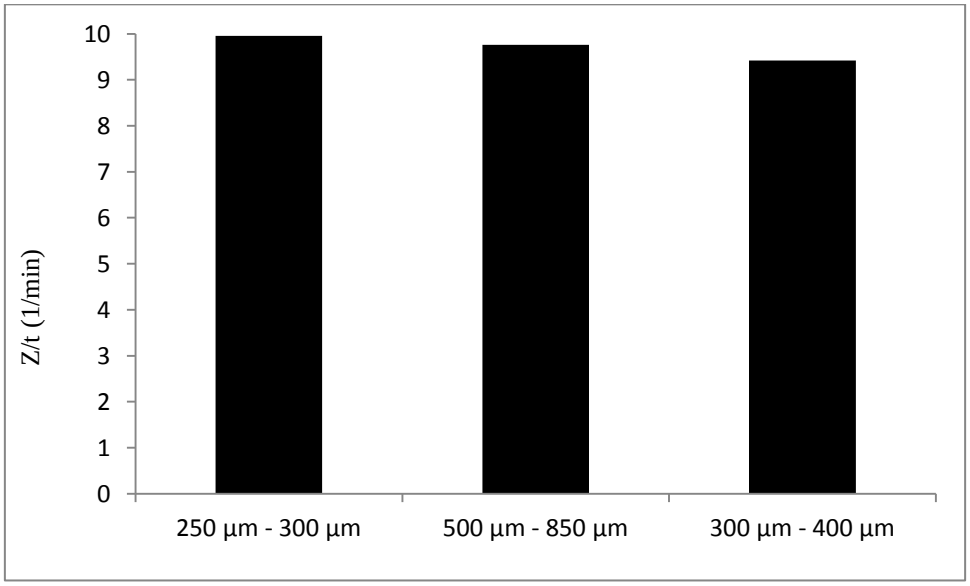

Figure 81: Time averaged number of zeros for Resilient Graphite containing fluids with various particle size ranges

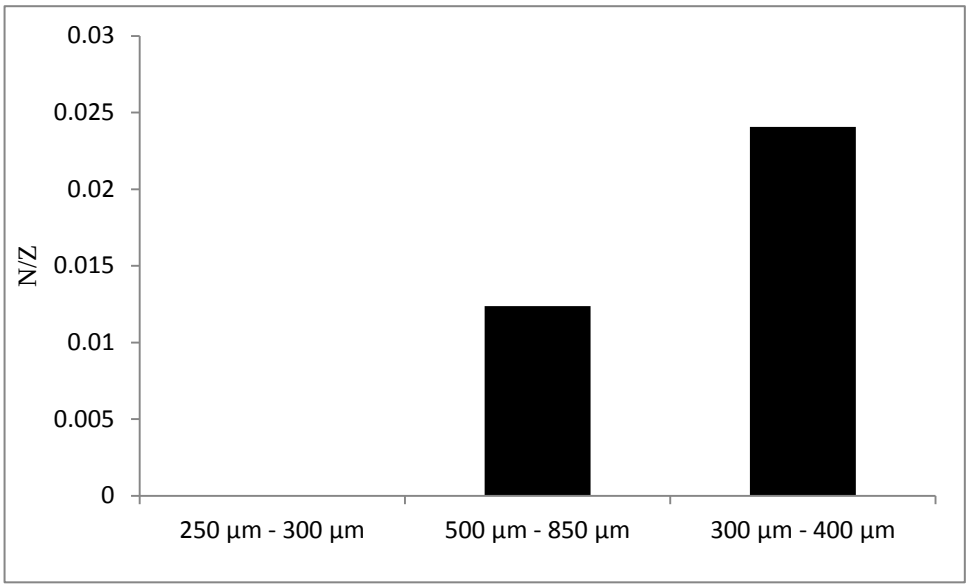

Figure 82: Number of peaks per zero values for Resilient Graphite containing fluids with various particle size ranges

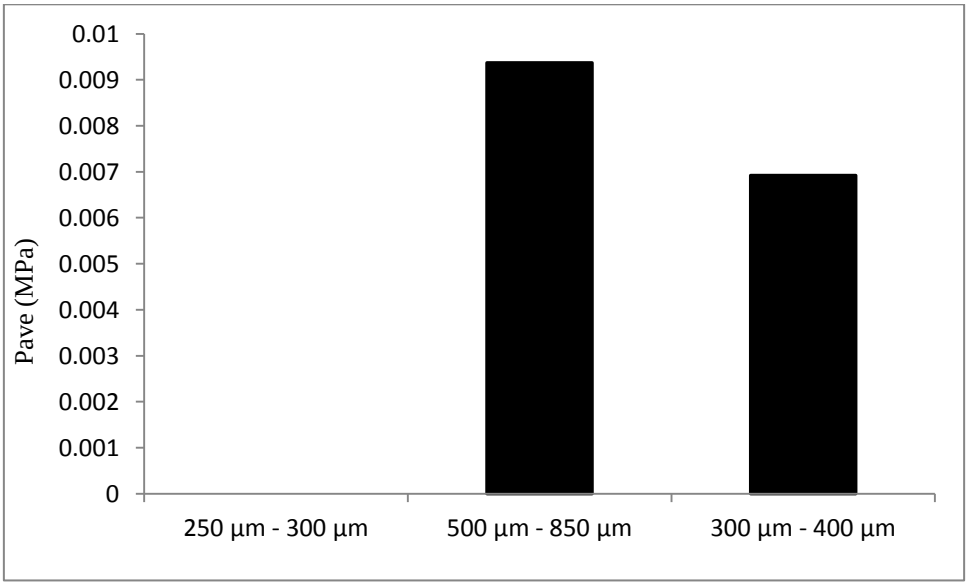

Figure 83: Average pressure values for Resilient Graphite containing fluids with various particle size ranges

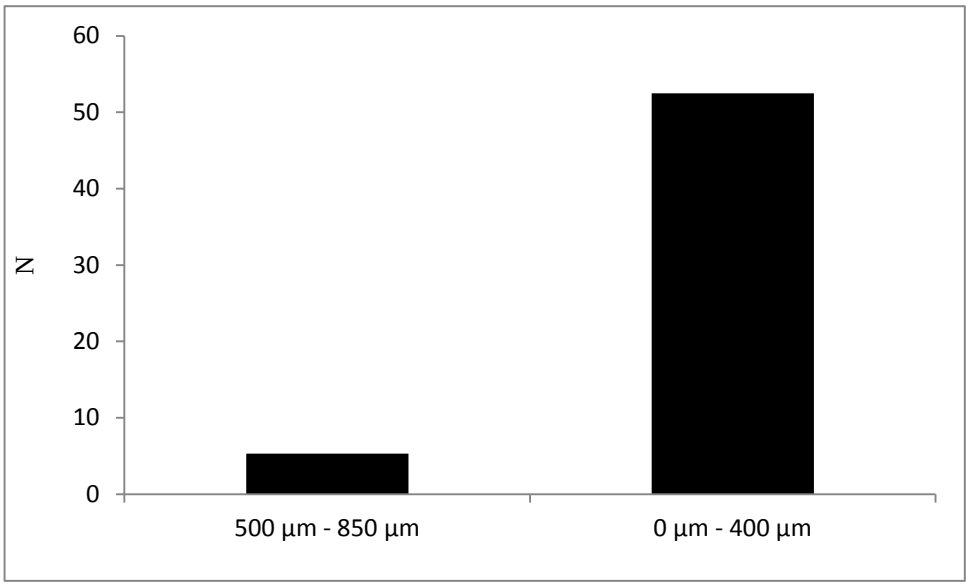

Figure 84: Total number of peaks for Mica containing fluids with various particle size ranges

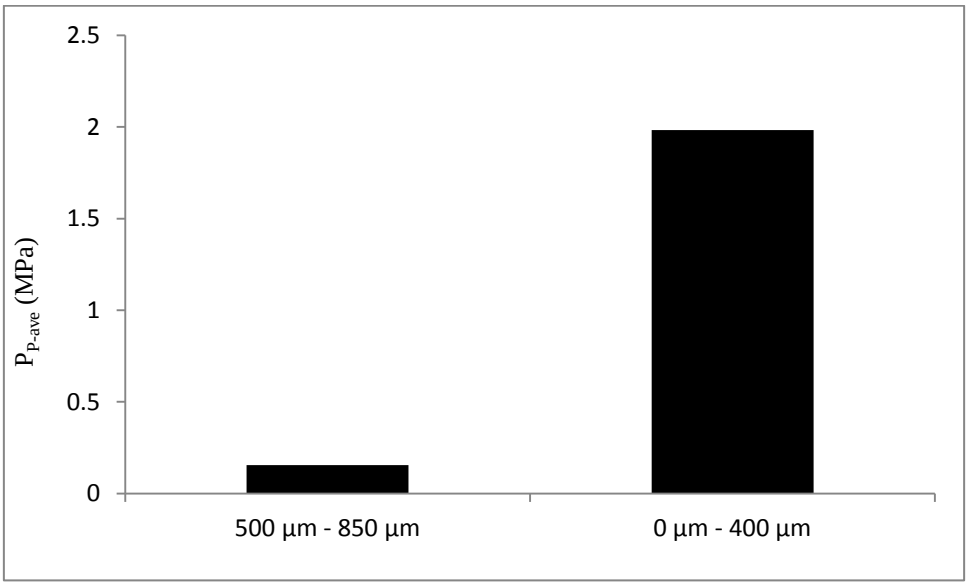

Figure 85: Average peak pressure values for Mica containing fluids with various particle size ranges

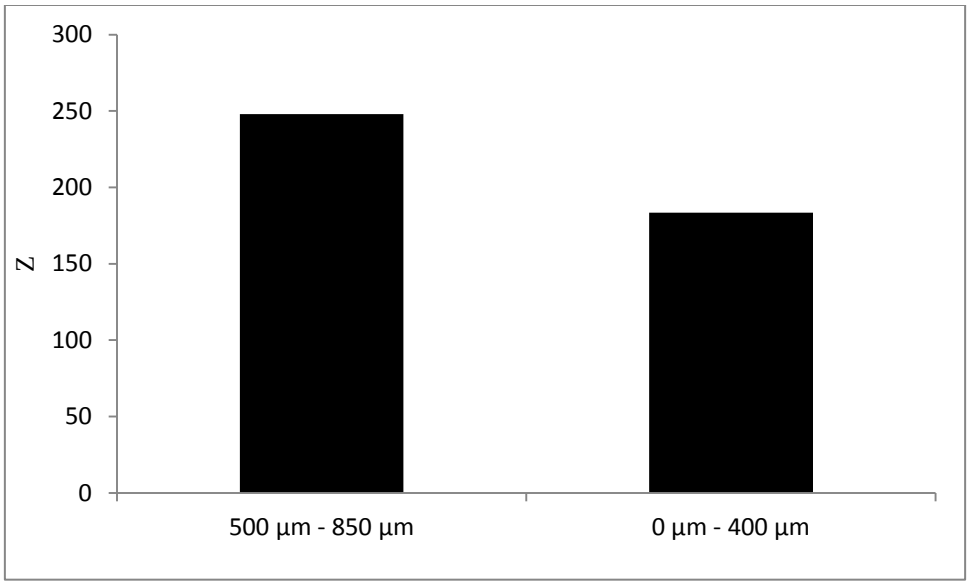

Figure 86: Total number of Zeros for Mica containing fluids with various particle size ranges

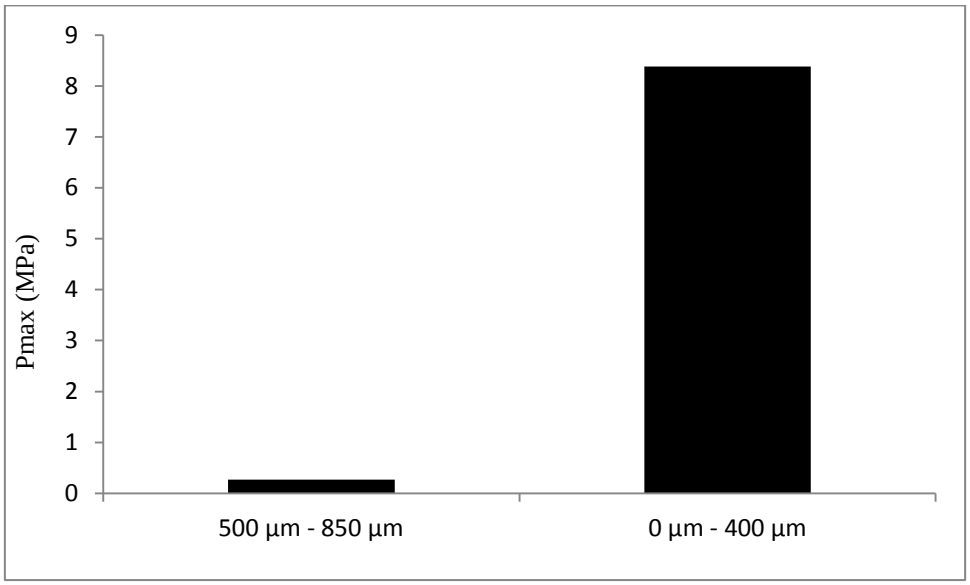

Figure 87: Maximum pressure values for Mica containing fluids with various particle size ranges

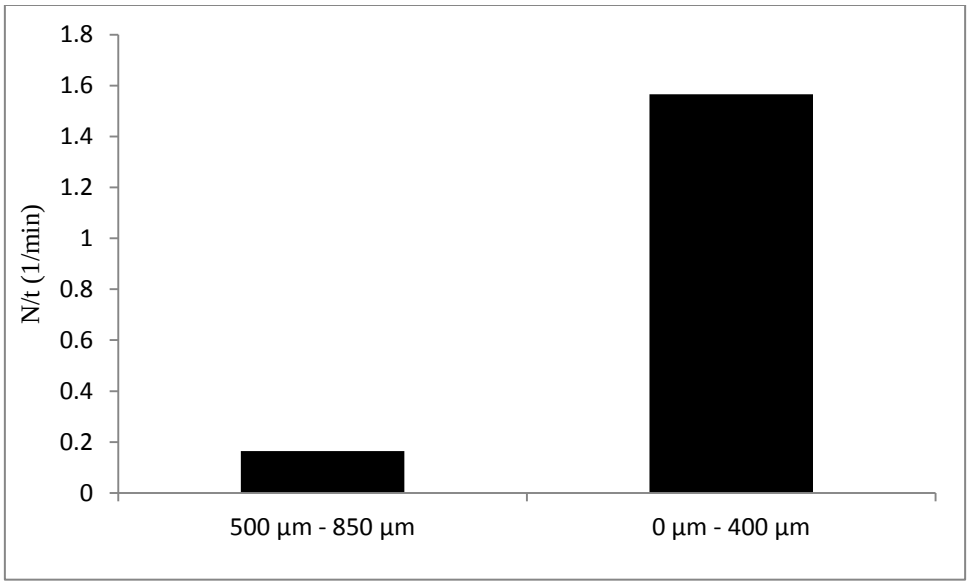

Figure 88: Time averaged number of peaks for Mica containing fluids with various particle size ranges

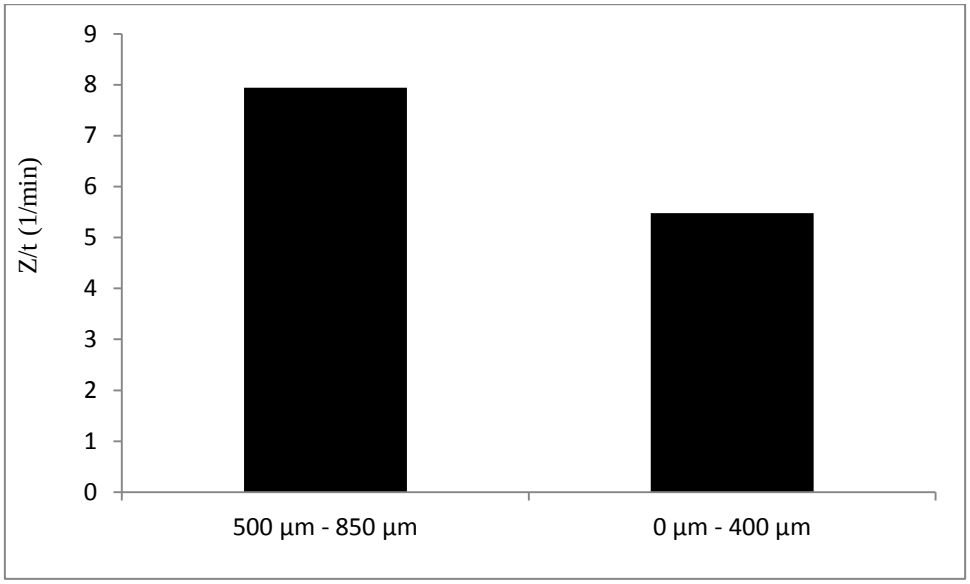

Figure 89: Time averaged number of zeros for Mica containing fluids with various particle size ranges

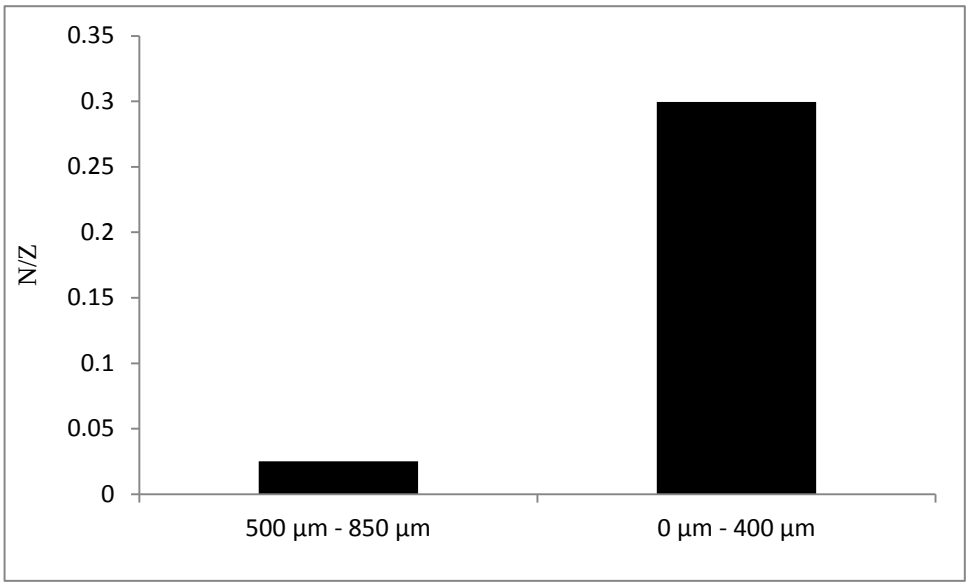

Figure 90: Number of peaks per zero values for Mica containing fluids with various particle size ranges

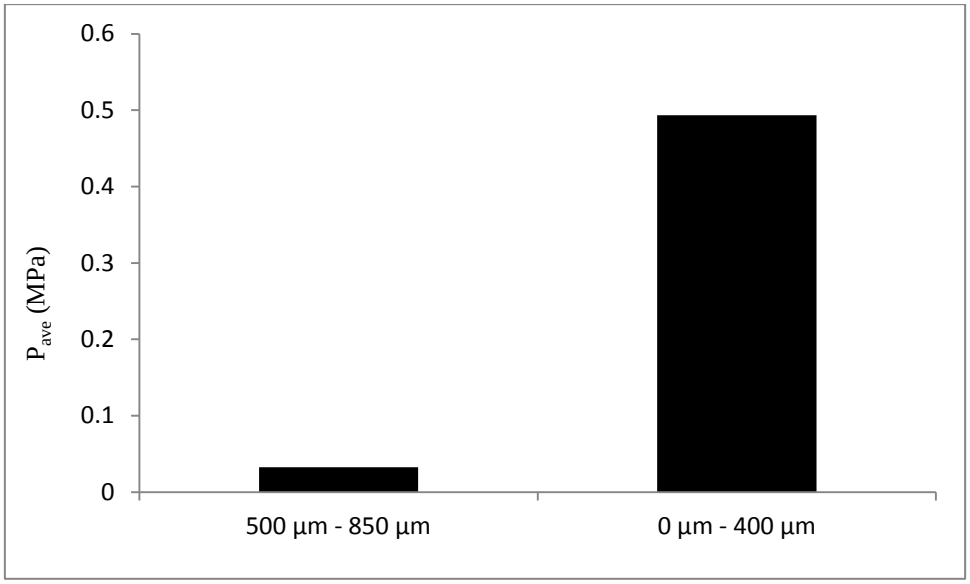

Figure 91: Average pressure values for Mica containing fluids with various particle size ranges

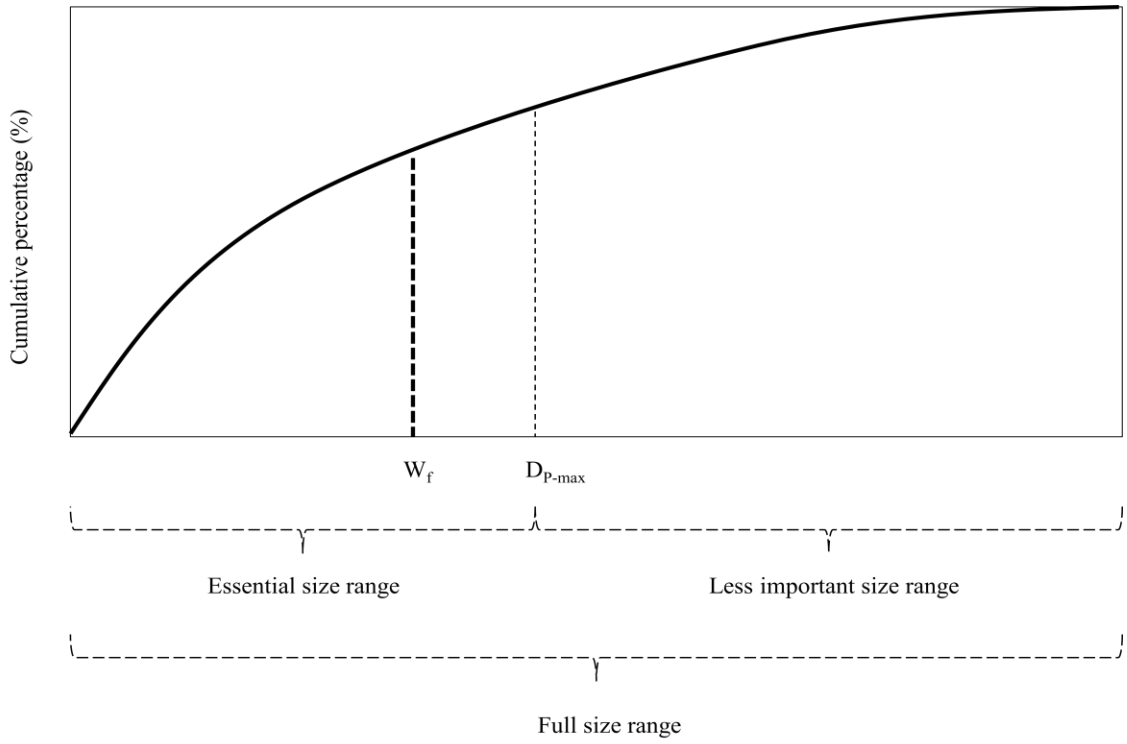

Figure 92: Schematic illustration of contribution of particle size ranges to the strengthening process

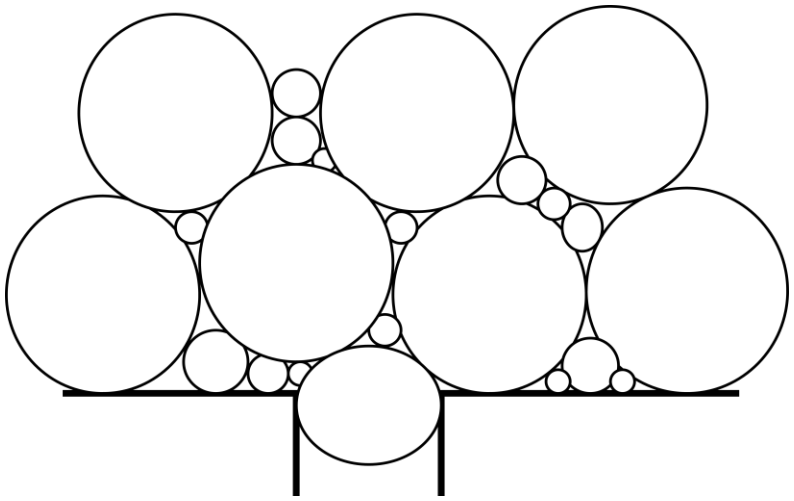

Figure 93: Schematic illustration of plugging and sealing during particle plugging tests

3.5.3.3. Effect of friction

As discussed in the previous section, particles that are close to the fracture width in size, contribute significantly to the plugging mechanism. In order to prove this theory, a series of tests were designed using fracture planes with wrinkled surfaces to increase the friction coefficient. Should the plugging mechanism govern the strengthening process then the wrinkled fractures must enhance the strength of the bridge. The wrinkles were orders of magnitude smaller than the fracture size and therefore did not significantly change the opening size. The tests were carried out using a 500 μm wide fracture. One of the fluids contained Resilient Graphite and the other contained Mica as the LCM. Results are presented in Figures 94 - 97. Except for the total number of peaks for a Mica containing fluid, the rest of the findings indicate a severe enhancement in the strengthening capacity of the fluid. However, in this case the strengthening is modified by making changes to the fracture surface and no alteration has been done to the fluid. Higher friction coefficient does not allow for easy removal of the particles and higher pressure values is required to remove the plug. This conclusion also strongly supports the theory of a governing plugging mechanism during wellbore strengthening processes.

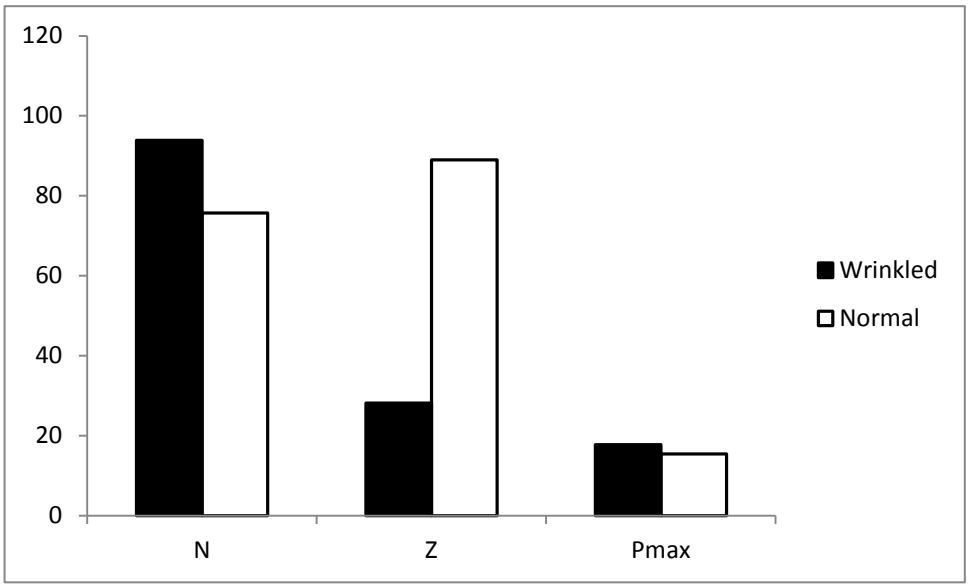

Figure 94: Effect of wrinkled fracture surfaces on total number of peaks, total number of zeros and maximum pressure values (MPa) during particle plugging tests using a Resilient Graphite containing fluid

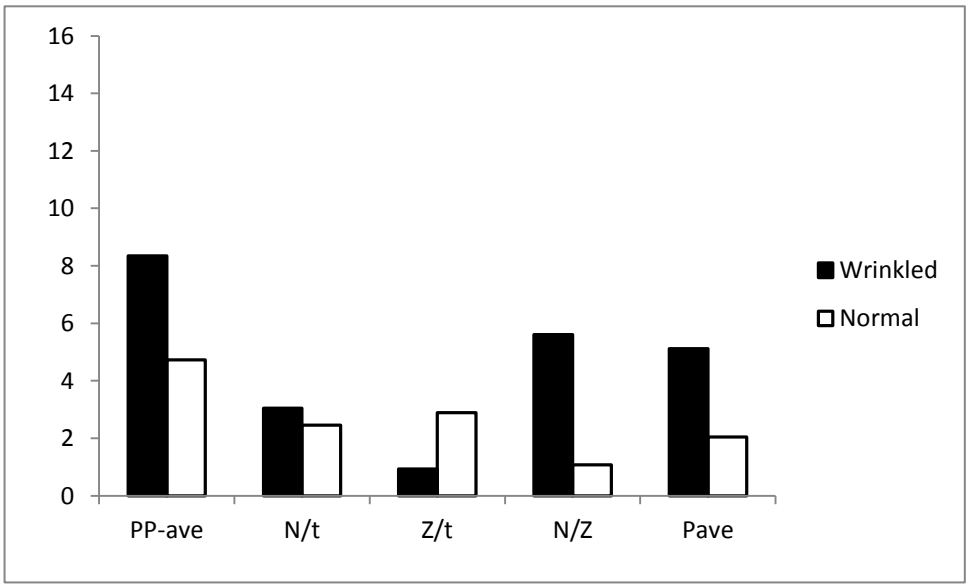

Figure 95: Effect of wrinkled fracture surfaces on average peak pressure values (MPa), time averaged number of peaks (1/min), time averaged number of zeros (1/min), average peak per zero values and average pressure values (MPa) during particle plugging tests using a Resilient Graphite containing fluid

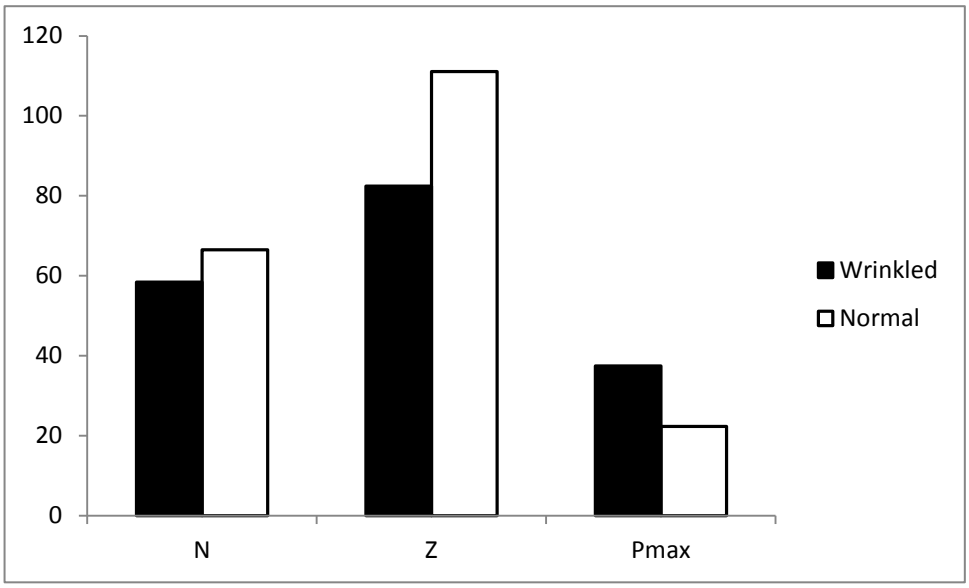

Figure 96: Effect of wrinkled fracture surfaces on total number of peaks total number of zeros and maximum pressure values (MPa) during particle plugging tests using a Mica containing fluid

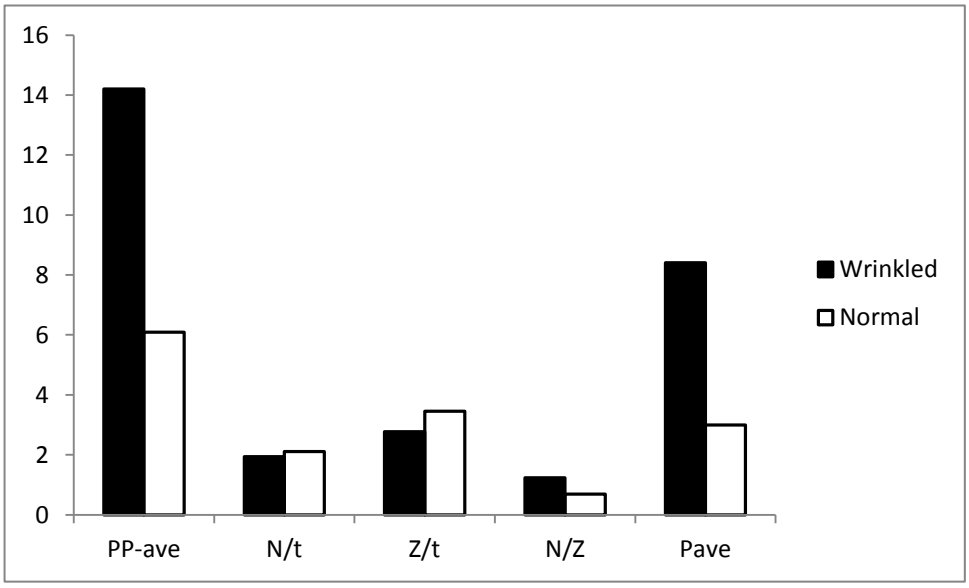

Figure 97: Effect of wrinkled fracture surfaces on average peak pressure values (MPa), time averaged number of peaks (1/min), time averaged number of zeros (1/min), average peak per zero values and average pressure values (MPa) during particle plugging test using a Mica containing fluid

3.5.3.4. Effect of solids concentration

Solids concentration of the fluid describes how many particles are available in the vicinity of the fracture mouth to perform the bridging process. Some researchers have stated that a critical solids concentration exists above which no significant improvement occurs in the strengthening capability of the fluid. In the current work, two concentrations of 8.49 lb/bbl (24.25 kg/m3) and 33.16 lb/bbl (94.70 kg/m3) were selected to be compared with the results using a fluid with a concentration equal to 16.85 lb/bbl (48.11 kg/m3). In the figures, they have been referred to as the high concentration, low concentration and normal concentration, respectively. Resilient Graphite, Mica, mixture of Resilient Graphite and Mica, mixture of Resilient Graphite, Mica and Solu-Flake, and mixture of Resilient Graphite, Mica and Fiber were selected as the LCMs. Particle plugging tests were performed using a 500 μm wide fracture. The results are presented in Figures 98 - 107.

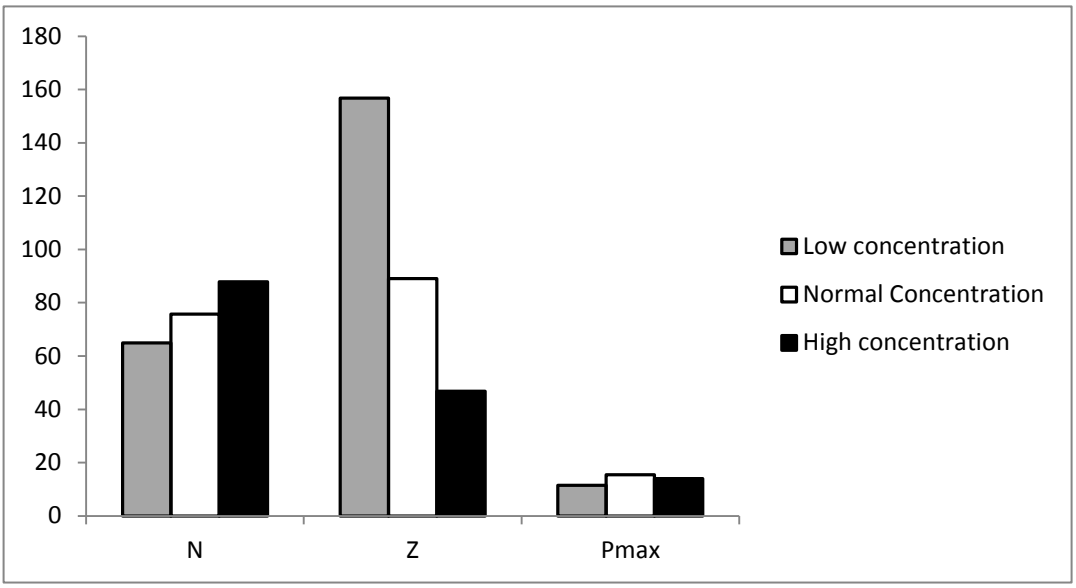

Figure 98: Impact of concentration on the total number of peaks, total number of zeros and the maximum pressure (MPa) during particle plugging tests using a Resilient Graphite containing fluid

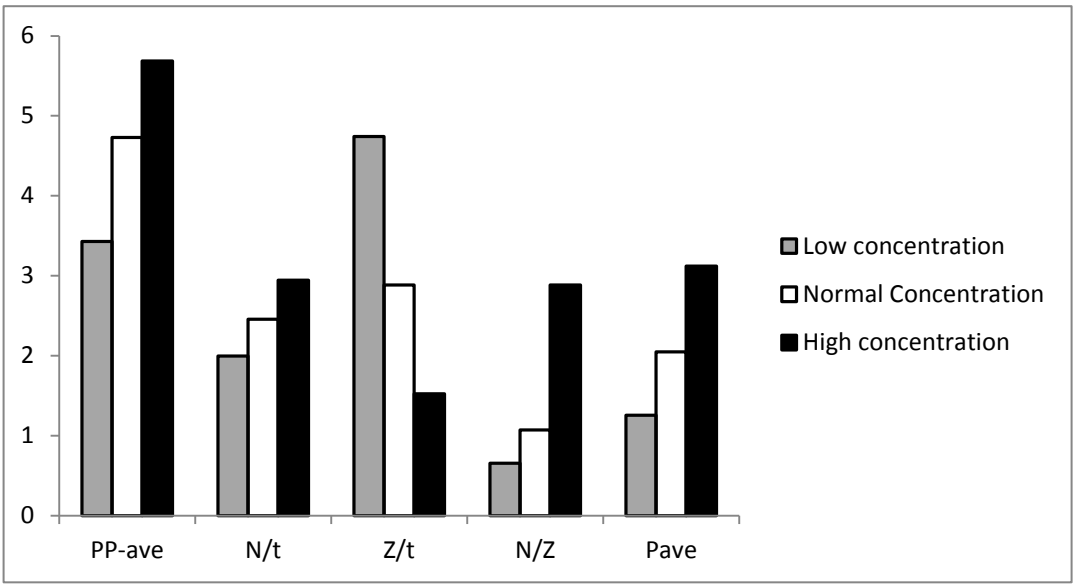

Figure 99: Impact of concentration on the average peak pressure (MPa), time averaged number of peaks (1/min), time averaged number of zeros (1/min), average number of peaks per zero values and the average pressure (MPa) during particle plugging tests using a Resilient Graphite containing fluid

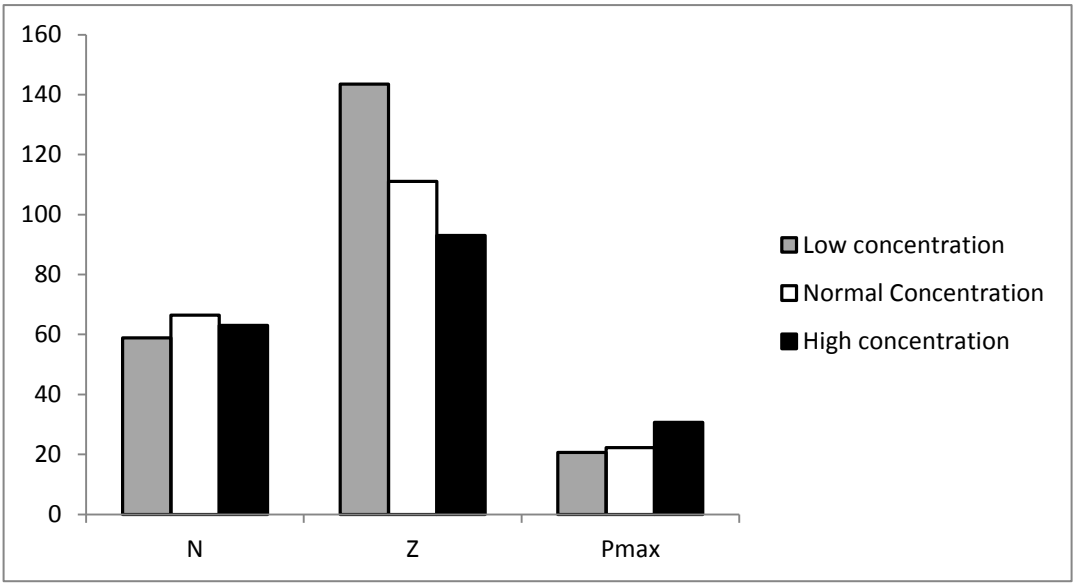

Figure 100: Impact of concentration on the total number of peaks, total number of zeros and the maximum pressure (MPa) during particle plugging tests using a Mica containing fluid

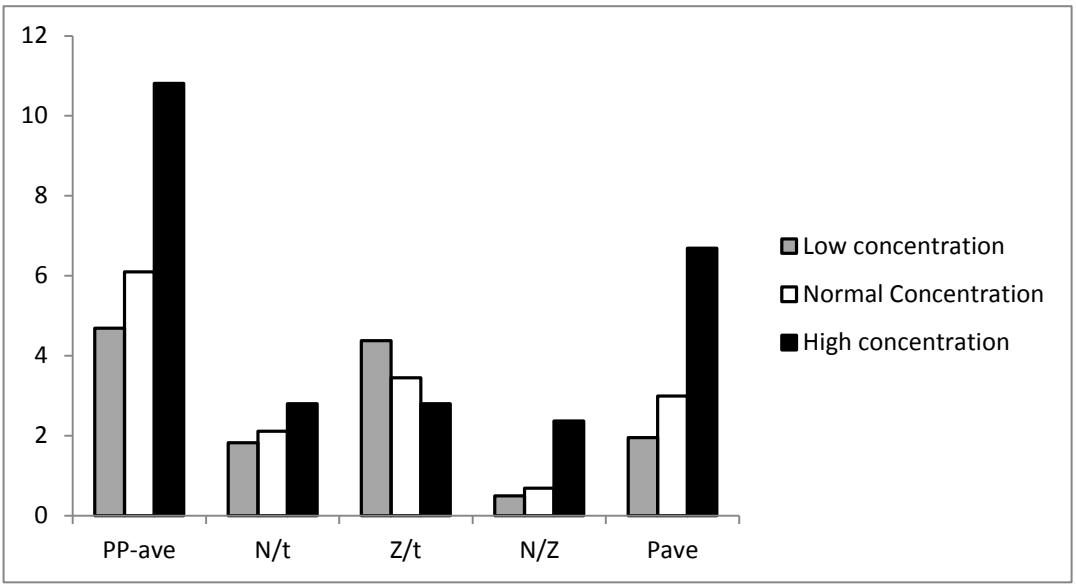

Figure 101: Impact of concentration on the average peak pressure (MPa), time averaged number of peaks (1/min), time averaged number of zeros (1/min), average number of peaks per zero values and the average pressure (MPa) during particle plugging tests using a Mica containing fluid

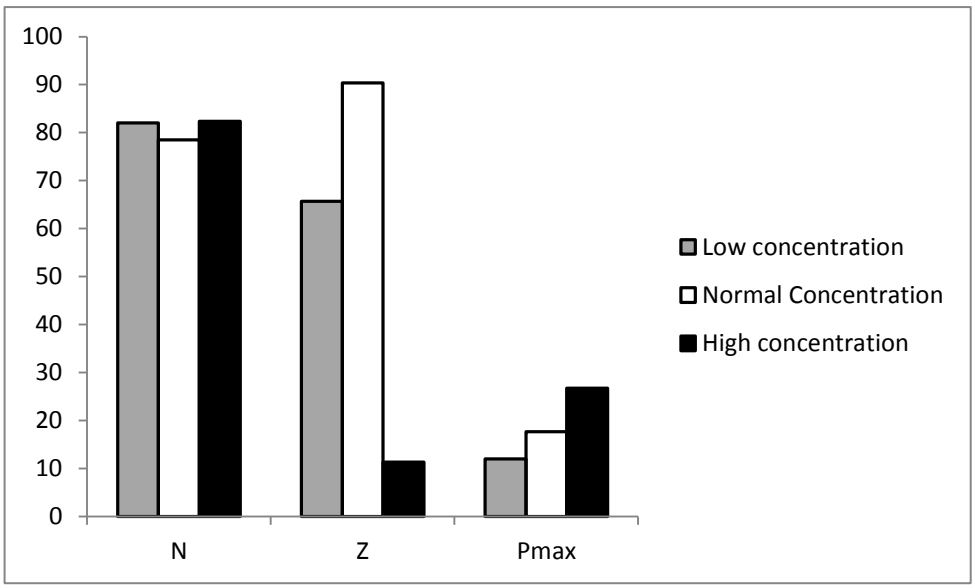

Figure 102: Impact of concentration on the total number of peaks, total number of zeros and the maximum pressure (MPa) during particle plugging tests using a Resilient Graphite and Mica containing fluid

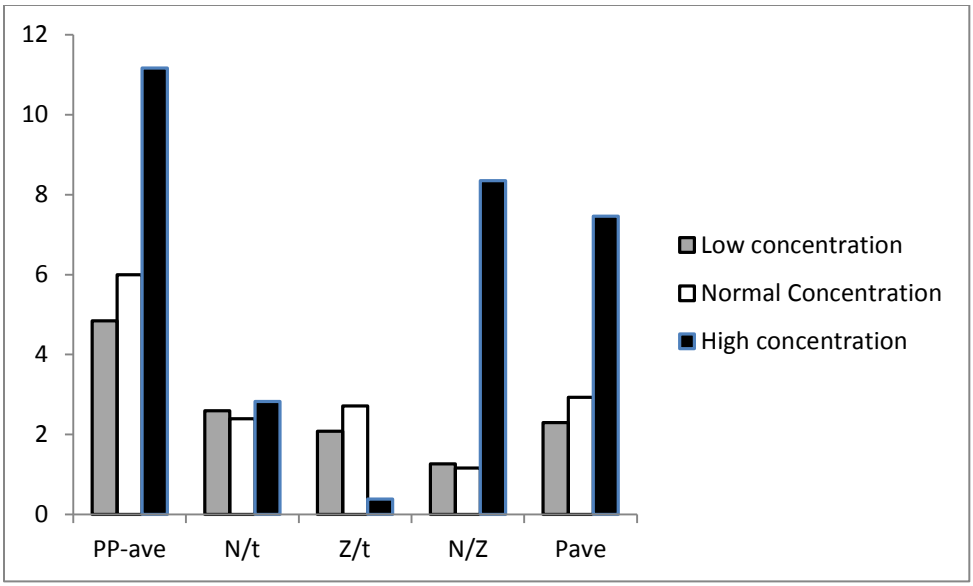

Figure 103: Impact of concentration on the average peak pressure (MPa), time averaged number of peaks (1/min), time averaged number of zeros (1/min), average number of peaks per zero values and the average pressure (MPa) during particle plugging tests using a Resilient Graphite and Mica containing fluid

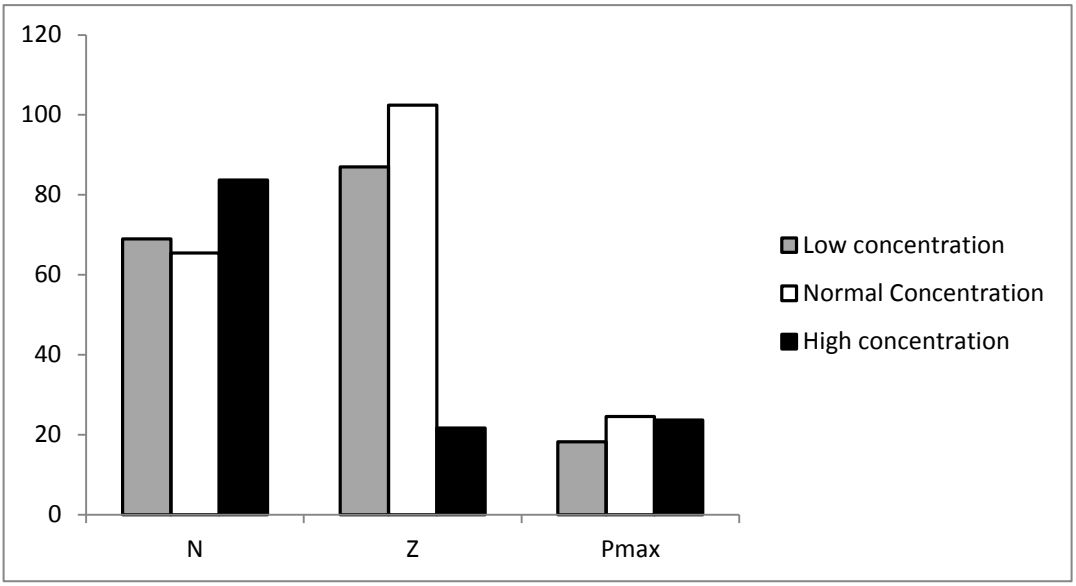

Figure 104: Impact of concentration on the total number of peaks, total number of zeros, and the maximum pressure (MPa) during particle plugging tests using a Resilient Graphite, Mica and Solu-Flake containing fluid

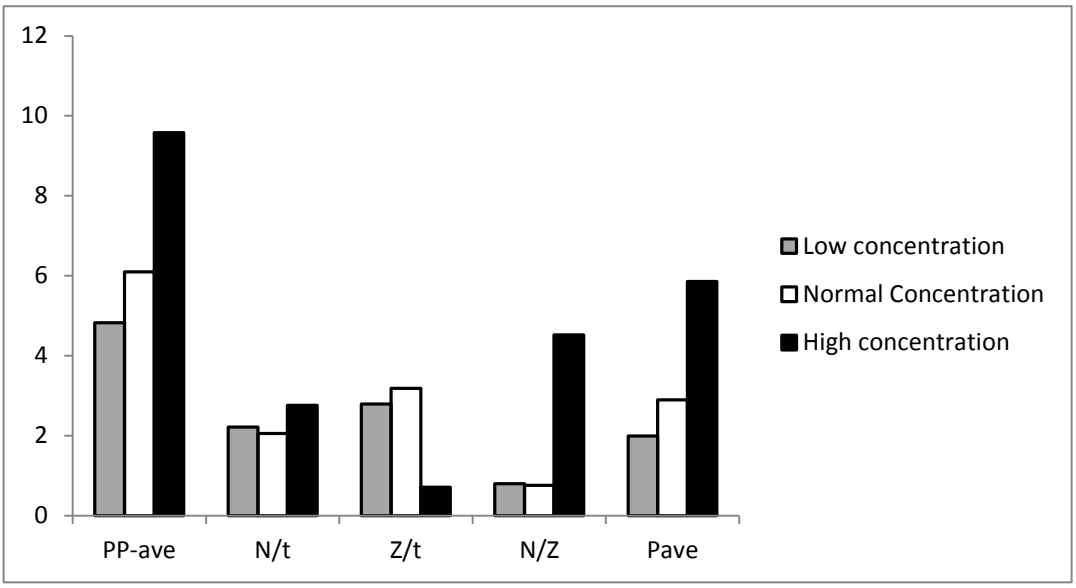

Figure 105: Impact of concentration on the average peak pressure (MPa), time averaged number of peaks (1/min), time averaged number of zeros (1/min), average number of peaks per zero values and the average pressure (MPa) during particle plugging tests using a Resilient Graphite, Mica and Solu-Flake containing fluid

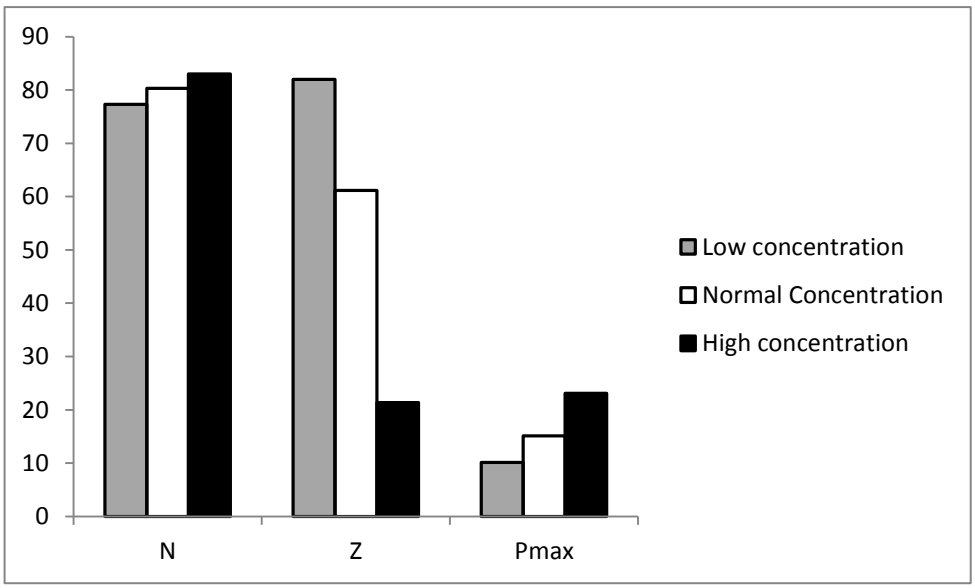

Figure 106: Impact of concentration on the total number of peaks, total number of zeros and the maximum pressure (MPa) during particle plugging tests using a Resilient Graphite, Mica and Fiber containing fluid

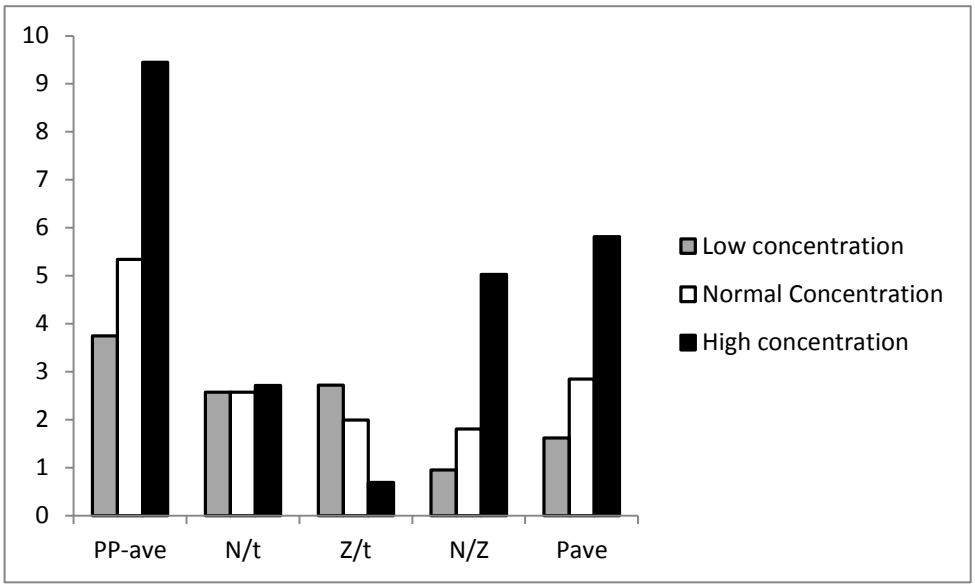

Figure 107: Impact of concentration on the average peak pressure (MPa), time averaged number of peaks (1/min), time averaged number of zeros (1/min), average number of peaks per zero values and the average pressure (MPa) during particle plugging tests using

With the exception of total number of peaks for a mica containing fluid, solids concentration has a positive impact on the strengthening capability of all types of tested fluids. No critical limit was encountered in our planned concentration range above which the strength of the bridge declines. For field scale applications, concentration is further limited by the pumping capacity and maximum mud weight.

3.5.3.5. Effect of opening size

Fracture width was studied using three sizes of 300 μm, 500 μm and 700 μm. The results are presented here in Figures 108 -115 for fluids which contained Resilient Graphite. As expected the opening size has a negative effect on the strengthening process when the rest of the parameters are constant.

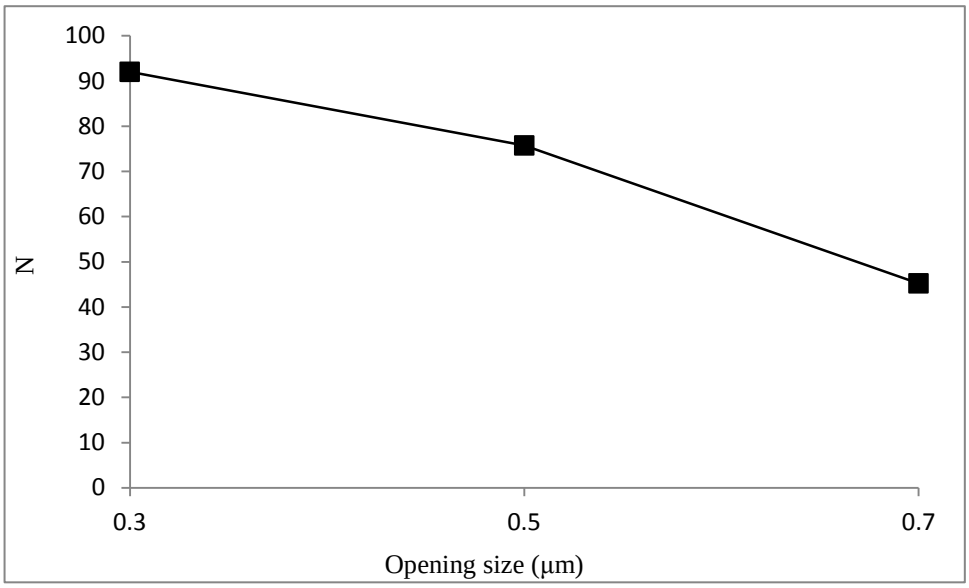

Figure 108: Variation of total number of peaks with respect to the opening size for a Resilient Graphite containing fluid during particle plugging tests

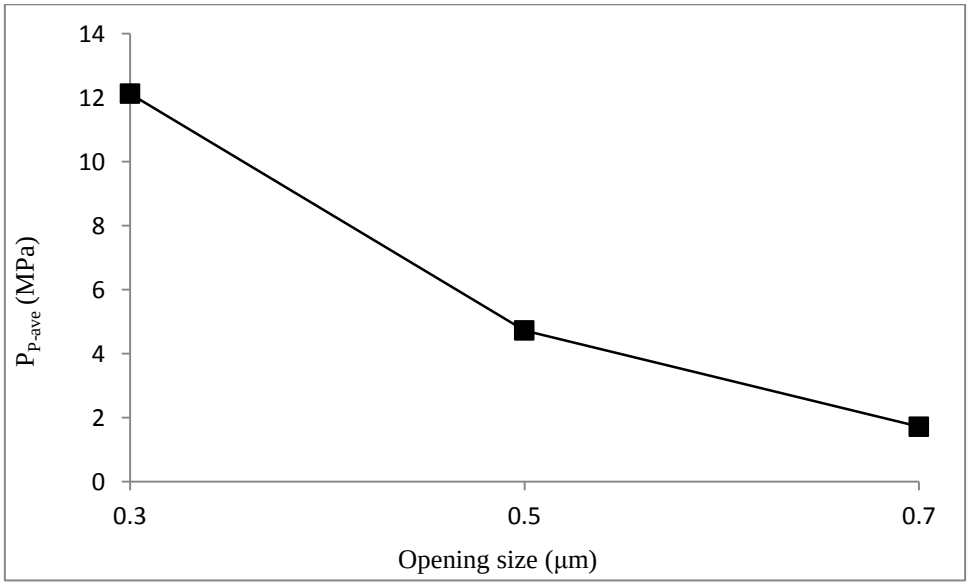

Figure 109: Variation of average peak pressure values with respect to the opening size for a Resilient Graphite containing fluid during particle plugging tests

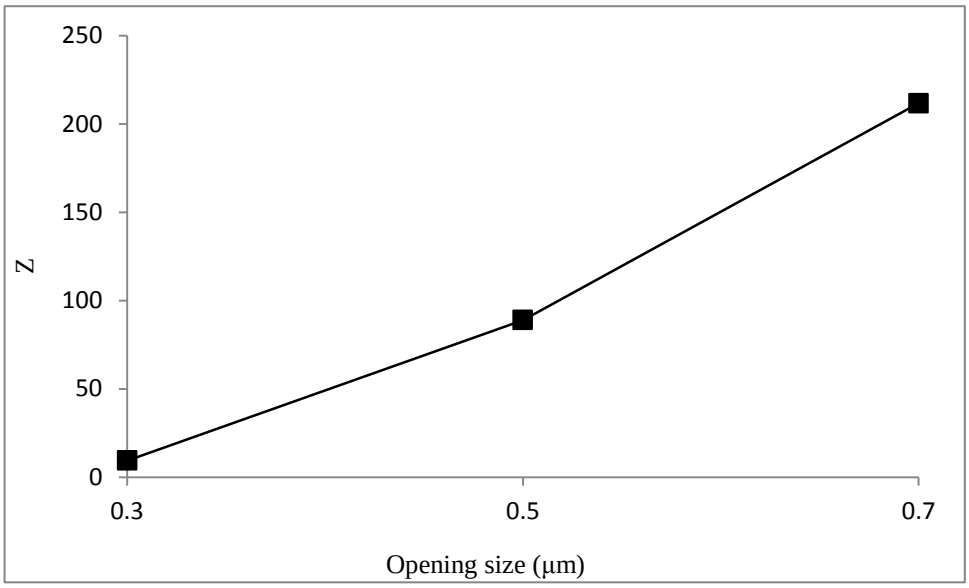

Figure 110: Variation of total number of zeros with respect to the opening size for a Resilient Graphite containing fluid during particle plugging tests

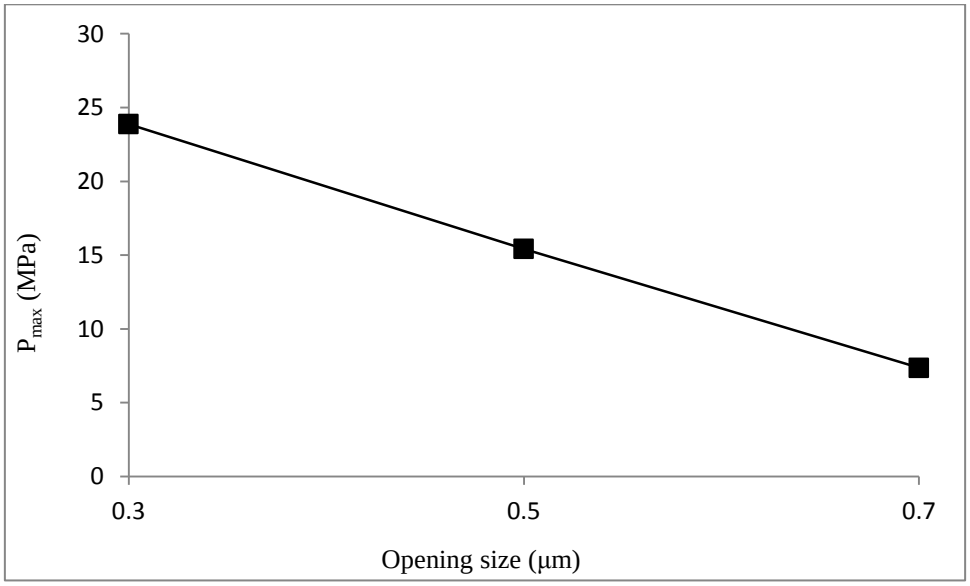

Figure 111: Variation of maximum pressure values with respect to the opening size for a Resilient Graphite containing fluid during particle plugging tests

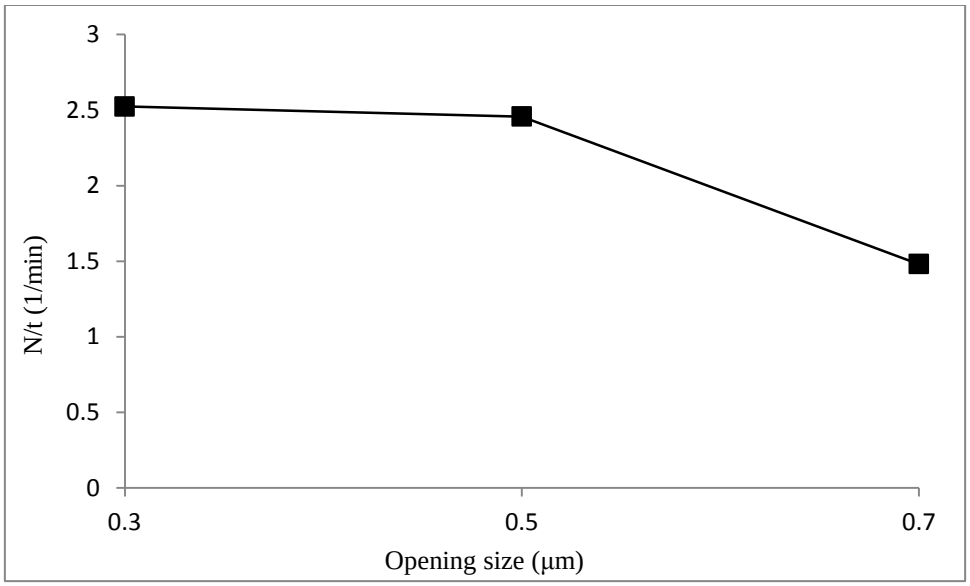

Figure 112: Variation of time averaged number of peaks with respect to the opening size for a Resilient Graphite containing fluid during particle plugging tests

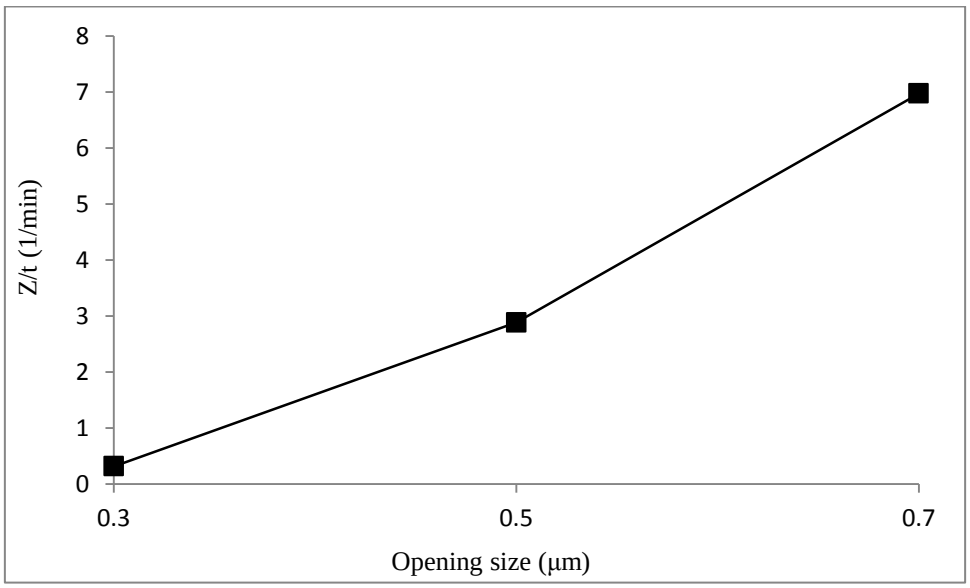

Figure 113: Variation of time averaged number of zeros with respect to the opening size for a Resilient Graphite containing fluid during particle plugging tests

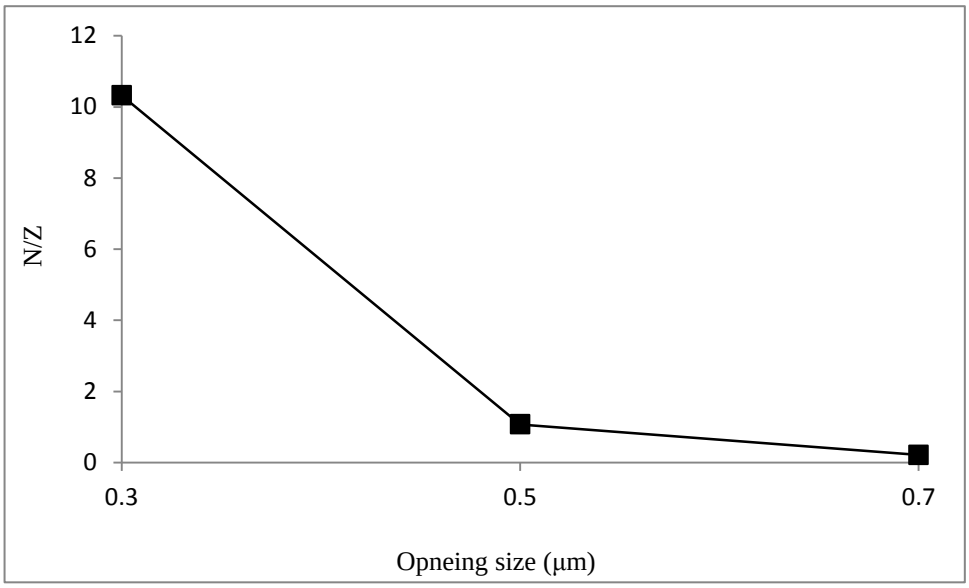

Figure 114: Variation of average number of peaks per zero with respect to the opening size for a Resilient Graphite containing fluid during particle plugging tests

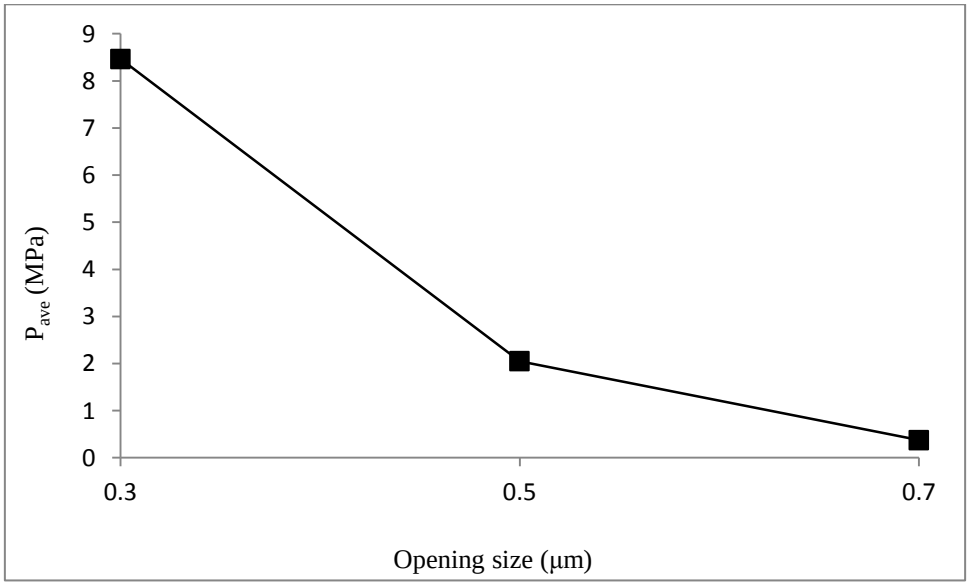

Figure 115: Variation of average pressure values with respect to the opening size for a Resilient Graphite containing fluid during particle plugging tests

3.6. Core fracturing tests

Core fracturing tests were performed using the hollow cylinder system explained in section 3.3 at the University of Stavanger. The system allowed for exerting the desired confining pressure around the core and circulation of drilling fluid in the wellbore prior to increasing the pressure and initiation of tensile fractures. Circulation of the fluid allows for mud cake deposition around the borehole. Three fracturing tests were performed in this stage. The fracturing tests were mainly conducted to inspect if the fracture reopening experiments and core fracturing tests lead to different results. In addition, the correlation of results from the particle plugging tests and core fracturing tests was planned to be examined. Results are shown in Figure 116 and indicate that Resilient Graphite particles exhibit a high strengthening capability when solely mixed in the fluid. This is in consistence with previous findings using Resilient Graphite additive.

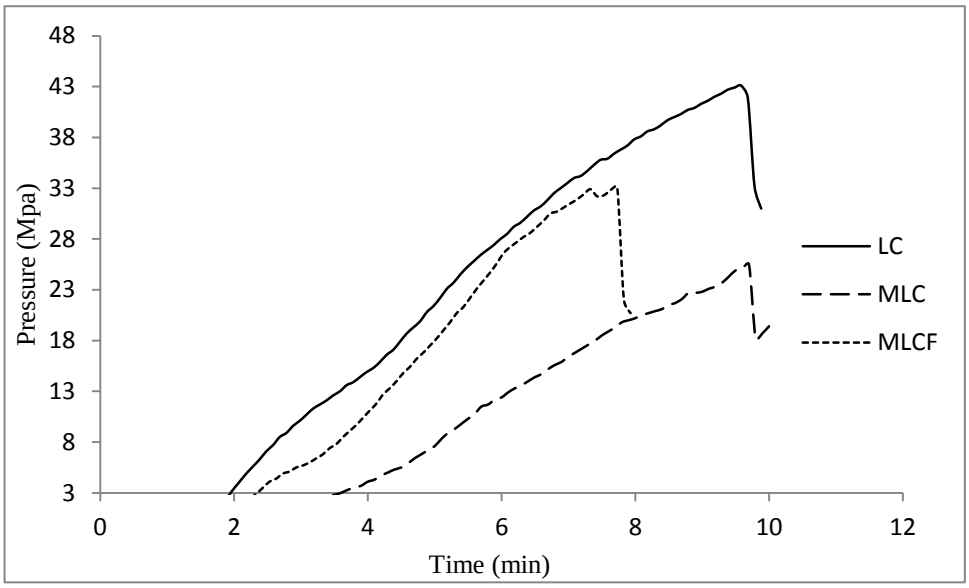

Figure 116: Fracture initiation pressure values of Resilient Graphite containing fluid, Resilient Graphite + Mica containing fluid, and Resilient Graphite + Mica + Fiber containing fluid

In addition, it can be observed that during the fracturing and fracture reopening tests the measured pressure values during the particle plugging tests ($P_{P\text{-}ave}$, P_{ave} and P_{max}) do not correlate

with the fracturing and fracture reopening pressure values. Resilient Graphite particles exhibited a good capability for building bridges over the fractures during the particle plugging tests, but the bridges were weak compared to several other particles. The promising results obtained by the Resilient Graphite containing fluid during the core fracturing and fracture reopening tests show that the experimental limitations of the particle plugging tests and the fact that the back pressure is always equal to atmospheric pressure do not allow for proper simulation of the strengthening process. However, some other parameters such as the average number of peaks per zero (N/Z) reveal the superiority of the Resilient Graphite particles. In other words, the particle plugging test is most reasonable for evaluation of capabilities of particles to build bridges over the fractures rather than average strength of the bridges. Frequent formation of bridges prevents filtration and elevation of fracture pressure in a core fracturing or fracture reopening test. Particles like Solu-Flake allow a significant amount of fluid to enter the opening prior to formation of the bridge. Although the formed bridges made of such particles are remarkably stronger compared to those formed by Resilient Graphite particles in the particle plugging tests, the chance of formation of such bridges are very low in the core fracturing tests. The high filtration increases the fracture pressure and leads to fracture propagation. This concept is presented and explained schematically in Figure 117.

As illustrated in the Figure 117, Resilient Graphite particles build a bridge over the fracture very quickly and stop the fluid leakage from the cell. This is achieved due to their physical and mechanical properties which will be discussed in the next chapter. The granular shape of the Resilient Graphite also assists in filling the gap efficiently. As a result of this process, a thin bridge is formed and the particles may not be very well attached together. On the other hand, Solu-Flake allows for more amounts of filtration to leak out of the cell due to its fiber like shape. Therefore it takes a longer time to form the bridge, which is significantly thicker and stronger than the one formed by the Resilient Graphite particles. This explain the higher N, N/t and N/Z and lower P_{ave}, P_{max}, and $P_{P\text{-}ave}$ for Resilient Graphite containing fluids compared to the ones which contain Solu-Flake particles.

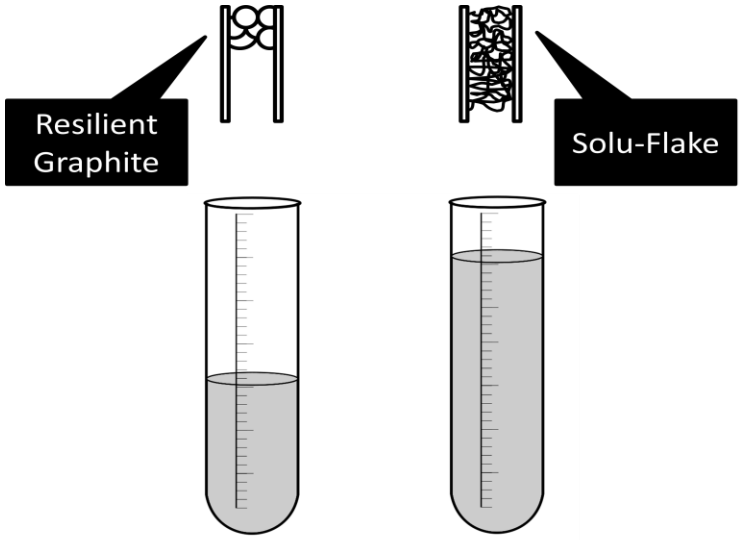

Figure 117: Comparison of filtration volume and bridge strength between Resilient Graphite containing fluid and Solu-Flake containing fluid during particle plugging tests

As previously pointed out, pressure parameters that are estimated during the particle plugging tests do not correlate well with results of the core fracturing and fracture reopening tests. This is because the fracture limitations and specifications in the rock are different to the metallic fractures in the particle plugging tests. During core fracturing and fracture reopening tests, the filtration needs to be minimized to build a solid firm bridge. A high amount of filtration allows the fracture pressure to increase and change the fracture shape. The fracture then may become wider which, in turn, enhances the filtration and is detrimental to the wellbore strengthening, or may propagate and become unstable and make the strengthening process impossible. It has also been mentioned in previous researches that immediate sealing of the fracture at the moment of its initiation is the key to successful wellbore strengthening. Therefore, particles such as Resilient Graphite which have the capability of frequently forming bridges over the fracture, show superior results in real case strengthening trials.

The data analysis parameters which were defined in the current work for the particle plugging tests allowed for in-depth understanding of the strengthening process as well as examining the reliability and validity of the particle plugging test procedures and data analysis methodologies.

Based on the achieved results, observations and explanations in this chapter, it was concluded that the average peaks per zero (N/Z) is the main parameter that can be extracted from particle plugging tests. Higher values of this parameter indicate the high capability of the fluid to form bridges over the fractures and low amount of filtration through the fracture. These two properties are both essential for wellbore strengthening and fracture isolation.

CHAPTER FOUR: MECHANISTIC MODELING OF THE STRENGTHENING PROCESS

In the previous chapter, the results of particle plugging, core fracturing and fracture reopening tests were presented and discussed. It was concluded that particles with the capability of bridging the openings in the shortest possible time and minimizing the flow to the fracture can increase the Wellbore Pressure Containment (WPC) effectively. In this chapter, results of the experiments are investigated to build a mechanistic model for the resistance of the fracture bridges as a function of the studied parameters. In the first section, influential parameters are reviewed and the second section describes the model and presents its verification.

4.1. Review of the experimental results

It was concluded during the experimental phase of this research that the particle size distribution and range, friction coefficient of the fracture planes, particle concentration of the drilling fluid, size of the opening and type of the particles impacted the strength of the bridge during particle plugging tests. Large particles were found to be essential in forming the bridge while wide particle size distributions enhanced the strength of the bridge. Based on these observations and the previously completed studies, it was concluded that plugging is the major mechanism which governs the strengthening process. Large particles plug the opening and smaller particles fill the smaller gaps between the larger particles and build a firm bridge. This theory was also supported by the fact that higher friction coefficients of the fracture planes increased the resistance of the bridge. The eight newly defined parameters allowed for more detailed examination of the performance of the fluids and particles. Comparison of the particle plugging and core fracturing results revealed that the pressure parameters recorded during the particle plugging tests (P_{max}, $P_{P\text{-}ave}$, and P_{ave}) may not be considered as reliable indicators of the strengthening performance of particles (which is the case in most of previous studies); instead, parameters which show the capability of particles in quick formation of bridges and reduction of the filtration to the fractures, exhibited a stronger correlation to the core fracturing results. The opening size of the

fracture had an adverse effect on the strength of the bridge, as expected. Concentration of the particle in the fluid increased the strength of the bridge during the particle plugging tests. Modeling of a real fracture case in this chapter will show that there is a limit to the impact of higher solids concentrations. We will also discuss how the effect of concentration may be altered and influenced by the fracture size and particle size distribution and range. Despite the limitations of the experimental systems, small scale of the setup and the controllability of the geometry allowed for in-depth understanding of the strengthening mechanism. This understanding was first applied to build a mechanistic model to describe the results during the particle plugging tests and was then modified to explain the process of strengthening in real tensile fractures. This modeling process is one of the few studies in which properties of solids have been taken into account. In the next two sections, stages of model derivation are described in detail.

4.2. Modeling of the bridging process in the particle plugging system

Bridging of openings in particle plugging tests is based on the plugging mechanism. Figure 118 shows the assumed process for plugging during a particle plugging test. Based on the proposed mechanism, particles form a uniform block between the fracture planes. Properties of the block change with particle type, concentration, size distribution and size range as well as the fracture geometry. The block is called the particle block in this text. Once the plug forms between the fracture planes, the particle block is under compression. In order to better visualize the plugging process, the particle block can be assumed to have a virtual original size in rest which is slightly larger than its size under compression, as shown in Figure 118. When it enters the opening between the fracture planes, the friction force between the fracture surfaces and the sides of the particle block determines the pressure required to remove the block. Once the block is removed, the flow of the drilling fluid to the fracture continues. The pressure required to remove the block is the average peak pressure ($P_{P\text{-}ave}$) measured during the particle plugging tests. Based on the explained plugging and plug removal mechanisms, the friction coefficient of the fracture surfaces comes into account as one of the major factors. The significance of the friction coefficient of the rock surface was vividly observed during the experimental tests. Since the

particle block needs to contract in order to enter the opening, the frictional force exerted on the sides of the block varies with its elastic properties.

Considering Figure 119, the spherical particles contract upon entering the fracture. Therefore, the particle block will have the dimensions of $W_f \times D^* \times L_f$, where W_f is the fracture width, D^* is the original particle diameter and L_f is the slot length. The strain exerted on the particle block can be estimated by Equation 4-1.

$$\varepsilon_P = \frac{D^* - W_f}{D^*} \qquad \text{Eq. 4-1}$$

where ε_P is the strain of the particle block. Using Equation 4-1, stress and consequently the force on each side of the particle block can be found.

$$\sigma_P = E_P \varepsilon_P$$

$$F_N = D^* L_f E_P \varepsilon_P \qquad \text{Eq. 4-2}$$

where F_N is the normal force exerted on each side of the particle block. The forces exerted on the two small ends of the particle block are neglected in this modeling process. Using the normal forces, the total static friction forces on the particle block can be estimated.

$$f = 2\mu_{sf} D^* L_f E_P \varepsilon_P \quad \text{Eq. 4-3}$$

Where f is the total friction forces applied on the two large sides of the particle block and μ_{sf} is the static frictional coefficient of the fracture planes. In order to find a relationship between the particle properties and the pressure required to remove the particle block, the plugging mechanism is considered, as pointed out previously. When the force exerted on the top side of the particle block in Figure 119 equals the total frictional forces, the block is removed and the flow out of the cell continues. Therefore the force required for the failure of the plug is equal to f in Equation 4-3.

$$F_{Cell} = 2\mu_{sf} D^* L_f E_P \varepsilon_P \quad \text{Eq. 4-4}$$

Where F_{Cell} is the force exerted by the fluid in the cell to remove the particle block. This force can be used to estimate the average peak pressure ($P_{P\text{-}ave}$) during a particle plugging test.

$$P_{P-ave} = \frac{F_{Cell}}{A_f}$$

$$P_{P-ave} = \frac{2\mu_{sf} D^* L_f E_P \varepsilon_P}{W_f L_f}$$

Inserting the equation for the particle block strain and simplifying the equations results in Equation 4-5 which can be applied to estimate the average peak pressure during a particle plugging tests using the mechanical properties of the solid constituents of the drilling fluid.

$$P_{P-ave} = 2\mu_{sf} E_P \left(\frac{D^*}{W_f} - 1\right) \qquad \text{Eq. 4-5}$$

The initial size of the particle block must be higher than the fracture width to form a plug. However, if the particle block size is much larger than the opening size, the particle block cannot enter the opening. In reality the particle block does not form out of the opening. Usually a large particle becomes stuck between the fracture planes and smaller particles accumulate and fill the smaller gaps as shown in Figure 118.

Presence of particles close to the size of the fracture has been highlighted in the literature, based on field experiences[1]. When using simulated fractures in particle plugging experiments, particles that are smaller than the opening size, pass through the fracture and do not contribute to the bridge formation unless a larger particle is present. In real tensile fractures, fracture width usually decreases away from the borehole and smaller particles can plug the fracture in a distant point along the fracture length. Another major difference between the real wellbore strengthening cases and the particle plugging tests lies within the dynamicity of the well condition. As mentioned earlier, one the main objectives of particle plugging tests in this work was to understand the governing mechanism of strengthening process.

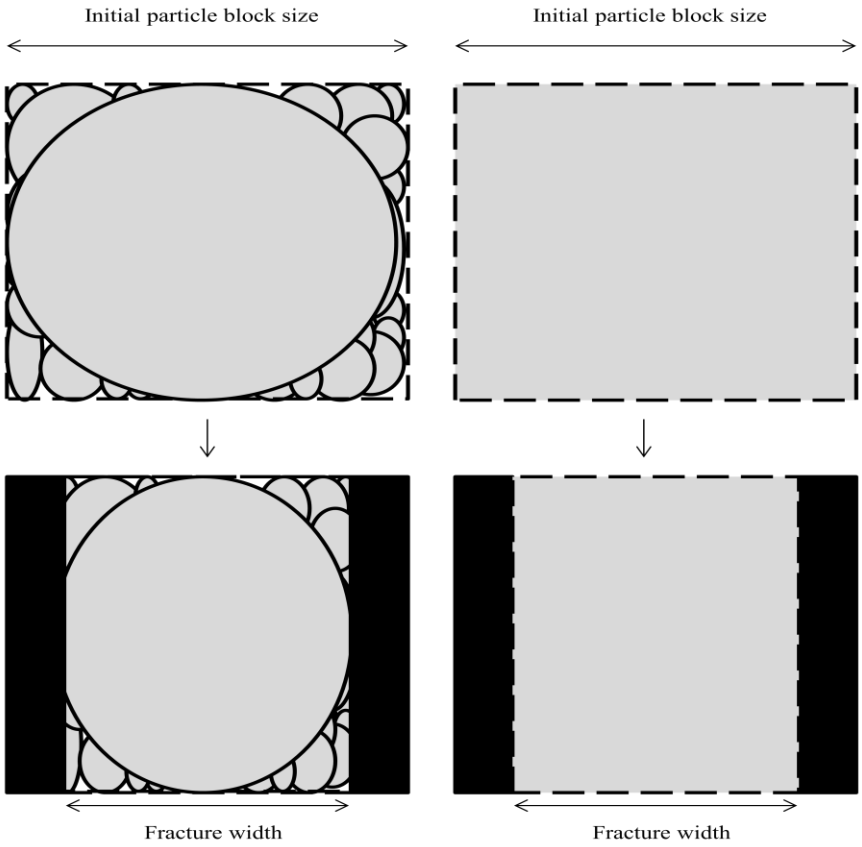

Figure 118: Schematic illustration of particle block formation between the fracture planes during particle plugging tests

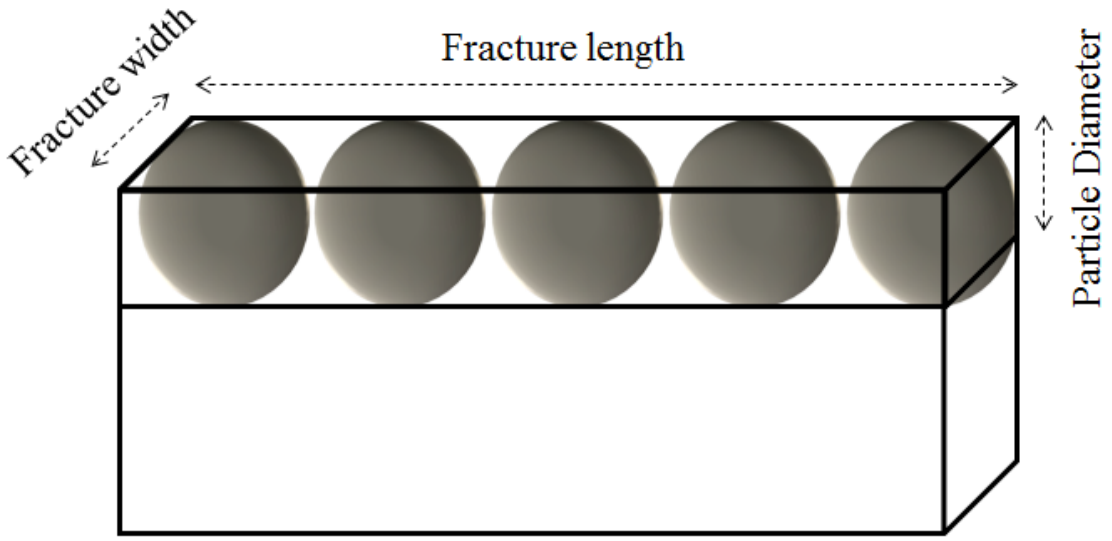

Figure 119: Particle block dimensions

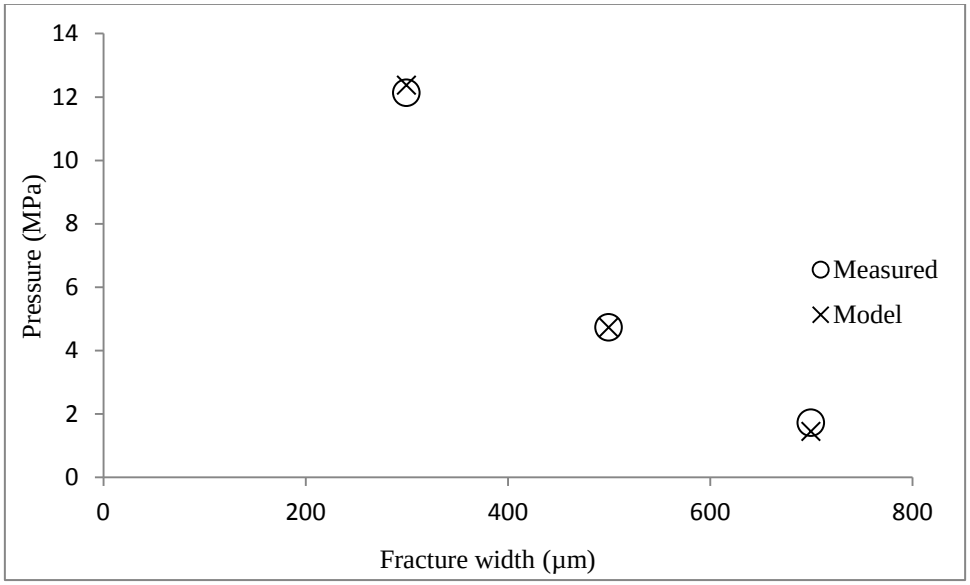

Figure 120: Comparison of measured average peak pressure values during particle plugging tests using Resilient Graphite containing fluid with the mechanistic model predictions

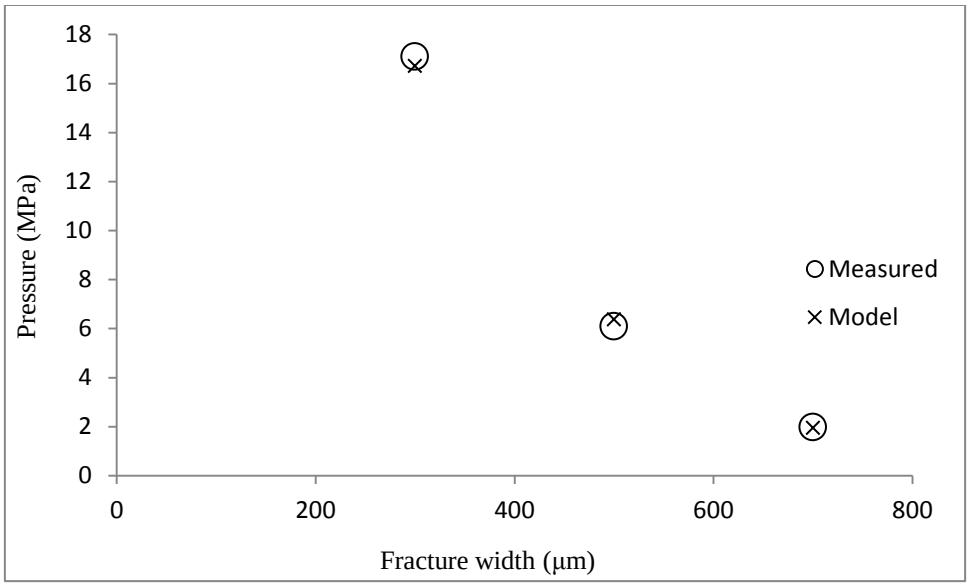

Figure 121: Comparison of measured average peak pressure values during particle plugging tests using Mica containing fluid with the mechanistic model predictions

Table 101: Comparison of model predicted values with measured pressure values during particle plugging tests

W_f (μm)	Particle type	Estimated pressure (MPa)	E_P (MPa)	Measured pressure (MPa)	μ_{sf}	D^* (μm)	Error (%)
300	LC	12.364	84.3	12.12571853	0.4	850	0.47
500	LC	4.7208	84.3	4.7277376	0.4	850	0.00
700	LC	1.445142857	84.3	1.719414297	0.4	850	4.38
300	M	16.72	114	17.09367763	0.4	850	0.82
500	M	6.384	114	6.094739137	0.4	850	1.37
700	M	1.954285714	114	1.978451208	0.4	850	0.03

The obtained mechanistic model for the average peak pressure ($P_{P\text{-}ave}$) presented in Equation 4-5, shows a good agreement with the experimental results as shown in Figures 120 and 121. The model accounts for the correlation between the strengthening capabilities of the fluids and the mechanical properties of the particles as well as the friction coefficient of the fracture planes. It also lays the ground work for modeling the strengthening process in real case tensile fractures which will be discussed later in this chapter. Table 11 presents the measured and predicted

values and the accuracy of the model. D^* has been assumed to be equal to the maximum particle size for the sake of simplicity, however, D^* is slightly higher than the opening size in reality. Correct estimation of D^* requires further testing focusing on the mechanical strength of the particles and their yield strains. In order to remove this complication and yet reach a reliable model for wellbore strengthening in real cases, it was assumed that particles which are only equal to or smaller than the fracture opening in size may enter the fracture.

4.3. Mechanistic modeling of the wellbore strengthening process in a tensile fracture

Tensile fractures initiate in the formations due to decreased tangential (hoop) stress around the well; i.e. when the tensile tangential (hoop) stress overcomes the tensile strength of the formation. If the fracture propagation is not controlled in the primary stages, the opening will grow in all dimensions and it becomes practically very difficult to plug. Fracture mechanics will not be discussed in this work but some applications will be briefly pointed out. Fracture mechanics is highly applicable in hydraulic fracturing engineering designs where controlling the fractures to propagate away from the wellbore enhances the productivity of the well. Based on the literature and the experimental analysis in this research, it was concluded that fracture initiation pressure can be predicted using Kirsch equations. Fracture initiation pressure modeling was briefly reviewed in Chapter 2. Once the fracture is initiated, the particles available in the vicinity of the fracture plug the opening and prevent further filtration. Filtration to the fracture leads to pressure build up in the fracture tip and consequently propagation of the fracture. More details about the pressure distribution in the fracture have been given by Wang[9]. Equations 4-2 and 4-3 are used for determination of fracture geometry based on the KDG model[56].

$$w_{f-max} = \frac{4(1-\upsilon_R^2)L_f P_f}{E_R} \qquad \text{Eq. 4-6}$$

$$w_{f-ave} = \frac{\pi(1-\upsilon_R^2)L_f P_f}{E_R} \qquad \text{Eq. 4-7}$$

where $W_{f\text{-}max}$ is the maximum fracture width, $W_{f\text{-}ave}$ is the average fracture width, L_f is the fracture half length, ν_R is the Poisson's ratio of the formation, E_R is the Young's modulus of the formation and P_f is the net fracture pressure which is the fracture pressure minus the minimum insitu stress. Figure 122 schematically shows the fracture geometry. In this Figure, W refers to fracture width, L refers to fracture length and H refers to fracture height. Figure 123 presents the cross sectional view of the well after initiation of a two wing tensile fracture.

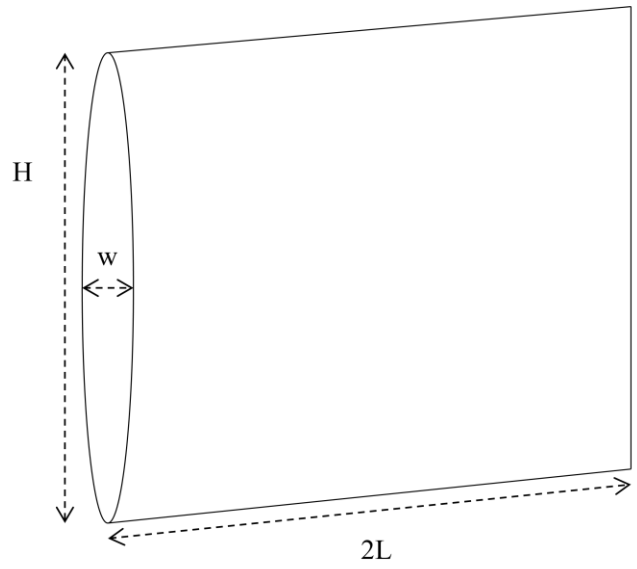

Figure 122: Schematic illustration of tensile fracture geometry

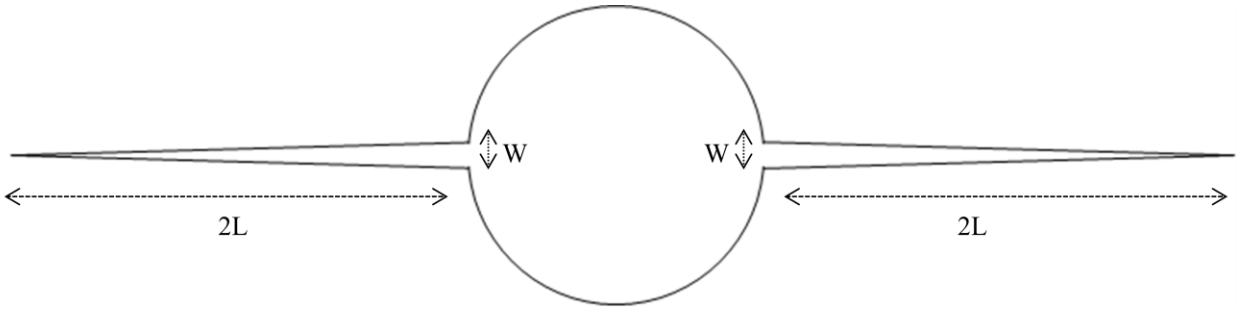

Figure 123: Cross sectional illustration of a two wing tensile fracture geometry

Based on the findings from the particle plugging experiments and modeling it is assumed that the particles fill the fracture partially. It also assumed that only particles that are equal to or smaller than the fracture opening in size can enter. Figure 124 shows a plugged fracture based on the mentioned assumptions. Although a range of particle types and sizes may contribute to the formation of the plug, average properties of the plug will be considered here.

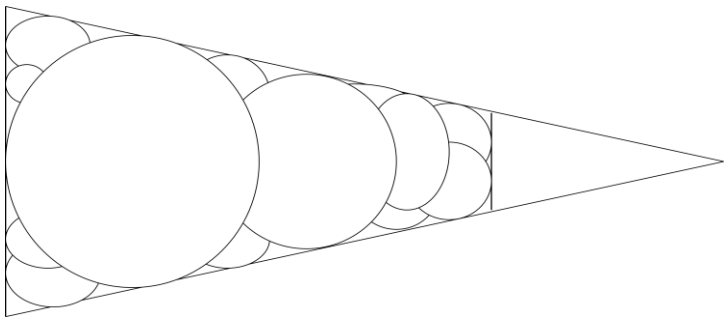

Figure 124: Deposition of the particles at the fracture mouth to form the plug

It is also assumed that the initial width of the plug is equal to the fracture mouth opening size (W_f). The plug contracts to penetrate deeper in the fracture. The limit for this compaction is defined by the yield strain of the plug, beyond which the particle pack will disintegrate and lose

its elastic properties which are essential to efficient plugging. The plug is assumed to behave similar to an unconsolidated sand pack. In Figure 125 the dimensions of the plug are shown. L_y is the distance from the fracture mouth to the point at which the plug yields. Therefore, if the solids concentration of the drilling fluid is sufficient to fill the fracture with particles, L_y will be equal to length of the plug. W_y is the width of the fracture at point at which the plug yields. It is assumed that the plug behaves elastically until it yields and the pressure at the yield point is equal to the compressive strength of the plug.

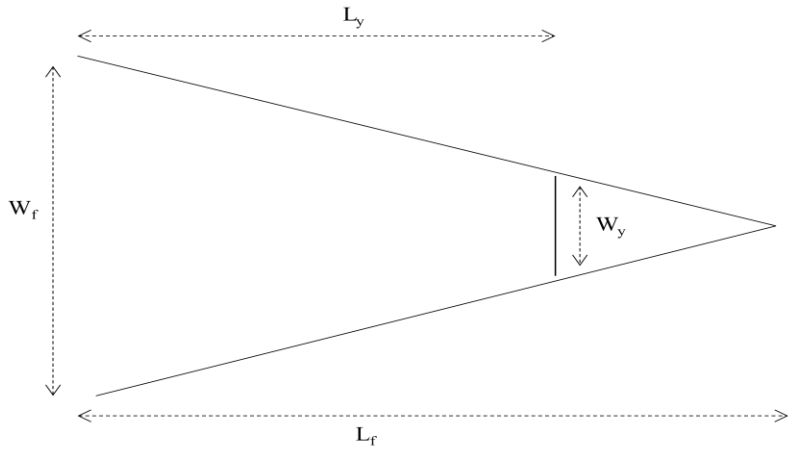

Figure 125: Dimensions of the plug in a tensile fracture

Once the plug is formed, the fracture pressure is not impacted by the pressure in the well and the fracture cannot propagate, assuming that the plug is firm and has a very low permeability. In order to initiate the circulation loss, the pressure in the well needs to elevate. The pressure at which the circulation loss starts is the pressure required to remove the plug. This pressure level is also called the Wellbore Pressure Containment (WPC) as pointed out previously in the literature. In order to be able to mathematically model the required pressure to remove the plug, elements of the plug with the length of dL are considered as shown in Figure 126. It is assumed that dL is very small and thus, rectangular blocks are formed despite the inclination of the fracture planes.

For each element, the applied force on the two ends is a function of the level of compression and the mechanical properties of the particles. An arbitrary element of the plug is shown in schematically in Figure 127. The end effects have been neglected in this modeling process and all elements are assumed to have a rectangular shape. Suppose a normal force equal to dF_N is exerted on the two ends of the element due to its contraction. The magnitude of the force is proportional to the strain level of the element. Equations 4-7 to 4-10 are used to estimate the amount of normal force as a function of elastic properties and strain of the plug element.

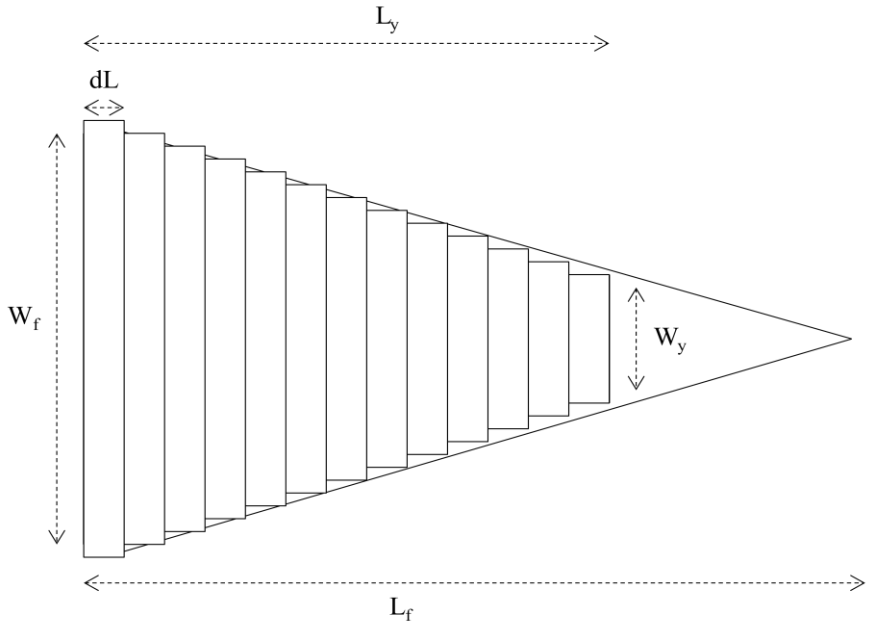

Figure 126: Elements of the plug inside the fracture

$$dF_N = \sigma_N dA \qquad \text{Eq. 4-7}$$

$$dF_N = \sigma_N H_f dL \qquad \text{Eq. 4-8}$$

$$\sigma_N = \varepsilon E_P \quad \text{Eq. 4-9}$$

$$dF_N = \varepsilon E_P H_f dL \quad \text{Eq. 4-10}$$

where dL is the length of the element as shown in Figure 126, H_f is the height of the fracture, ε is the strain of the element and E_P is the elastic modulus of the particle block which is assumed to be constant throughout the plug. The static friction force exerted on the plug can be estimated by multiplying the static friction coefficient μ_f by the normal force. The static friction force is the force which holds the plug element between the fracture planes. The static friction coefficient of the fracture planes is a function of rock surface roughness and is typically between 0.3 and 0.4.

$$df = 2\mu_{sf} \varepsilon E_P H_f dL \quad \text{Eq. 4-11}$$

As pointed out above and shown in Figure 128, the friction on the other two sides of the block facing the top and bottom sides of the fracture, have been neglected due to their relatively small area. The strain of the block is found by its width or its distance from the fracture mouth and the fracture dimensions.

$$\varepsilon = \frac{W_f - W}{W_f} \quad \text{Eq. 4-12}$$

$$\frac{W}{W_f} = \frac{L_f - L}{L_f} \rightarrow \frac{L}{L_f} = \varepsilon \qquad \text{Eq. 4-13}$$

where W and L are the width and the distance from the fracture mouth for an arbitrary element.

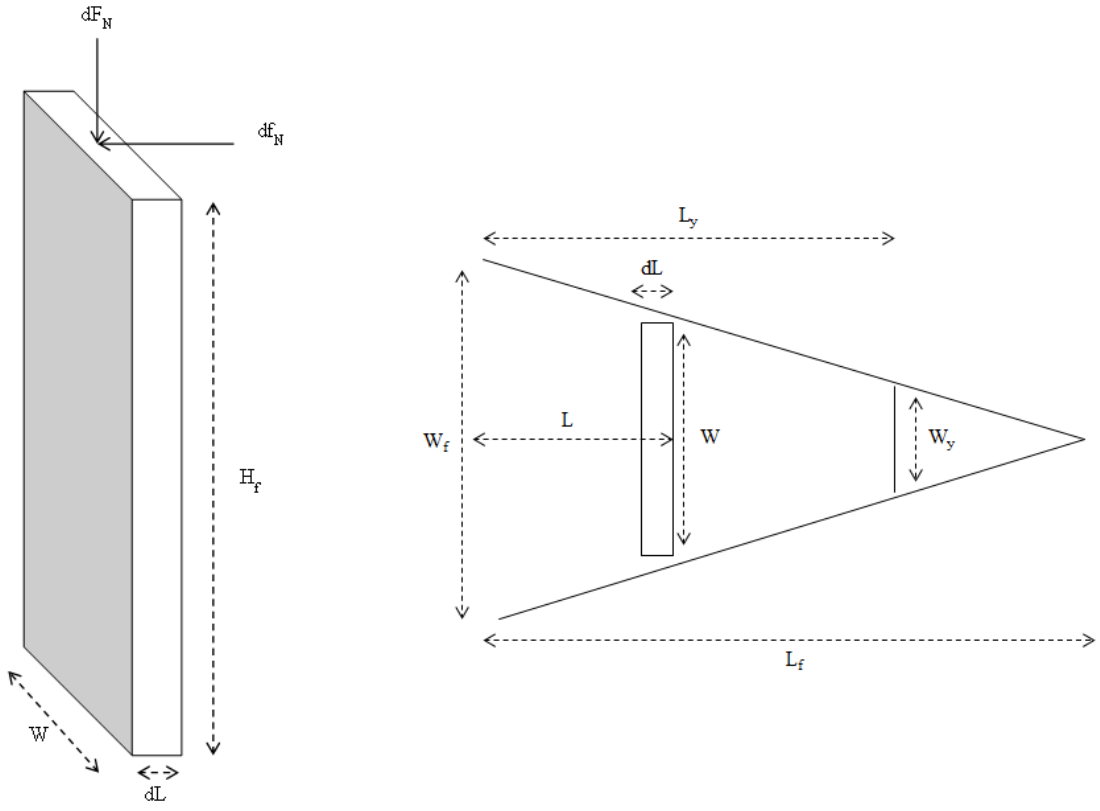

Figure 127: An element of the plug in the fracture

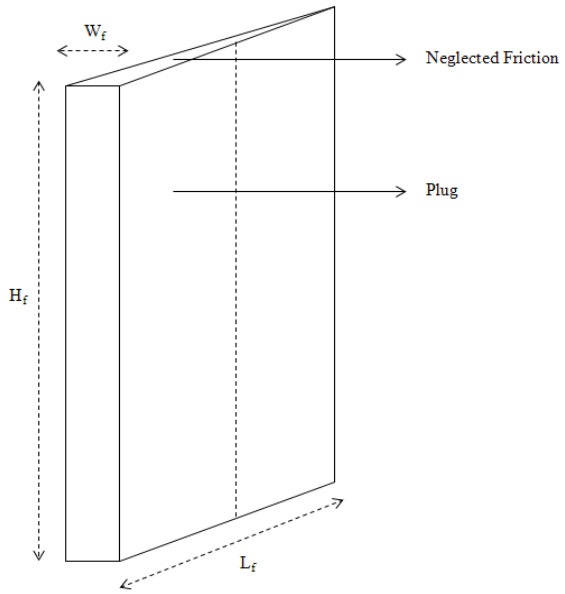

Figure 128: Illustration of the assumption of negligible friction on two sides of the plug

Using equations 4-12 and 4-13, df can be rewritten and integrated over the full length, from the fracture mouth to the point at which the plug yields and the strain is equal to ε_y. ε_y is the yield strain and represents the maximum deformation of the plug as it still behaves elastically. Strains above this value are partly permanent and are referred to as the plastic strains.

$$dL = L_f d\varepsilon \qquad \text{Eq. 4-14}$$

$$df = 2\mu_f \varepsilon E_P H_f L_f d\varepsilon \qquad \text{Eq. 4-15}$$

$$f = \int_0^{\varepsilon_y} 2\mu_f \varepsilon E_P H_f L_f d\varepsilon = 2\mu_f E_P H_f L_f \int_0^{\varepsilon_y} \varepsilon d\varepsilon \quad \text{Eq. 4-16}$$

$$f = \mu_f E_P H_f L_f \varepsilon_y^2 \quad \text{Eq. 4-17}$$

As mentioned above, the static frictional force estimated by Equation 4-17 holds the plug in spot and opposes its removal by the fluid pressure in the well. The force required to remove the plug needs to overcome the frictional force. Based on this force which is exerted by the fluid and the fracture dimensions, the pressure required to remove the plug can be estimated.

$$F_{Str} = f \quad \text{Eq. 4-18}$$

Where F_{Str} is the force required to be provided by the drilling fluid in the well to initiate the circulation loss. Therefore P_{Str}, the pressure in the well required to remove the plug can be estimated as a function elastic properties of the particles.

$$P_{Str} = \frac{F_{Str}}{A_f} = \frac{\mu_f E_P H_f L_f \varepsilon_y^2}{H_f W_f} = \frac{\mu_f E_P L_f \varepsilon_y^2}{W_f} \quad \text{Eq. 4-19}$$

It is important to revisit the term $E_P\varepsilon_y^2$. Replacing the term $E_P\varepsilon_y$ by σ_y which is the maximum stress at which the plug behaves elastically (i.e. the yield strain), the result will equal twice the

area under the stress-strain plot as shown in Figure 129, assuming the plug behaves elastically up to the yield point. This value is the resilience modulus of the material, U_r. The resilience modulus indicates the extent of elastic deformation of a material and increase with the yield stress and strain. This mechanical property determines how much a plug can deform and enter the fracture before yielding and is mathematically defined as below.

$$U_r = \frac{\sigma_y \varepsilon_y}{2} = \frac{E_P \varepsilon_y^2}{2} \qquad \text{Eq. 4-20}$$

Higher modulus of resilience leads to both larger length of the plug, L_y and thus higher friction between the plug and the fracture plane. Therefore more resilient plugs enhance the strengthening process. Substituting the resilience modulus in equation 4-19 yields:

$$P_{Str} = \frac{\mu_f L_f U_r}{W_f} \qquad \text{Eq. 4-21}$$

P_{Str} is basically the strength of the plug formed by the fluid in the fracture. When fracture initiates, the fluid may form a plug and prevent circulation loss. As pointed out previously, Kirsch equation can be used reliably to predict the fracturing gradient, P_{init}. However, wellbore strengthening technology can elevate the circulation loss pressure, P_{LC}, well above the fracturing gradient. The circulation loss pressure is also known as the wellbore containment pressure.

$$P_{LC} = P_{init} + P_{Str}$$ Eq. 4-22

Assuming the equality of the yield point and the compressive strength of the plug, Equation 4-21 can be rewritten as below.

$$P_{Str} = \frac{\mu_f L_f C_o^2}{W_f E_P}$$ Eq. 4-23

where C_o is the compressive strength of the plug.

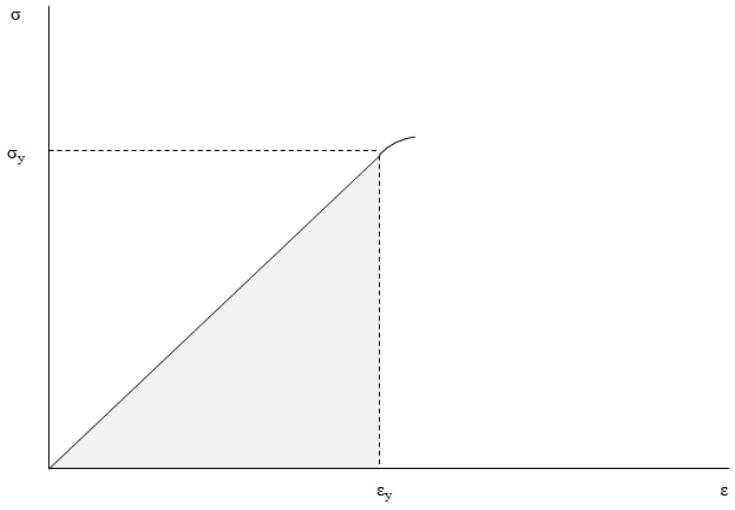

Figure 129: Stress - strain plot of a fully elastic material

The model developed in this research and presented in this section enables the engineers to preplan the strengthening operations and estimate the maximum strengthening that can be expected in the well. The developed mechanistic model explains the superior performance of Resilient Graphite in the field. Resilient Graphite particles can deform substantially before yielding and thus exerting sufficient force on the fracture planes to form a hard to remove plug. The developed model is one of the main outcomes of the present work and can relate the measurable properties of formation and particles to the strengthening capabilities of the drilling fluid. In the modeling procedure explained above, it was assumed that the solids concentration of the drilling fluid is sufficient for immediate deposition of particles and filling the fracture from the mouth to the yield point. However, in most cases very high solids concentrations are required for this condition to be achieved. High solids content increases the mud weight and circulation loss probability in the well. Therefore partial filling of fractures is obtained using typical drilling fluid concentrations. Therefore, it is important to model the strength of the plugs when partial plugging occurs. In a full plugging of the fracture, all the fracture from its mouth to the point that the plug yields is filled with particles as shown in Figure 124. The volume of the plug in this case, V_{Pf} can be estimated using Equation 4-24.

$$V_{pf} = \frac{H_f L_f W_f}{2} - \frac{H_f (L_f - L_y) W_f}{2} \quad \text{Eq. 4-24}$$

Equation 4-12 and 4-13 can be rewritten to for the yield point.

$$\varepsilon_y = \frac{W_f - W_y}{W_f} \quad \text{Eq. 4-25}$$

$$\varepsilon_y = \frac{L_y}{L_f}$$ Eq. 4-26

Using a few rearrangements and Equations 4-24, 4-25 and 4-26, volume and mass of the plug can estimated.

$$V_{pf} = H_f L_f W_f \varepsilon_y \left(1 - \frac{\varepsilon_y}{2}\right)$$ Eq. 4-26

$$m_{pf} = \rho_p H_f L_f W_f \varepsilon_y \left(1 - \frac{\varepsilon_y}{2}\right)$$ Eq. 4-26

where m_{pf} and ρ_p are the mass and density of the plug. It is important to remember that this is valid for the full fracture filling case. In this modeling process it is assumed that the full fracture filling case occurs when the drilling fluid entering the fracture contains a mass of particles equal to m_{pf}. In other words, it is assumed that as the fracture initiates, a certain volume of the drilling fluid equal to the volume of the fracture enters the opening, and if this volume contains sufficient particles, the full fracture plugging can happen. Therefore, equation 4-26 can assist in finding the maximum effective concentration of particles.

$$C_{Cr} = 2\rho_P \varepsilon_y [1 - 0.5\varepsilon_y] \left(\frac{d_{max}}{W_f}\right)^m$$ Eq. 4-27

where d_{max} is the maximum particle size present in the drilling fluid and C_{Cr} is the critical maximum concentration of the drilling fluid. When the fracture is partially filled as shown in Figure 130, the plug penetrates to the point at which it yields, but the mass of particles is not sufficient to fully occupy the void space and a part of the fracture is left with no particle pack. In this figure L_i refers to the length of the void space and W_i is the width of the outer side of the plug. Therefore L_y - L_i is equal to the length of the plug. The strain on the inner side of the plug is ε_y and on the outer side the strain is ε_i and is a function of the solids concentration.

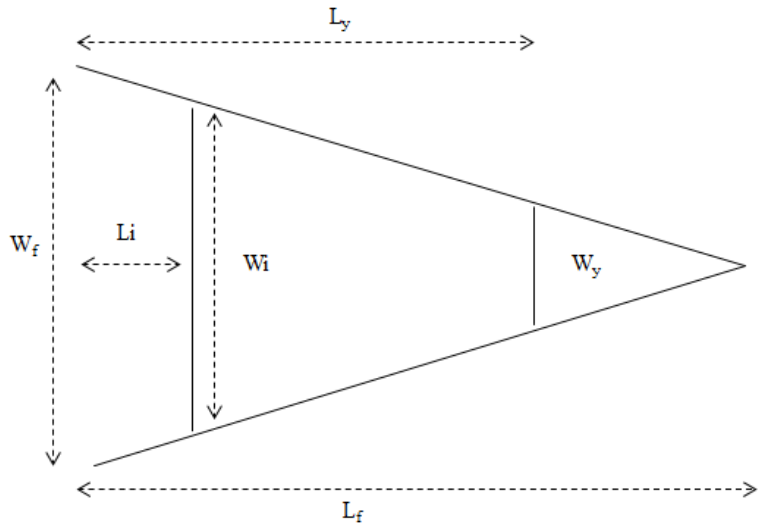

Figure 130: Partial plug formation in the fracture

In order to estimate the strength of the plug when the fracture is partially packed with particles, it is required to know exactly what portion of the opening is filled. Equation 4-28 finds the volume of the plug.

$$V_p = \frac{H_f(L_f - L_i)W_f}{2} - \frac{H_f(L_f - L_y)W_f}{2}$$ Eq. 4-28

Based on trigonometric relations, the following equations can be drawn from Figure 130.

$$\varepsilon_i = \frac{W_f - W_i}{W_f} = \frac{L_i}{L_f}$$

$$\varepsilon_y = \frac{W_f - W_y}{W_f} = \frac{L_y}{L_f}$$

Using the relations above and a few rearrangements, Equation 4-28 can be rewritten based on which Equation 4-30 is derived to estimate the mass of the plug.

$$V_p = \frac{H_f L_f W_f}{2}\left[(1 - \varepsilon_i)^2 - \left(1 - \varepsilon_y\right)^2\right]$$ Eq. 4-29

$$m_p = \rho_p \frac{H_f L_f W_f}{2}\left[(1 - \varepsilon_i)^2 - \left(1 - \varepsilon_y\right)^2\right]$$ Eq. 4-30

The ratio of concentration of the drilling fluid in the case of partial filling of fracture to the maximum effective concentration can be estimated by dividing m_p by m_{pf}. This ratio is defined as the concentration efficiency in this work and is showed by κ.

$$\kappa = \frac{m_p}{m_{pf}} = \frac{C_p}{C_{Cr}} = \frac{(1-\varepsilon_i)^2 - \left(1-\varepsilon_y\right)^2}{1-\left(1-\varepsilon_y\right)^2} \quad \text{Eq. 4-31}$$

Since the concentration of the drilling fluid is usually a known value, Equation 4-31 can be rearranged to estimated ε_i.

$$\varepsilon_i = 1 - \sqrt{\kappa\left(1-\left(1-\varepsilon_y\right)^2\right) + \left(1-\varepsilon_y\right)^2} \quad \text{Eq. 4-32}$$

Once ε_i is estimated it is possible to estimate the integration in Equation 4-16 between different boundaries, to find the static fictional force holding a partial plug in the fracture.

$$f^p = \int_{\varepsilon_i}^{\varepsilon_y} 2\mu_f \varepsilon E_P H_f L_f d\varepsilon = \mu_f \varepsilon E_P H_f L_f \left(\varepsilon_y^2 - \varepsilon_i^2\right) \quad \text{Eq. 4-33}$$

where f^p is the static frictional force exerted on a partial plug. A force equal to f^p is required to be provided by the drilling fluid in the well to remove the partial plug and initiate the circulation

loss. Similar to to the process followed for derivation of the pressure required to overcome the plug, the extra pressure required to initiate the circulation loss in the case of partial plugging, P_{Str}^{P} is derived and presented below.

$$P_{Str}^{p} = \frac{\mu L_f (U_r - \varepsilon_i^2)}{W_f (1 - \varepsilon_i)} \quad \text{Eq. 4-34}$$

$$P_{LC} = P_{init} + P_{Str}^{p} \quad \text{Eq. 4-35}$$

Equations 4-34 and 4-35 can be applied in engineering designs of wellbore strengthening operations when the concentration of the solids in the drilling fluid is lower than the critical concentration. This is mostly the case during drilling operations since the maximum effective concentration may be too high to be safely applied.

4.4. Model simulation

Simulation of the newly developed model requires the consideration of concentration and the size distribution of the particles in the fluid with respect to the opening size. Figure 131 schematically shows the effect of concentration on the plug resistance. When the concentration of the particles is not sufficient in the fluid, the formed bridge is easier to remove. On the other hand high concentrations may not assist in enhancing the bridge strength since the plug cannot grow in size once the fracture is filled with particles. In the last section, two separate equations were derived to estimate the strengthening provided by the drilling fluid based on the mechanical properties of solids present in the drilling fluid.

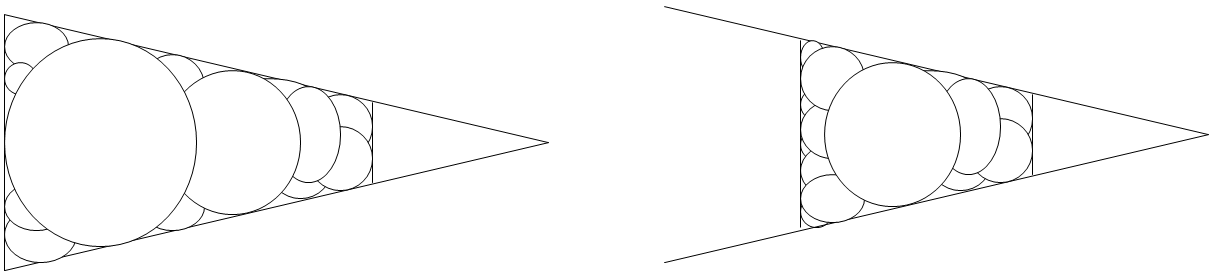

Figure 131: Significance of concentration of particles in plug formation

Particle size distribution determines the portion of the particles that can enter the opening. If most of the particles in a fluid are larger than the opening size, a resistant plug cannot form even if the concentration is high. Therefore it is essential to calculate the amount of the particles that can enter the opening. In this section, a simple simulation of the plug resistance is carried out. The initial values are presented in Table 12.

Table 12: Initial values applied to estimate the plug strength

Parameter	**Value**
Maximum particle size, mm	1.5
Particle size distribution parameter (m)	0.5
Fracture length, cm	50
Fracture height, cm	100
Density of particles, gr/cm3	3
Friction coefficient of rock	0.3
Resilience modulus, Pascal	1600
Concentration of the fluid, kg/m^3 (lb/bbl)	160 (60)

Figures 132 and 133, shows the particle size distribution of the fluid and the strength of the plug versus the fracture width. As expected, the plug becomes weaker as the fracture size grows. The graph shows that the Wellbore Pressure Containment (WPC) can increase up to 1.8 MPa (273 psi) in this case.

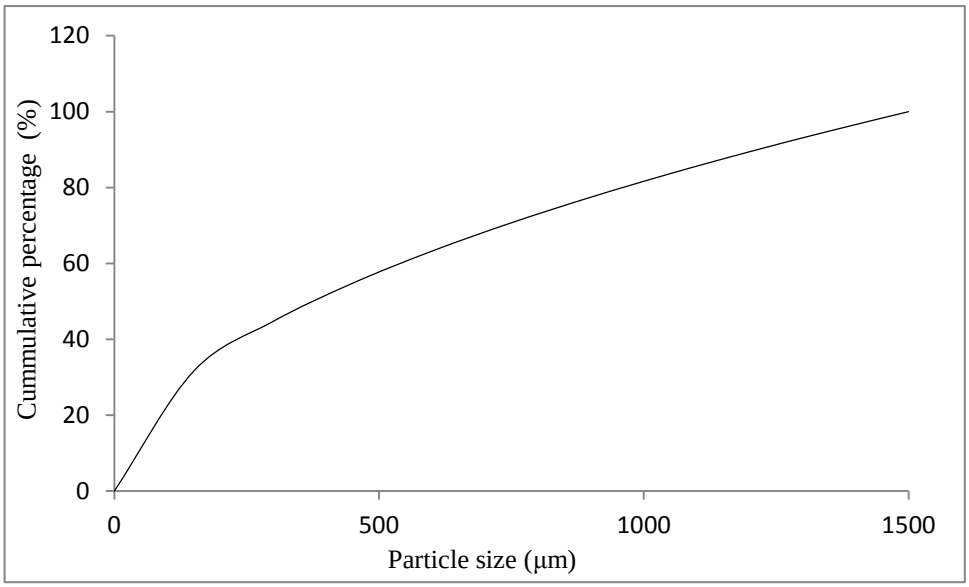

Figure 132: Distribution of the particle size in the simulated strengthening case

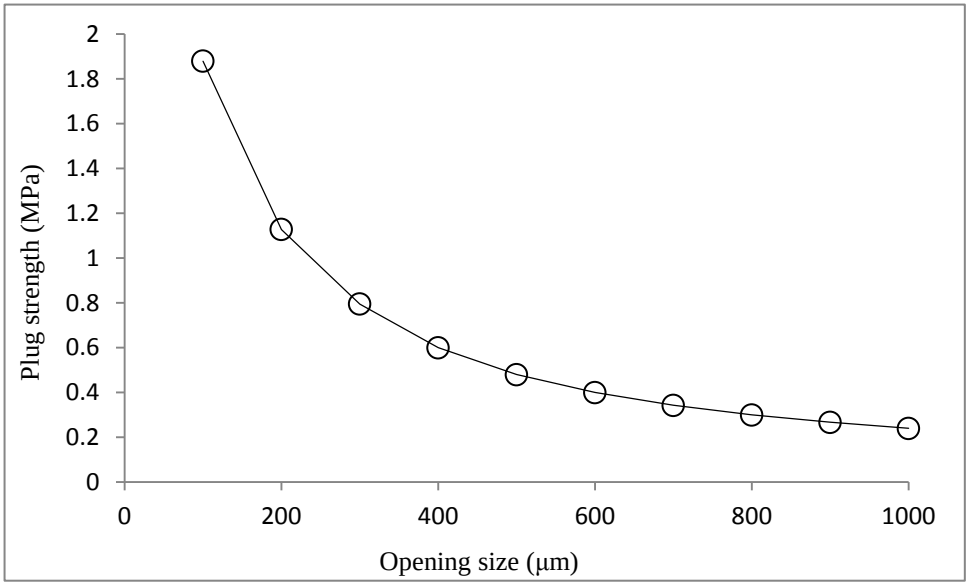

Figure 133: Estimated plug strength versus the fracture width

Figure 134 presents the thickness of the plug for various opening sizes. The formed plug is thinner for fractures narrower than 400 μm and becomes constant as for wider fractures. This is

because the fracture is filled with particles and no further increase in the thickness of the plug is possible.

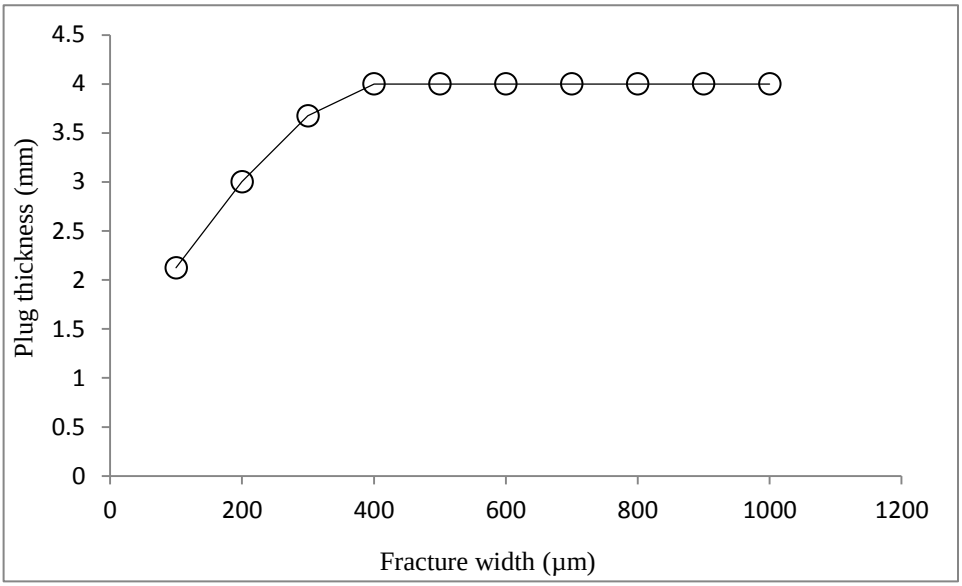

Figure 134: Estimated plug thickness with respect to fracture width

The maximum thickness of the plug T_{max}, is equal to L_y. Using Equation 4-26, Equations 4-36 and 4-37 can be derived.

$$T_{max} = L_y = L_f \varepsilon_y \quad \text{Eq. 4-36}$$

$$T_{max} = \frac{L_f C_o}{E_P} \quad \text{Eq. 4-37}$$

Concentration of the drilling fluid is one of the important controlling parameters for wellbore strengthening operations. A critical limit for the concentration, is mentioned in the literature as a limit above which no further improvement can be achieved in the strength of the plug. Figure 135 shows the sensitivity of the plug strength in a 700 µm fracture with respect to particle concentration. All other parameters are equal to those mentioned in Table 12. It can be concluded that there is a critical concentration, above which the fracture plug resistance cannot be improved. This critical concentration is a function of particle type and size distribution as well as the fracture size. Equation 4-22 is developed in this work to estimate the critical concentration.

$$C_{Cr} = 2\rho_P \frac{C_o}{E_P}\left[1 - 0.5\left(\frac{C_o}{E_P}\right)\right]\left(\frac{d_{max}}{W_f}\right)^m \quad \text{Eq. 4-22}$$

where d_{max} is the maximum particle size and ρ_P is the density of the particles.

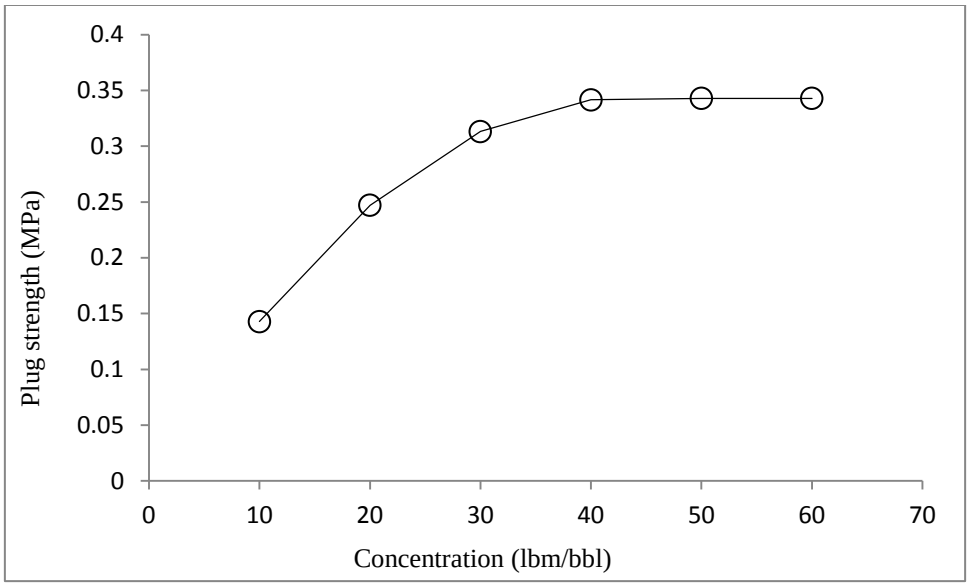

Figure 135: Variation of plug strength with respect to particle concentration

The significance of small particles can also be studied using the developed model. As discussed previously, the particle size distribution parameter, m, indicates the amount of each portion of size range mixed in the fluid. When m grows significantly, i.e., more large particles are present in the fluid, lesser amounts of particles can enter small openings and build the bridge. Therefore, despite the small fracture size, the plug becomes very narrow and weak. This phenomenon can be observed in the model output shown in Figure 136 where a simulation of the model has been carried out. In this case m is equal to 2 and the rest of the parameters are equal to those presented in Table 12. Small particles can take the role of plugging the fractures in the very early stages of initiation. In addition, they fill the gaps between larger particles, reduce the permeability and enhance the plug strength. Based on the fact that micro size particles cannot reach nano size pores in shale formations to form an internal plug and prevent water invasion, application of nano-particles has been recommended in some studies[57,58].

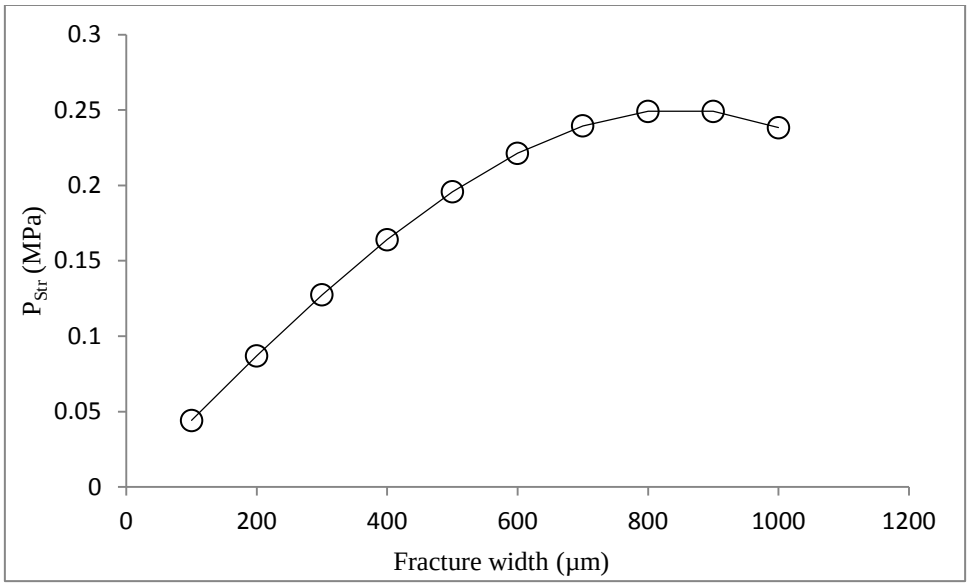

Figure 136: Variation of plug strength with respect to fracture width for m=2

Results of this research highlighted the significance of properties of drilling fluid and its constituents in the strengthening process. The wellbore may be strengthened using an engineered drilling fluid up to a limit which is mainly imposed by the mechanical properties of the solids, their size distribution and concentration as well the fracture geometry and friction coefficient. The most widely accepted theory for wellbore strengthening called stress caging is laid upon the hypothesis of increased tangential (hoop) stress around the wellbore due to increased strain once the fracture is initiated and sealed. However, Salehi *et al.* proved that the tangential (hoop) stress cannot be increased beyond the pre-determined limit according to the wellbore pressure. Figure 137 shows the tangential (hoop) stress around the wellbore for various pressure levels. As the pressure decreases, the fracture initiates and is then sealed off by the solids in the fluid. In the most ideal case, the wellbore is restored completely and the initial tangential (hoop) stress is recovered. Therefore the theory of increasing the tangential (hoop) stress to a level beyond what is estimated using the analytical or numerical models, is invalidated. On the other hands, stress caging theory highlights the importance of increased tangential (hoop) stress as a basis for increased fracture gradient. However previous studies and specially laboratory experiments clearly revealed circulation loss occurs at the location of the initial fractures at a higher pressure

level. This shows the importance of plug properties rather than tangential (hoop) stress around the borehole.

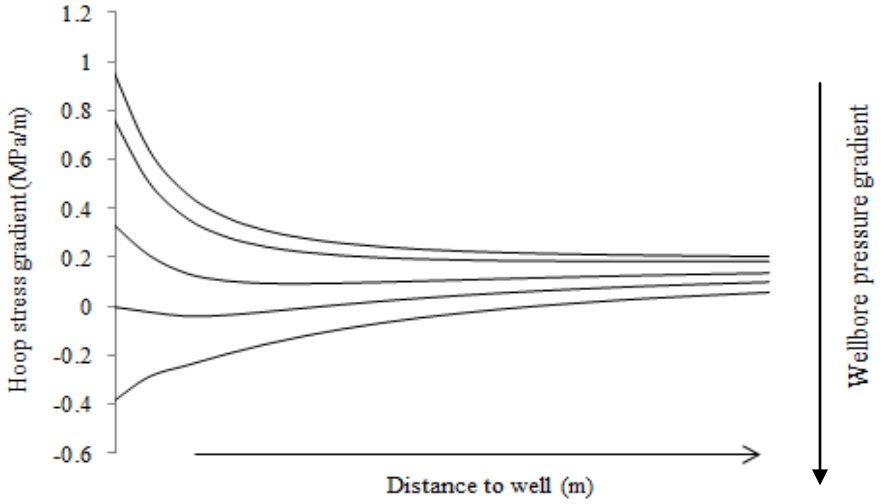

Figure 137: Tangential (hoop) stress gradient distribution away from the wellbore

4.5. Case study

A wellbore strengthening field case was studied using the developed model to verify its applicability for field practices. In general wellbore strengthening field operations are performed either during the drilling operations by adding the required particles to the fluids, or by carrying out a pill treatment. The former has the advantage of lower Non Productive Time (NPT) of the rig and therefore lower operational costs, while the latter introduces the possibility of designing a specific fluid for strengthening purposes. The dataset analyzed in this work was obtained by performing a pill treatment in a long open hole section. The operator was aware of a weak zone which was expected to be prone to fracturing at the depth of 1000 m. A formation integrity test was performed first at the depth of 1400 m using an inert fluid system with the density of 1000 kg/m^3 and a surface pressure of 1962 kPa was recorded before formation broke down, which was equivalent to 1200 kg/m^3 mud density at the reference depth of 1000 m. The strengthening pill was mixed in the fluid in the approximate concentration of 160 kg/m^3 and was spotted through the entire annulus, increasing the Equivalent Mud Density (EMD) to more than 1300 kg/m^3. The final surface pressure achieved was 2562 kPa over a period of 10 hours of the strengthening operation which represented an Equivalent Mud Density (EMD) of 1346 kg/m^3 at a reference depth of 1000 m. During the operation, the surface pressure was recorded. Part of the information regarding the properties of the particles in the strengthening pill and the formation characteristics were provided by the service company and the missing data were assumed in a reasonable range or extracted from other references. The strengthening operation initiated by injecting the fluid into the annulus and the drill pipe in order to reduce downhole pressure fluctuations. The pressure was increased by injection and released periodically. The pressure release was allowed when a decline in surface pressure was observed. In Table 13, the initial parameters which were applied in the model are presented.

Table 113: Initial parameters applied in the field verification of the developed strengthening model

Parameter	Value
Maximum particle size, mm	1.5
Particle size distribution parameter (m)	1
Fracture length, cm	20
Fracture height, cm	100
Density of particles, gr/cm3	2.6
Friction coefficient of rock	0.3
Resilience modulus, Pascal	20000
Concentration of the fluid, lb/bbl	56
Elastic modulus of the formation, GPa	1
Poisson's ratio of the formation	0.45

Figure 138 and 139 show the recorded surface pressure and the estimated downhole pressure, respectively. The maximum achievable pressure increases in each period of squeeze and release. In order to model this strengthening process, fracture geometry is required. The fracture was assumed to have two wings and its dimensions were assumed in a reasonable range. In order to have a better estimate on its width, the KGD model presented in equation 4-6 was used.

Figure 140 shows the maximum differential pressure achieved by the strengthening process at the depth of 1000 m during the squeezing periods. The differential pressure refers to the pressure minus the fracturing gradient obtained by the formation integrity test.

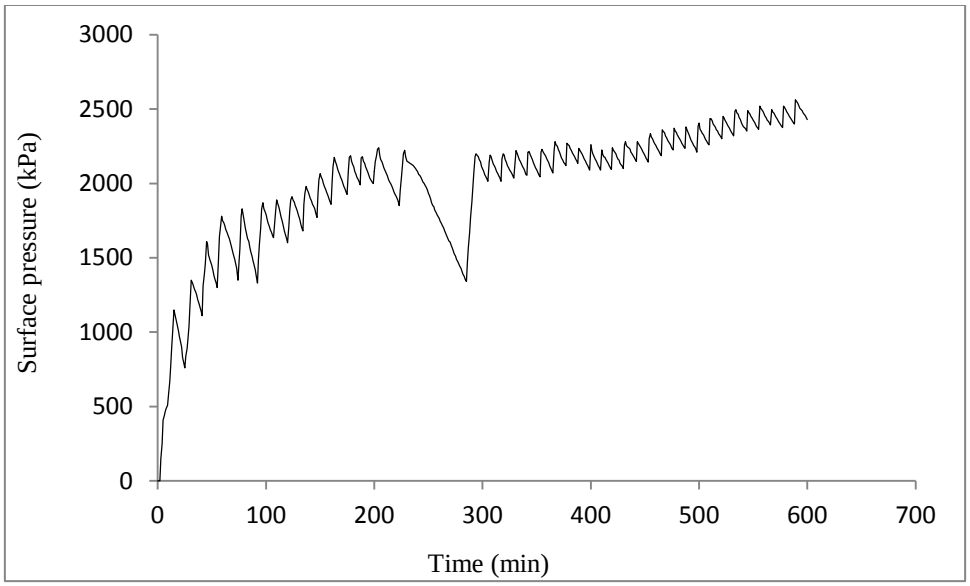

Figure 138: Surface pressure recorded during the wellbore strengthening field trial

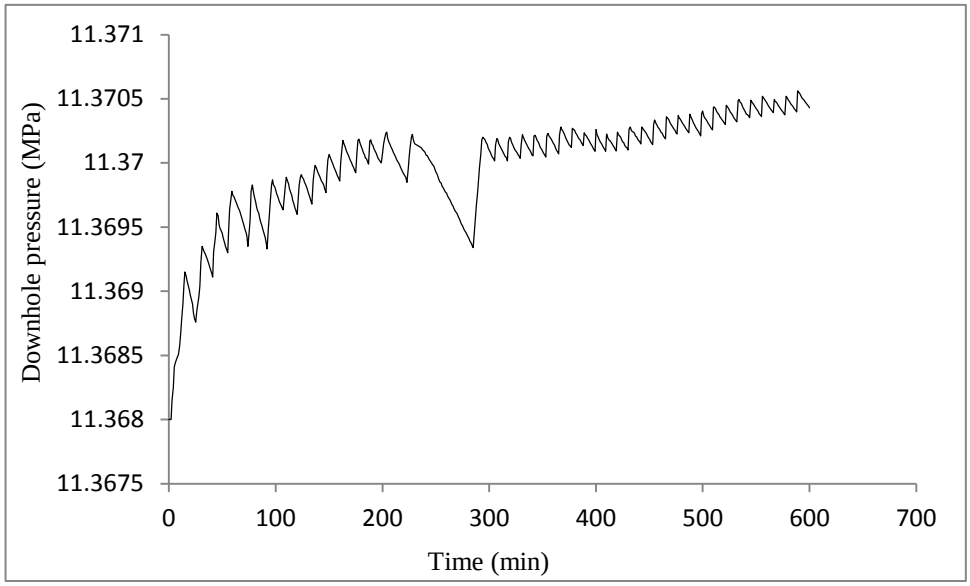

Figure 139: Downhole pressure estimated during the wellbore strengthening field trail

Since the formation was believed to be weak and unconsolidated, it can be concluded that the fracture gradient almost equals the minimum horizontal stress. If this process was performed using a clear water fluid and no plug was formed, these values could have been applied in

Equation 4-6 to find the fracture geometry. However in this case, since a plug is formed within the fracture, the exact net fracture pressure cannot be estimated. In order to overcome this limitation, the lowest pressure differential was assumed to be equal to the net fracture pressure. This assumption was made based on the fact that the plug formed in the initial stage of the strengthening process was thin and weak. Therefore the fluid pressure has most probably overcome its strength. Based on the assumed length of the fracture and KGD equation, the fracture width was estimated to be equal to 500 µm.

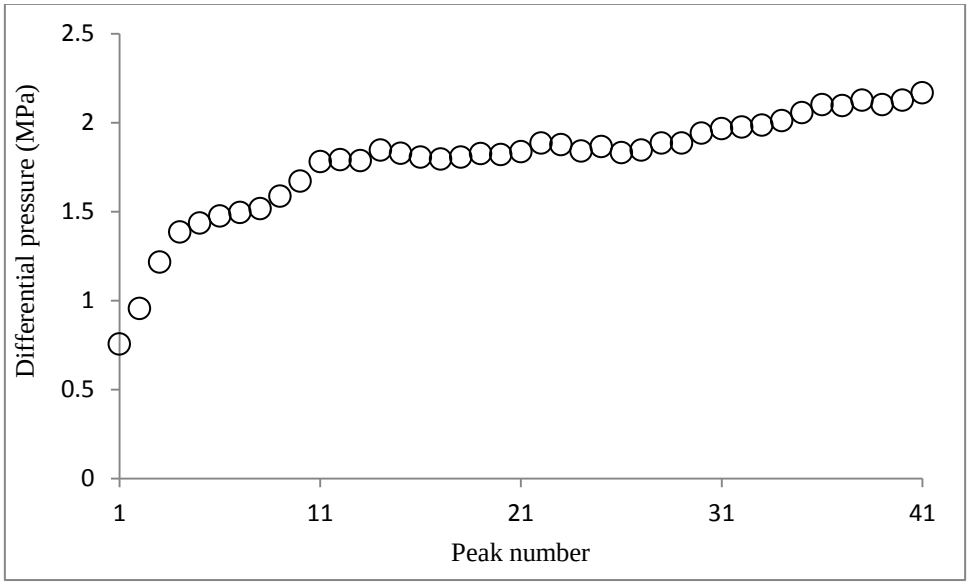

Figure 140: Strengthening pressure values (P_{Str}) achieved in different strengthening stages

Using the newly developed model, it was concluded that the concentration of the strengthening fluid was not sufficient to fill the fracture completely in one stage. Therefore a part of the fracture was filled during each squeeze period until the fracture was fully filled with particles at some point, beyond which no significant increase in the plug strength was observed and the rate of strength improvement declined. Due to the dynamic conditions in the well and the uneven distribution of the particles in the vicinity of the fracture, it is impossible to find the exact amount of deposition of particles in each stage of squeezing. However, it is possible to find the

maximum amount of deposition, should the concentration have remained constant. Figure 141 schematically shows the stages of deposition based on the model. The amount of particle deposition decreases in each stage until the plug reaches its maximum size.

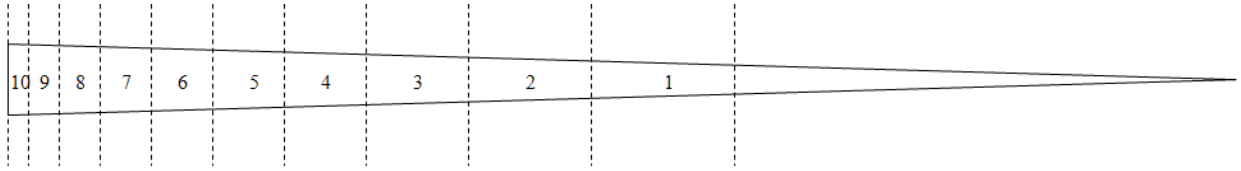

Figure 141: Schematic illustration of deposition stages based on the newly developed model

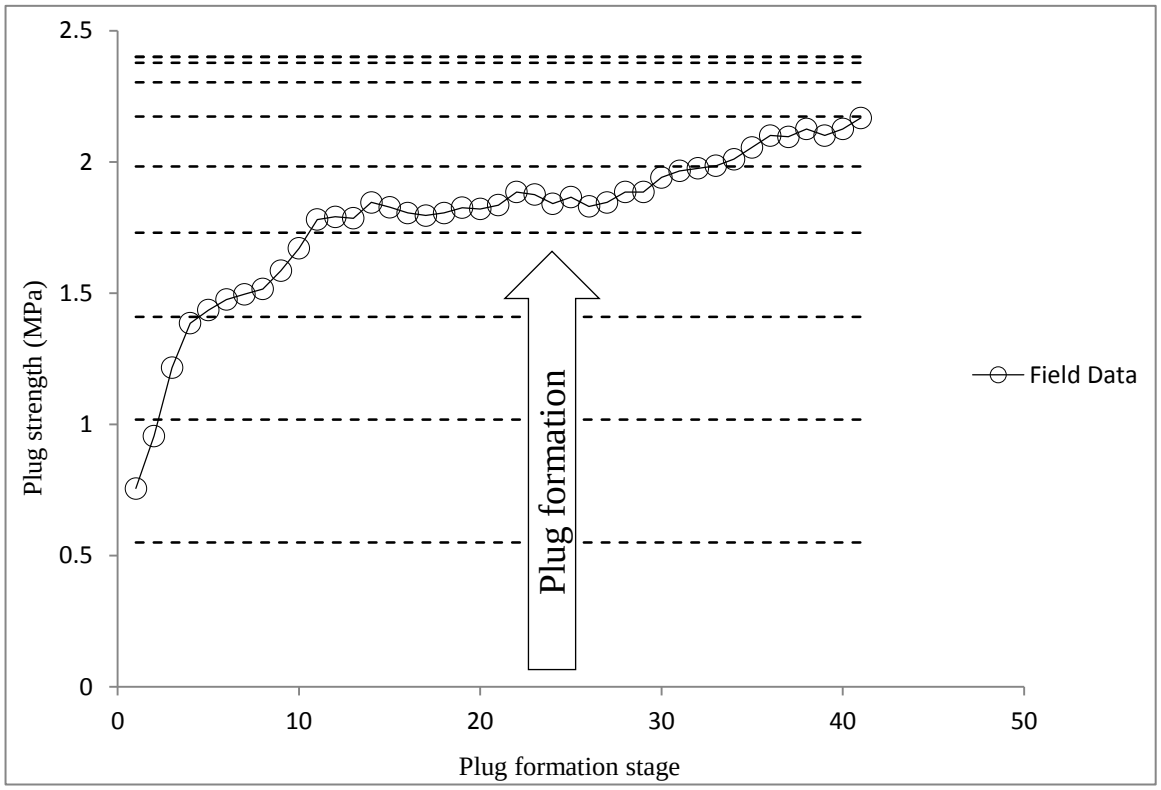

Figure 142: Predicted strengthening levels at each stage using the newly developed model against the field measurements

The level of differential pressure achievable after each stage of plug deposition is estimated and presented by dash lines in Figure 142. In the primary stages more particles can enter the fracture and the differential pressure increases more rapidly, but as the fracture becomes partially filled by particles, the rate of plug growth decreases. Normalizing the model predicted differential pressure values with the number of peaks, the results show a good agreement with the field data as presented in Figure 143. By normalizing, the ten full plug formation stages will be distributed over forty one partial deposition stages which was the case during the field trial. The differential pressure values equal the strength of the formed plug. Based on the model, it can be predicted that the maximum strengthening of the formation cannot exceed 2400 kPa.

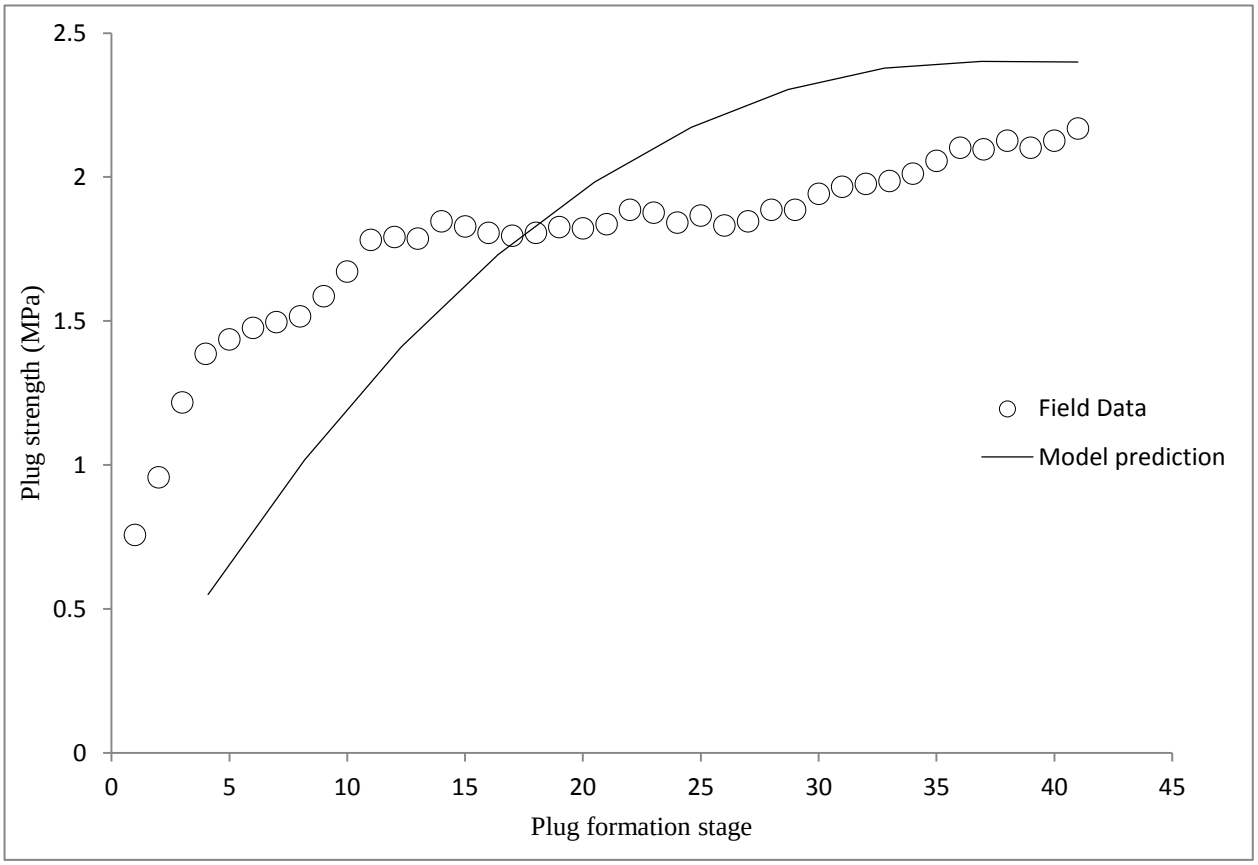

Figure 143: Agreement of the model predicted values of plug strength with the field data

Despite the limitations imposed by lack of required data and unmeasured parameters, the model was verified by a field case and was able to predict the maximum strength of the wellbore based on the drilling fluid properties. Application of the model can assist in prediction of the maximum possible strengthening around the well, specifically in weak zones which are prone to tensile fracturing. The model can also be applied to tune the drilling fluid properties such as particle size distribution and concentration to achieve the highest level of plug strength for the lowest cost.

The developed algorithm for modeling wellbore strengthening presents one of the first methodologies that considers the drilling fluid and particle properties to estimate the allowed pressure in the wellbore. Previously, controlling parameters were partially detected and mentioned in the literature, but a quantified evaluation of their contribution was scarce in the literature. Further to the estimation of the formation strength against circulation loss prior to a real operation, this model can provide valuable information during the post analysis stage to be applied in designing future operations.

CHAPTER 5: CONCLUSIONS AND RECOMMENDATIONS

5.1. Introduction

A wide range of conclusions may be withdrawn from the presented work. Since a thorough review of previous laboratory, numerical and field endeavors was performed in the initial stage of this research, the available knowledge was extracted and classified. This knowledge was then applied in carefully designing the experimental phase of the work to avoid repetition and fill the gap in the analysis and understanding of the wellbore strengthening process. In this chapter conclusions are presented in three sections: conclusions withdrawn from the literature, experimental conclusions and modeling conclusions. In the final section of this chapter, some recommendations will be presented for future research in this area.

5.2. Conclusions drawn from the literature

I. Plugging has been suggested by most previous studies as the governing mechanism of the wellbore strengthening process. It is worth noting that detection of the mechanism in the literature has been based on qualitative observations and field experience for the most part.

II. The stress caging mechanism has attracted attention during the past decade as the main mechanism of strengthening. However, there are some skeptics about the mechanical foundation of the theory. Stress caging is also built upon the plugging mechanism.

III. Resilient Graphite particles mixed with Calcium Carbonate granules have been tested in the laboratory and field in the past leading to promising strengthening results. Therefore this mixture forms the basis of the most recommended strengthening products and pills.

IV. Particle type has been investigated comparatively in previous research and the contributing properties of the particle have been rarely detected and revealed. In a few cases, the importance of angle of internal friction and shear strength of particle has been highlighted. Mohs scale is also recommended as a practical method of evaluation of strengthening capabilities of particles. There are some controversial ideas regarding the

effect of high compressive strength of particles in the literature. Some researchers believe that it prevents particles from reaching the fracture tip while others mention the importance of compressive strength in building a strong bridge over the openings.

V. Particle size distribution has not been investigated quantitatively in the past for strengthening purposes. Maintaining the value of D_{50} equal to the fracture opening size was recommended to handle uncertainties. Importance of particles close to fracture opening in size was also highlighted. Mixture of different particle shapes were proven to be efficient in field and lab trials.

VI. Concentration of solids in the drilling fluids proved to improve the strengthening process as expected. A critical limit for concentration is also reported in some studies above which the strengthening capability of the fluid declines or stays constant.

5.3. Experimental conclusions

I. Particle plugging and core fracturing systems were applied in this work. Pressure values recorded during particle plugging tests were concluded to be unable to provide reliable information regarding the strengthening capabilities of particles.

II. A new system of data analysis was devised and applied in this research which assists in revealing more information about the capabilities of particles in the wellbore strengthening process. Eight new parameters were defined to describe the number of bridges formed by each fluid, amount of filtration, maximum pressure, average pressure, average strength of the formed bridges and the amount of filtration required to form one bridge.

III. Resilient graphite containing fluid showed the best performance in the core fracturing and fracturing reopening experiments while it was unable to form strong bridges in the particle plugging tests. Calcium Carbonate was found to be ineffective both in granular and fiber form when applied alone in core fracturing and fracture reopening tests.

IV. Despite the superior performance of Calcium Carbonate in the fiber form in terms of building strong bridges during the particle plugging tests, it failed to form resistant sealing barriers in the fractures initiated in the cores.

V. Based on the close analysis and investigation of the experiments and the governing mechanisms, the average number of peaks per zero (N/Z) was found to be the most indicative of the strengthening capability of the drilling fluid.

VI. The upper range of particle size was found to be more essential in forming a bridge since fluids with higher m factor resulted in stronger bridges.

VII. In a part of the experimental phase, fluids were tried in the particle plugging system that lacked a specific part of the particle size range and the results were compared to the fluids that contained the full size range of particles. Results indicated that the particles which are in the same size of the opening or close to it are the most essential range of particles. However, a wide range of particles enhances the strengthening capabilities of the fluid.

VIII. Investigation of the effects of friction coefficient of fracture planes showed that higher friction coefficient improves the strengthening process. This conclusion also highlights the importance of the plugging mechanism and the presence of particles of the same size as the fracture opening in the fluid.

IX. Higher concentration of solids proved to improve the strengthening capability of the fluids. However, the solid content of the fluid is constrained by the pumping capacity and the safe downhole pressure range in real cases. In the particle plugging experiments, no critical solids concentration limit was encountered.

X. Opening size had an adverse effect on the strengthening process as expected for all fluids during the particle plugging tests.

5.4. Modeling conclusions

I. Based on the plugging mechanism, a mechanistic model was put forth in this work to predict the average peak pressure ($P_{P\text{-}ave}$) during particle plugging tests. The model accounts for mechanical properties of the solids, friction coefficient of the fracture planes and the fracture width. Comparison of the model predicted values and the measured values proved the accuracy of the model.

II. Based on the above mentioned model, a mechanistic model was developed for tensile fractures in real cases, which considers the size distribution and concentration of the

particle in the drilling fluid in addition to the fracture geometry, mechanical properties of the particles and the friction coefficient of the fracture planes.

III. The model shows that there is a critical limit for concentration of the particles above which no further enhancement can occur in the strengthening process. An equation was also developed based on the mechanistic model to estimate the maximum efficient concentration. Another equation is presented to estimate the maximum thickness of the plug in tensile fractures.

IV. A successful field trial of wellbore strengthening was analyzed in this work and the model was verified using the real data. The model exhibited the capability of predicting the maximum allowed pressure in the formation based on the fluid properties.

V. Based on the developed mechanistic model, it was concluded that given a specific particle size distribution and fracture geometry, the plug formed in small fractures might be weaker than those formed in larger fractures. Therefore, the particle size distribution should include all size ranges to make it possible for the fluid to bridge the openings. Based on this observation, application of nano-particles was recommended for nano-size pores and other types of openings. Nano-particles can also fill the gaps between larger solid particles and assist in building a bridge with lower permeability. They also have extraordinary mechanical properties and can assists in enhancing the resistance of the bridge.

5.5. Recommendations

I. Investigation of nano-fluids for wellbore strengthening purposes may lead to remarkable improvements in circulation loss mitigation based on the findings in the presented work. As it was shown, high compressive strength of nano-particles in addition to their small size results in firmer plugs with lower permeability. The nano-particles can also partly replace the costly Resilient Graphite which is commonly applied and reduce the overall cost of the pill or the drilling fluid.

II. More field studies with less uncertain values may lead to further modification of the developed model, specifically for fluid loss through permeable pores and natural

fractures. Application of image logs can help in reducing the uncertainties of the fracture opening geometry.

III. In this work, a low fracture toughness and very low formation permeability was assumed in the modeling phase. In future steps it may be possible to derive formation specific models that consider the field approved toughness and permeability values to predict the strengthening level of the rock.

REFERENCES

1. Messenger J., “Lost Circulation”, Pennwell Corp. Publications, 1981.
2. Ivan C., Bruton J. and Bloys B., “Lost circulation can be managed better than ever”, World Oil, June 2003.
3. Murchison W. J.,” Rule of thumb for man on the rig”, Murchison Drilling Schools, Inc Publications, 2001.
4. Sweatman R.E., Kessler C.W., and Hillier J.M., “New Solutions to Remedy Lost Circulation, Crossflows, and Underground Blowouts”, Paper SPE /IADC 37671 presented at the 1977 SPE/IADC drilling conference held in Amsterdam, Netherlands 4-6 March 1997.
5. Rabia H., “Well Engineering and Construction”, Entrac Consulting Publications, 2001.
6. Cowan J.C., House F. F., and Harrington A. H., “Seepage Loss Reducing Additive for Well Working Compositions and Uses Thereof”, Patent 5076944, December 31, 1991
7. Nayberg, T. M., “Laboratory Study of Lost Circulation Materials for Use in both Oil-Based and Water-Based Drilling Muds”, Paper SPE 14723, SPE Drilling Engineering, September 1987.
8. Nasirov S., “Drilling Fluid Optimization to Mitigate Lost Circulation”, Master of Petroleum Engineering Dissertation, Volume No: Thesis / N-UIS 2005, University of Stavanger, Stavanger, Norway, 2005
9. Wang H., “Near Wellbore Stress Analysis for Wellbore Strengthening”, Ph.D. Dissertation, Department of Chemical and Petroleum Engineering, University of Wyoming, May 2007.
10. Robert F. M., “Petroleum Engineering Handbook”, Society of Petroleum Engineers Publications, 2007.
11. Howard G. C., and Scott Jr P.P., “An Analysis and the Control of Lost Circulation”, Petroleum Transactions, AIME, Volume 192, 1951.
12. Soroush H. and Sampaio J.H.B., “Investigation Into Strengthening Methods for Stabilizing Wellbores in Fractured Formations”, Paper SPE 101802, Proceedings of the SPE Annual Technical Conference and Exhibition held in San Antonio, Texas, US, 24-27 September 2006.

13. Morita N., Black A.D., and Fuh G. F., “Theory of Lost. Circulation Pressure”, Paper SPE 20409, Proceedings of the 65th Annual Technical Conference and Exhibition of the Society of Petroleum Engineers held in New Orleans, LA, 23-26 September 1990.
14. Fuh G. F., Morita N., Boyd P.A., and McGoffin S.J., “A New Approach to Preventing Lost Circulation While Drilling”, Paper SPE 24599, Proceedings of the 67th Annual Technical Conference and Exhibition of the Society of Petroleum Engineers held in Washington, DC, 4-7 October 1992
15. Catalin D., Ivan C.D., Bruton J. R., Thiercelin M, and Bedel J., “Making a Case for Rethinking Lost Circulation Treatments in Induced Fractures”, Paper SPE 77353, Proceedings of the SPE Annual Technical Conference and Exhibition held in San Antonio, Texas, US, 29 September – 2 October 2002.
16. Scott Jr. P. P., and Lummus J.L., “New Developments in the Control of Lost Circulation” Paper SPE-516G, presented at the 30th Annual Fall Meeting of the Petroleum Branch of the American Institute of Mining and Metallurgical Engineers in New Orleans, October 2-5, 1955.
17. White J. R., “Lost circulation materials and their evaluation”, Presented as part of a panel discussion on lost circulation at the spring meeting of the Pacific Coast District, Division of Production, Los Angeles May 1956.
18. Whitfill D. L., and Hemphill T, “Pre-treating fluids with lost circulation materials”, Drilling Contractor, May/June 2004.
19. Song J.H., and Rojas J. C., “Preventing Mud Losses by Wellbore Strengthening:, Paper SPE 101593, Proceedings of the SPE Russian Oil and Gas Technical Conference and Exhibition held in Moscow, Russia, 3-6 October 2006.
20. Fett D., Martin F., Dardeau C, Rignol J., Benaissa S., Adachi J., and Pastor J., Paper Journal of SPE Drilling and Completion, Pages 500 – 508, December 2010.
21. Goud M.C., and Joseph G., “Drilling Fluid Additives and Engineering to Improve Formation Integrity”, Paper SPE/AIDC 104002, Proceedings of the Indian Drilling Technology Conference and Exhibition held in Mumbai, India, 16-18 October 2006.
22. Whitfill D. L., Hemphill T., “All Lost-Circulation Materials and Systems Are Not Created Equal”, Paper SPE 84319, Proceedings of the SPE Annual Technical Conference and Exhibition held in Denver, Colorado, USA, 5-8 October 2003.

23. Whitfill D., “Lost Circulation Material Selection, Particle Size Distribution and Fracture Modeling with Fracture Simulation Software “, Paper IADC/SPE 115039, Proceedings of the IADC/SPE Asia Pacific Drilling Technology Conference and Exhibition held in Jakarta, Indonesia, 25-27 August 2008
24. Aston M. S., Alberty M.W., McLean M.R., Jong H.J., and Armagost K., “Drilling Fluids for Wellbore Strengthening”, Paper IADC/SPE 87130, Proceedings of the IADC/SPE Drilling Conference held in Dallas, Texas, 2-4 March 2004
25. Aadnoy B.S., Belayneh M., Arriado M., and Flateboe R., ”Design of Well Barriers To Combat Circulation Losses”, Journal of SPE Drilling & Completion, Volume 23, Number 3, September 2008
26. Sweatman R., Wang H., and Xenakis H., “Wellbore Stabilization Increases Fracture Gradients and Controls Losses/Flows During Drilling”, Paper SPE 88701, Proceedings of the Abu Dhabi International Conference and Exhibition held in Abu Dhabi, United Arab Emirates , 10-13 October 2004
27. Hayatdavoudi A., “An Inquiry into the Development of a Modern Lost Circulation Material”, Paper SPE 5185
28. Canson, B. E., “Lost Circulation Treatments for Naturally Fractured, Vugular, or Cavernous Formations”, Paper SPE/AIDC 13440, Proceedings of the SPE/IADC Drilling Conference held in New Orleans, Louisiana, 5-8 March 1985
29. Cameron C., Helmy H., and Haikal M., “Fibrous LCM Sweeps Enhance Hole Cleaning and ROP on Extended Reach Well in Abu Dhabi”, Paper SPE 81419, Proceedings of the Middle East Oil Show held in Bahrain, 9-12 June 2003
30. El-Sayed M., Ezz A., Aziz M., and Waheed A., “Successes in Curing Massive Lost-Circulation Problems with a New, Expansive LCM”, Proceedings of the SPE/IADC Middle East Drilling and Technology Conference held in Cairo, Egypt, 22-24 October 2007
31. Taib, Anuar M., “Carbonate Drilling with Mud Loss Problems in Offshore Sarawak”, Paper IADC/SPE 36394, Proceedings of the SPE/IADC Asia Pacific Drilling Technology held in Kuala Lumpur, Malaysia, 9-11 September 1996
32. Sanad M., Butler C., Waheed A., and Sweatman R., “A New Treatment Increases the Fracture Gradient to Cure Lost Circulation and Control a Flowing HPHT Well in the East

Mediterranean Sea", Paper SPE 84318, Proceedings of the SPE Annual Technical Conference and Exhibition held in Denver, Colorado, USA, 5-8 October 2003

33. Kurochkin B., "Clay/Latex mixture stops lost circulation in large carbonate fractures", Oil and Gas Journal, August 28, 1995
34. Kramer J., Acosta F., and Thornton P., "New technique combats lost circulation", Oil and Gas Journal, Aug 18, 2003; 101, 32, ABI/INFORM Global, page 46
35. Monroy R.R., Mandujano H., Tejeda, J., Solis E., and Rueda, F., "Pemex controls lost circulation in south Mexico", Oil and Gas Journal, 97, 31, pages 66-68, 1999
36. Dumans C.F.F., Quantification of the Effect of Uncertainties on the Reliability of Wellbore Stability Model Predictions", PhD Dissertation in the University of Tulsa, 1995
37. Morita, N. 1995 "Uncertainty Analysis of Borehole Stability Problems", Paper SPE 30502, Proceedings of the SPE Annual Technical Conference and Exhibition held in Dallas, Texas, 22-25 October 1995
38. Abousleiman Y. N., Mguyen V., Hemphill T., and Kanj M. Y., "Time-Dependant Wellbore Strengthening in Chemically Active or Less Active Rock Formations", Paper AADE–07–NTCE–67, Proceedings of the AADE National Technical Conference and Exhibition held in Houston, Texas, USA, 10-12 April 2007
39. Wang H., Soliman M. Y., and Towler B. F., "Investigation of Factors for Strengthening a Wellbore by Propping Fractures", Paper SPE 112629, SPE Journal of Drilling and Completion, Volume 24, 3, Pages441-451, September 2009
40. Wang H., Soliman M. Y., Towler B. F., and Mukai D., "Avoiding Drilling Problems by Strengthening the Wellbore while Drilling", Paper ARMA 08-200, Proceedings of the 42nd U.S. Rock Mechanics Symposium (USRMS) held in San Francisco, CA, USA, 29 June – 2 July 2008
41. Wang H., Sweatman R., Engelman B., Deeg W., Whitfill D., Soliman M., and Towler B. F., "Best Practice in Understanding and Managing Lost Circulation Challenges". SPE Journal of Drilling and Completion, Pages 168 – 175, June 2008
42. Wang H., Towler B. F., and Soliman M., "Fractured Wellbore Stress Analysis: Sealing Cracks to Strengthen a Wellbore", Paper SPE 104947, Proceedings of the SPE/IADC Drilling Conference held in Amsterdam, Netherlands, 20-22 February 2007

43. Wang H., Soliman M. Y., Towler B. F., and Shan Z., "Strengthening a Wellbore With Multiple Fractures: Further Investigation of Factors For Strengthening a Wellbore". Paper ARMA 09-067, Proceedings of the 43rd U.S. Rock Mechanics Symposium & 4th U.S. - Canada Rock Mechanics Symposium held in Asheville, North Carolina, 28 June 1 July 2009
44. Wang H., Towler B. F., Soliman M. Y., and Shan Z, "Wellbore Strengthening Without Propping Fractures: Analysis for Strengthening a Wellbore by Sealing Fractures Alone", Paper SPE 12280, Proceedings of the International Petroleum Technology Conference held in Kuala Lumpur, Malaysia, 3-5 December 2008
45. Wang H., Soliman M. Y., Shan Z, Meng F., and Towler B. F. "Understanding the Effects of Leak-off Tests on Wellbore Strength", Paper SPE 132981, Proceedings of the SPE Annual Technical Conference and Exhibition held in Florence, Italy, 19-22 September 2010
46. Whitfill D. L., Wang M., Jamison D., and Angove-Rogers A., "Preventing Lost Circulation Requires Planning Ahead", Paper SPE 108647, Proceedings of the International Oil Conference and Exhibition held in Veracruz, Mexico, 27-30 June 2007
47. Whitfill D. L., Jamison D E., Wang M., and Thaemlitz C., "New Design Models and Materials Provide Engineered Solutions to Lost Circulation", Paper SPE 101693, Proceedings of the SPE Russian Oil and Gas Technical Conference and Exhibition held in Moscow, Russia , 3-6 October 2006
48. Whitfill D., and Wang H., "Making Economic Decisions To Mitigate Lost Circulation", Paper SPE 95561, Proceedings of the SPE Annual Technical Conference and Exhibition held in Dallas, Texas, 9-12 October 2005
49. Daqi L., Yili K., and Jiajie L., "The Mechanism Study on Lost Circulation Prevention and Plugging of Marine Fractured Carbonate Formation", http://www.seiofbluemountain.com/upload/product/201002/126562680253s7p8r.pdf
50. Aadnøy B. S., and Belayneh M., "Elasto-plastic Fracturing Model for Wellbore Stability Using Non-penetrating Fluids", Journal of Petroleum Science and Engineering, Volume 45, 3-4, Pages 179-192, December, 2004

51. Aadnoy B. S., Mostafavi V., and Hareland,G., “Fracture Mechanics Interpretation of Leak-Off Tests”, Paper SPE 126452, Proceedings of the Kuwait International Petroleum Conference and Exhibition held in Kuwait City, Kuwait, 14 -16 December 2009
52. Aadnoy B. S., Kaarstad E., and Belayneh M., “Elastoplastic Fracture Model Improves Predictions in Deviated Wells”, Paper SPE 110355, Proceedings of the SPE Annual Technical Conference and Exhibition held in Anaheim, California, U.S.A. , 11-14 November 11 2007
53. Belayneh M., “Experimental and Analytical Borehole Stability Study”, PhD Dissertation, University of Stavanger, Stavanger, Norway, 2004
54. “Material Safety Data Sheet”, http://www.bakerhughes.com/
55. Peronius N., and Sweeting T. J., “On the Correlation of Minimum Porosity with Particle Size Distribution”, Journal of Powder Technology, Volume,42, Pages 113 – 121, 1985
56. Fjaer E., Holt R. M., Raaen A. M. and Rinses R., “Petroleum Related Rock Mechanics”, Elsevier Publications, 2008
57. Sensoy T., Chenevert M.E., and Sharma M. M., “Minimizing Water Invasion in Shale Using Nano Particles”, Paper SPE 124429, Proceedings of 2009 SPE Annula Technical Conference and Exhibition held in New Orleans, Louisiana, USA, October 4 – October 7, 2009.
58. Amanullah M., Al-Arfaj M. K., and Al-Abdullatif Z., “Preliminary Test Results of Nano-Based Drilling Fluids for Oil and Gas Field Application”, Paper SPE 139534, Proceedings of SPE/AIDC Conference and Exhibition held in Amsterdam, Netherlands, March 1 – March 3, 2011.
59. Nygaard R., and Salehi S., “A Critical Review of Wellbore Strengthening: Physical Model and Field Deployment”, Paper AADE-11-NTCE-24, Proceedings of the 2011 AADE National Technical Conference and Exhibition held in Houston, USA, April 12 – April 14, 2011